UNIVERSITA' DEGLI STUDI DI PADOVA

Sede Amministrativa: Università degli Studi di Padova

DIPARTIMENTO DI GEOSCIENZE

SCUOLA DI DOTTORATO DI RICERCA IN SCIENZE DELLA TERRA
CICLO XXI

ARCHAEOMETRICAL INVESTIGATIONS ON MORTARS AND PAINTINGS AT POMPEII AND EXPERIMENTS FOR THE DETERMINATION OF THE PAINTING TECHNIQUE

Direttore della Scuola: Ch.mo Prof. Gilberto Artioli
Supervisore: Ch.mo Prof. Claudio Mazzoli

Dottoranda: Rebecca Piovesan

Alla mia famiglia

Riassunto

La caratterizzazione dei materiali da costruzione quali malte e intonaci può fornire indicazioni utili ed esclusive per rispondere a quesiti di carattere tecnologico, artistico e storico, come la distinzione tra diversi periodi costruttivi, la comprensione delle conoscenze tecnologiche e l'identificazione della provenienza delle materie prime. Ciò vale anche per lo studio delle finiture pittoriche murali, svolto prevalentemente per indicare la natura dei pigmenti, i tipi di ricette e le tecniche pittoriche adoperate.

Numerosi campioni di malta e finiture pittoriche provenienti da ambienti funzionalmente e cronologicamente differenti sono stati prelevati dal sito archeologico del Tempio di Venere a Pompei. La maggior parte di tali campioni appartiene ad unità archeologiche di età compresa tra la fine del IV secolo AC e il I secolo DC. Lo scopo di questo studio è stato quello di caratterizzare i materiali da costruzione, di determinarne le tecnologie di produzione e di correlare tali informazioni con il ruolo funzionale degli edifici da cui provengono, riconoscendo così anche eventuali evoluzioni nel tempo. E' stata inoltre svolta una ricerca sperimentale allo scopo di determinare criteri oggettivi per il riconoscimento delle tecniche pittoriche murarie utilizzate.

Le tradizionali tecniche analitiche impiegate per la caratterizzazione dei materiali, comprendenti microscopia ottica, elettronica (SEM, ESEM), diffrazione di raggi X (XRD), spettroscopia infrarossa (micro-ATR, FT-IR), spettroscopia Mössbauer, EMPA e colorimetria, sono state integrate dall'applicazione della tecnica di analisi di immagine, al fine di ricavare con maggior dettaglio i rapporti esistenti tra le differenti componenti tessiturali della malta (aggregato, legante e porosità).

Le malte campionate sono state inizialmente suddivise in tre macro-gruppi, basandosi sulla natura delle strutture architettoniche di provenienza. L'insieme dei dati indica che l'aggregato utilizzato nelle malte è costituito prevalentemente da frammenti di rocce vulcaniche, spesso contenenti leucite, da cristalli di clinopirosseno (diopside), sanidino, plagioclasio e raramente da granato e biotite. Questa composizione è tipica dei depositi vulcanoclastici del Somma-Vesuvio e indica che la materia prima dell'aggregato è di origine locale. Una differenziazione dei campioni, basata sulle diverse proporzioni dei componenti dell'aggregato, ha individuato un primo gruppo contenente prevalentemente frammenti di scorie vulcaniche ed un secondo costituito principalmente da cristalli di clinopirosseno. Nella maggior parte dei campioni si è osservata la presenza di uno o più strati di finitura, molto sottili, costituiti da un intonaco caratterizzato da aggregato a granulometria fine. Sulla base della composizione petrografica dell'aggregato tali strati di intonaco sono stati suddivisi in tre differenti tipi: i) intonaco costituito da frammenti di silicati e rocce silicatiche (*intonachino*); ii) intonaco costituito da frammenti di ceramica appositamente frantumata (*cocciopesto*); iii) intonaco costituito da frammenti di calcari o cristalli di calcite (*marmorino*).

Sia i pavimenti che le strutture idrauliche sono risultati essere composti da due tipi

di malta, la prima costituita da *cocciopesto* e la seconda caratterizzata da un aggregato a base di frammenti di natura vulcanica. I frammenti di *cocciopesto* sono stati ulteriormenti suddivisi in due gruppi sulla base della natura degli inclusi in essi presenti. Un gruppo di *cocciopesto* presenta come inclusi frammenti vulcanici, e ciò ne indica la produzione locale; l'altro, invece, presenta prevalenza di cristalli di quarzo e feldspato, suggerendo il riutilizzo di materiali ceramici di importazione. Sulla base delle osservazioni in microscopia ottica e dei valori dell'indice di idraulicità (HI), calcolato dall'elaborazione dei dati ricavati da microanalisi EDS, è stato possibile distinguere due diversi tipi di legante, entrambi a base di calce, ma con diverso indice di idraulicità, parametro correlato alle reazioni idrauliche occorse con l'aggregato presente nella malta. Alcuni aggregati di natura pozzolanica (*cocciopesto* e sabbia di natura vulcanica), infatti, reagendo con la calce aerea hanno prodotto un legante di tipo idraulico. Tutti i dati testimoniano come gli artigiani selezionassero i materiali di partenza con accuratezza in conformità a particolari caratteristiche, per ottenere malte con ben precisi caratteri fisici e/o estetici.

Per definire la possibile provenienza delle materie prime costituenti le malte, l'aggregato identificato nelle stesse è stato confrontato dal punto di vista petrografico con delle sabbie campionate in 14 località collocate lungo la costa napoletana e con depositi alluvionali antichi concentrati nell'area limitrofa al tempio di Venere, prelevati mediante 4 sondaggi. I risultati hanno confermato la provenienza di tali materiali da depositi locali, indicando una maggior compatibilità degli aggregati delle malte con le sabbie provenienti dai depositi alluvionali. Ciò supporta una recente ed innovativa ipotesi archeologica che vede la collocazione dell'antico porto commerciale di Pompei esattamente davanti al tempio di Venere ed inoltre suggerisce che i depositi alluvionali localizzati in questa zona venissero prelevati con il doppio scopo di allargare ed approfondire il porto e allo stesso tempo disporre di materiale da costruzione ben selezionato in una zona prossima al tempio in costruzione.
Per quanto riguarda l'evoluzione nel tempo, le ricette e le materie prime si presentano omogenee dal IV secolo AC al I secolo DC, indicando come le conoscenze tecnologiche fossero già ben sviluppate nel IV secolo AC, nonché una certa persistenza nella tradizione tecnologica. I differenti tipi di malta risultano correlati alla particolare funzione delle strutture architettoniche a cui appartengono. Un esempio è dato delle strutture idrauliche, dove viene sempre impiegato un aggregato di tipo pozzolanico, che ne conferisce il carattere idraulico.
Al fine di riconoscere le tecniche pittoriche adottate nelle pitture murarie di Pompei, nell'ambito di questa ricerca è stato svolto uno studio sperimentale mirato a definire criteri oggettivi e procedure analitiche per distinguere le tecniche pittoriche ad *affresco* e a *mezzofresco* (pittura alla calce). Due serie di fasce di 15 colori diversi sono state dipinte utilizzando vari pigmenti tradizionali, compreso il bianco di calce, secondo le tecniche pittoriche ad *affresco* e a *mezzofresco*. Da ciascuna fascia sono state ricavate delle sezioni lucide le quali sono state analizzate in microscopia ottica ed elettronica a scansione, al fine di determinare la microstratigrafia e le caratteristiche microtessiturali. Il confronto

tra la sequenza microstratigrafica e la distribuzione degli elementi chimici in entrambe le serie ha rivelato differenze sistematiche tra la tecnica ad *affresco* e quella a *mezzofresco*, indipendentemente dal pigmento utilizzato, stabilendo criteri oggettivi di distinzione ed una procedura operativa di indagine standardizzata.

Per convalidare i criteri diagnostici proposti sono stati analizzati e paragonati ai dati sperimentali ricavati cinque campioni provenienti dall'abazia di Chiaravalle (Milano) per i quali l'utilizzo di *affresco*, *mezzofresco* e pittura a secco è certificato e documentato.
Nell'ultima parte del lavoro, impiegando un'ampia gamma di metodologie analitiche (OM, ESEM, XRD, micro-ATR, FT-IR, spettroscopia Mössbauer, colorimetria and EMPA), sono stati approfonditamente caratterizzati 68 frammenti di pittura murale prelevati da riempimenti ritrovati nel tempio di Venere. Lo studio di questo tipo di campioni non permette di avanzare considerazioni sull'intera parete dipinta, ma fornisce comunque uno strumento utile per la caratterizzazione dei pigmenti e delle ricette utilizzati nel tempio. I dati dimostrano che la tavolozza utilizzata nel tempio di Venere è molto varia, anche se non così estesa come quella ritrovata in altri palazzi di Pompei; racchiude pigmenti largamente utilizzati sia a Pompei che in molte altre località dell'Impero romano. Essa coincide anche con i materiali descritti sia da Vitruvio che da Plinio ed è composta da diverse terre naturali come le ocre rosse, gialle e brune e la terra verde (costituita prevalentemente da celadonite) e da altri pigmenti artificiali come il bianco di calce, il nero fumo ed il blu egizio. E' stato riconosciuto anche l'utilizzo di cinabro, un pigmento alquanto prezioso. Tutti i pigmenti mostrano buona qualità. Anche la spettroscopia Mössbauer, eseguita con una innovativa strumentazione portatile non distruttiva, ha confermato l'identificazione di alcune ocre rosse e gialle. Le pellicole pittoriche risultano inoltre essere costituite prevalentemente da sottili strati (0,01-0,10 mm di spessore) che mostrano elevata adesione allo strato preparatorio sottostante. In alcuni casi sono stati tuttavia identificati strati con spessori maggiori (fino a 0,40 mm), spesso stesi su precedenti strati pittorici. L'analisi FTIR non ha rilevato in nessun campione componenti rapportabili a leganti di tipo organico. L'interpretazione della microstratigrafia rilevata nei campioni del tempio di Venere, sulla base dei criteri identificati e sviluppati su base sperimentale in relazione all'identificazione delle tecniche pittoriche, dimostra che i pigmenti sono stati stesi prevalentemente sull'intonaco ancora umido, come richiesto dalla tecnica pittorica ad *affresco*, mentre nel caso degli strati di maggior spessore è stata utilizzata la tecnica a *mezzofresco*.

Summary

The characterization of building materials, such as mortars and plasters, can give useful and unique indications when different technological, artistic and historical questions need to be answered (such as the definition of different construction periods, the understanding of technology knowledge and the identification and provenance of raw materials). This can be applied also to the study of wall paintings, which aims to identify the nature of pigments, recipes and adopted techniques.

A series of samples of mortars, paintings and floors from different functional and chronological contexts were collected from the Temple of Venus (south-western Pompeii). The majority of the samples were archaeologically dated from the end of the 4th century BC to the 1st century AD. The aim of this study was to characterise these building materials and to determine their production techniques, to relate them with functionality of the buildings or rooms, and to recognise their evolution in time. Experiments were also performed in order to determine objective criteria for the identification of the wall-painting technique adopted. Optical Microscopy (OM), Scanning Electron Microscopy (SEM, ESEM), X ray diffraction (XRD), infrared spectroscopy (micro-ATR, FT-IR), Mössbauer spectroscopy, microprobe (EMPA) and colorimetric analyses were carried out to characterise materials, and integrated with image analysis to define with more accuracy ratios among textural elements of the mortars (i.e. aggregate, binder, porosity).

The mortars were preliminary grouped into three macro-groups, based on architectural building they belong to. Results showed that aggregate in mortars is mainly composed of volcanic rock fragments, often containing leucite, and crystals of clinopyroxene (diopside), sanidine, plagioclase and, more rarely, garnet and biotite. These components are typical of the Somma-Vesuvio volcanoclastic deposits and indicate an aggregate made with raw materials of local provenance. Their differing amount of components allowed distinguish two main groups; the former, that include most of samples, is characterize by the prevalence of fragments of volcanic rocks, and the latter by abundant clinopyroxene crystals. Mortars often revealed thin cover fine-grained layers of plaster, and the results of petrographic composition of its aggregate allowed the differentiation of the plasters into several subtypes: i) a plaster made of fragments of silicates and silicate rocks (intonachino); ii) a plaster made of fragments of crushed pottery (cocciopesto); iii) a plaster made of fragments of limestone or crystals of calcite (marmorino).

Both floors and hydraulic structures were made of two types of mortar, the first one made of a cocciopesto and the second one characterised by an aggregate composed of volcanic fragments. Pottery inclusions are helpful in further subdividing the cocciopesto fragments into two subgroups: cocciopesto made of vulcanite fragments and cocciopesto made of crystals of quartz and feldspar; the former can be related to local production, the latter indicates re-use of imported materials. At the same time, optical microscopy study and calculation of

hydraulicity index (HI - derived from EDS data) were carried out on representative binder of the mortars. Some specific peculiarities may be observed and allowed the differentiation of the binders in two main types, both constituted by lime but displaying different hydraulicity index, which is correlated to the hydraulic reactions occurred between binder and aggregate. Some pozzolanic aggregates (i.e. cocciopesto and volcanic sand), indeed, reacted with the lime producing a hydraulic binder with useful hydraulic performances. The data showed that craftsmen selected the materials with accuracy on the basis of these characteristics, to obtain particular physical and/or aesthetical performances.

In order to establish the possible provenance of the raw materials, the aggregates identified in the mortars were petrographically compared with samples of sand collected from 14 different localities along the Neapolitan coastline and with alluvial sand deposits drilled from an area that lies in front of the Temple of Venus. These analyses confirmed the use of local deposits. More interestingly, sand from boreholes provided a better match with petrography of the mortar aggregates, supporting recent innovative archaeological hypothesis on the location of the trading harbour of Pompeii in front of the Temple of Venus, and suggesting that alluvial deposits were explored in this area with the double purpose of enlarging and deepening the docks, and providing well sorted building material close to the building area. Archaeologists might also speculate on the symbolic meaning of the use of raw materials coming from the harbour, for the construction of the Temple of Venus, patron of trades.

As regards time evolution, recipes and raw materials seem to be homogeneous from the 4th century BC to the 1st century AD, indicating that technological knowledge was already well established in the 4th century BC, and suggesting the persistence of technological tradition. The different types of mortars resulted to be correlated with architectonic structures and therefore with their specific functionality, such as in the case of hydraulic structures, where pozzolanic aggregate was always used.

The recognition of the painting technique adopted by an artist is often a matter of debate in studies for the characterization, restoration and conservation of mural paintings. During this research an experimental study was undertaken in order to define objective criteria and analytical procedures for the recognition of the fresco (buon fresco that means true fresco) and the mezzofresco painting (lime-painting) techniques. Two groups of fifteen coloured strips were painted using various traditional pigments, including lime white, according to both the fresco and mezzofresco painting techniques. Samples were prepared in polished sections and analysed by optical and scanning electron microscopy for determination of microstratigraphy and microtextural features. The comparison of microstratigraphic sequences and distribution of chemical elements in each of the two sets of samples displayed systematic differences between the fresco and mezzofresco painting techniques, independently on the pigment used, suggesting objective distinctive criteria and standardized operational procedures.
Five samples from the Chiaravalle Abbey (Milan) for which the use of fresco, secco and

mezzofresco is well documented, were also analysed and results were compared with experimental data to validate the proposed diagnostic criteria.

In the last section 68 fragments of wall paintings, prevalently from infillings, unearthed at the Temple of Venus were exhaustively characterised by a wide range of analytical methods (OM, ESEM, XRD, micro-ATR, FT-IR, Mössbauer spectroscopy, colorimeter and EMPA). The study of these kind of samples does not allow make remarks about the whole wall paintings, since removed from the original location, but is a useful method for the identification of pigments and recipes used in the temple. The data showed that the palette of the temple of Venus is various, although not so extended as that found in other buildings in Pompeii, and is consistent with pigments used elsewhere in Pompeii and in the Roman Empire and also with the palette described both by Pliny and Vitruvius. It is composed by several natural earths such as red, yellow and brown ochres and green earth (mostly celadonite); and by other artificial pigments such as whitewash, carbon black and Egyptian blue. Also the precious pigment cinnabar was detected. All the pigments displayed good quality; this was also confirmed for some red and yellow ochre by Mössbauer spectroscopy, performed with a non-destructive new portable equipment. Paintings mainly resulted to be made of thin pictorial layers (0.01-0.10 mm thick) strongly adhering to the underlying preparation layer. Nonetheless, in some cases thicker layers (up to 0.40 mm) were recognised, often spread on other previous painting layer. No traces of organic binder have been identified by the FTIR analysis in any sample. The application of the criteria developed to distinguish the paint technique to the interpretation of the microstratigraphy observed on the paintings of the Temple of Venus, demonstrated that pigments were mainly spread on the plaster while wet, such as in the fresco pictorial technique; but that in the thicker layers above mentioned the mezzofresco technique were used.

Note to the thesis

As the chapters of the thesis are to be viewed as “independent” scientific papers, there is, inevitably, a certain degree of repetition.

Acknowledgements

Special thanks to Claudio Mazzoli who worked together on this project and helped me so much during this thesis, and to Ruth Siddall for the indispensable teaching.
Many Thanks to the Soprintendenza archeologica di Pompei, to Emmanuele Curti, Director of the archaeological excavation at the Temple of Venus and to all the archaeological staff for the samples and the helpful collaboration.
Thanks for the samples to the Soprintendenza al patrimonio storico artistico ed etnoantropologico di Milano and to Sandrina Bandera, Director of the restoration project of the Chiaravalle Abbey. Thanks are due to the C.S.G. Palladio s.r.l. for sponsoring this PhD.
Acknowledgements are given to Luca Nodari, Luca Menegon and the staff of the Institute of Geosciences and Georesources, CNR, Padova, for the useful suggestions and their analytical support.

Contents

Chapter 3
The pigments of the temple of Venus (Pompeii)

Chapter 1

Ancient mortar technology: petrographic and microstratigraphic analysis of mortar-based building materials from the Temple of Venus, Pompeii

Introduction

Recipes for mortar-based building materials may change over time and differ in the various construction and restoration phases. They normally reflect craftspeople's knowledge, the availability of raw materials, and also the importance of the building in which they are found. The present research focuses on mortar-based materials from various construction and renovation phases of the Temple of Venus (Pompeii), in order to identify any changes over time in production recipes.

The Temple of Venus, who was both the main and polyad divinity of Pompeii, is located on the south-western side of the town (Figure 1), and underwent numerous reconstructions and renovations until the eruption of Vesuvius sealed Pompeii under a thick layer of pyroclastic deposits in 79 AD. The site of the temple had probably been a place of worship since Archaic times, connected with the Etruscan worship of Venus. The area was certainly occupied again in the late 4th-3rd centuries BC, when the Sannites entered it. It was completely redesigned in about 130 BC, during definitive Romanisation. The sanctuary of Roman Republic times was then renovated during the Julian and Claudian ages, but was almost completely destroyed during the earthquake of 62 AD. At the time of the eruption of Vesuvius in 79 AD, rebuilding was still under way, as attested by findings of building elements. A recent new hypothesis on the debated location of the harbour of Pompeii suggests that the Temple of Venus had not only religious but also trade connotations (Curti, 2007; Curti, 2008). This new interpretation places the harbour on the south-western side of Pompeii, outside the town walls, near the market and right in front of the temple. Therefore, the Temple of Venus becomes an extremely interesting case study with which to follow continual religious and political changes through architectural renovations in Pompeii.

1. Sample selection

During excavations at the Temple of Venus by the Postgraduate School of Archaeology, University of Matera, between 2004 and 2008, thousands of fragments of mortar-based building materials were unearthed. In this study, we analysed a selection of these samples

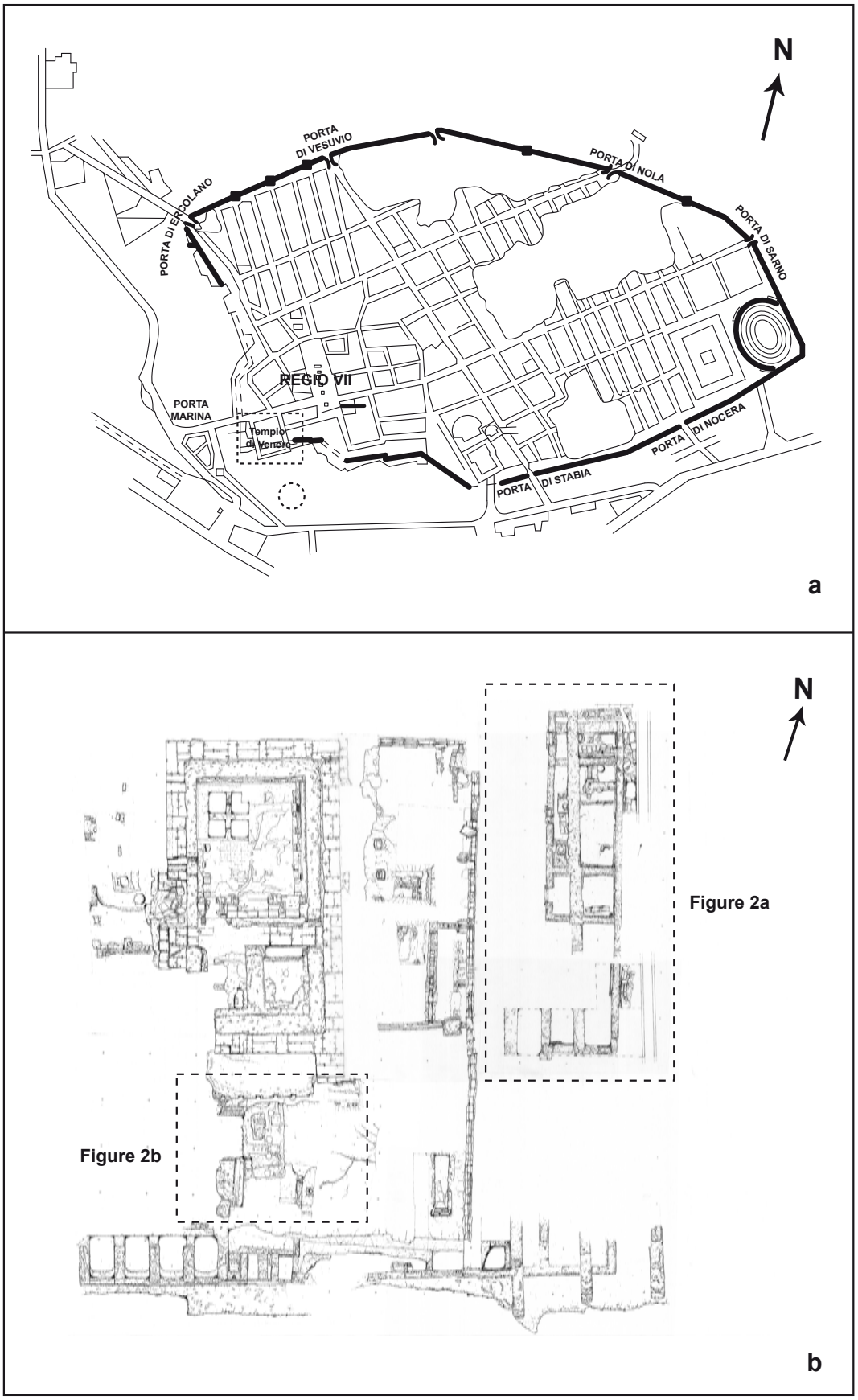

Figure 1. Map of archaeological site of Pompeii (a) with location of Temple of Venus (dotted square) and of the hypothetical location of the harbour (dotted circle). Plan of Temple of Venus (b).

(127 fragments of mortars), mostly from the southern northern areas of the site (Figure 1b, 2). The samples were archaeologically dated from the end of the 4th century BC to the 1st century AD and divided into six age groups (Table 1). Stratigraphic units were dated and chronologically related on the basis of ceramic types. The samples were also subdivided into three groups according to the architectural features of their provenance: walls, floors and hydraulic structures (conduits, wells and cisterns) (Table 1), and then analysed petrographically and microstratigraphically.

Identified aggregate particles were also compared with samples of sand collected from fourteen localities along the Neapolitan coastline, from Cuma to Castellammare di Stabia (Figure 3), and with four alluvial sand samples from borehole cores drilled in the area in front of the Temple of Venus, to study the areas from which raw materials came.

Table 1
Time distribution of differing types of mortars and relative abundances in various architectural features of provenance structures.

		Walls					Floors		Hydraulic S.	
		Arriccio		*Intonaco*						
		VSRA	**CRA**	**I**	**C**	**M**	**VSRF**	**CRF**	**VSRH**	**CRH**
Republican times	**End 4th-3rd BC**	9	1	1	3	1	4	1	2	-
	Second half 2nd BC	25	3	3	11	8	12	7	5	4
	1st BC	8	1	2	2	7	-	-	-	-
Imperial times	**Augustan age**	3	-	-	1	2	1	-	1	1
	Julio-Claudian age	13	-	1	5	4	4	2	1	1
	Flavian age	2	-	-	-	-	-	-	-	-
Unknown age		18	1	-	1	-	4	4	-	-
	Samples									
Walls	89	93%	7%	15%	31%	54%	-	-	-	-
Floors	28	-	-	-	-	-	69%	31%	-	-
Hydraulic structures	10	-	-	-	-	-	-	-	58%	42%

VSRA: Volcanic scoria-rich arriccio; CRA: Clinopyroxene-rich *arriccio*; I: *Intonachino*; C: *Cocciopesto*; M: *Marmorino*; VSRF: Volcanic scoria-rich floors; CRF: Ceramic-rich floors; VSRH: Volcanic scoria-rich hydraulic structures; CRH: Ceramic-rich hydraulic structures.

2. Analytical methods

All samples were analysed by optical microscopy (OM), following macroscopic and microstratigraphic analytical procedures for study of mortar-based building materials described in UNI Norm 11176:2006 “Cultural heritage - Petrographic description of a mortar” proposed by the Italian Organization for Standardization (UNI), a member of the International Organization for Standardization (ISO). These procedures are applicable to mortars and plasters, where “mortar” is a material composed of an inorganic binder plus an aggregate with dimensions of less than 5 mm (Prentice, 1990), and “plaster” is a type of fine-grained, often multi-layered, mortar which provides a smooth coat to a wall or other surface.

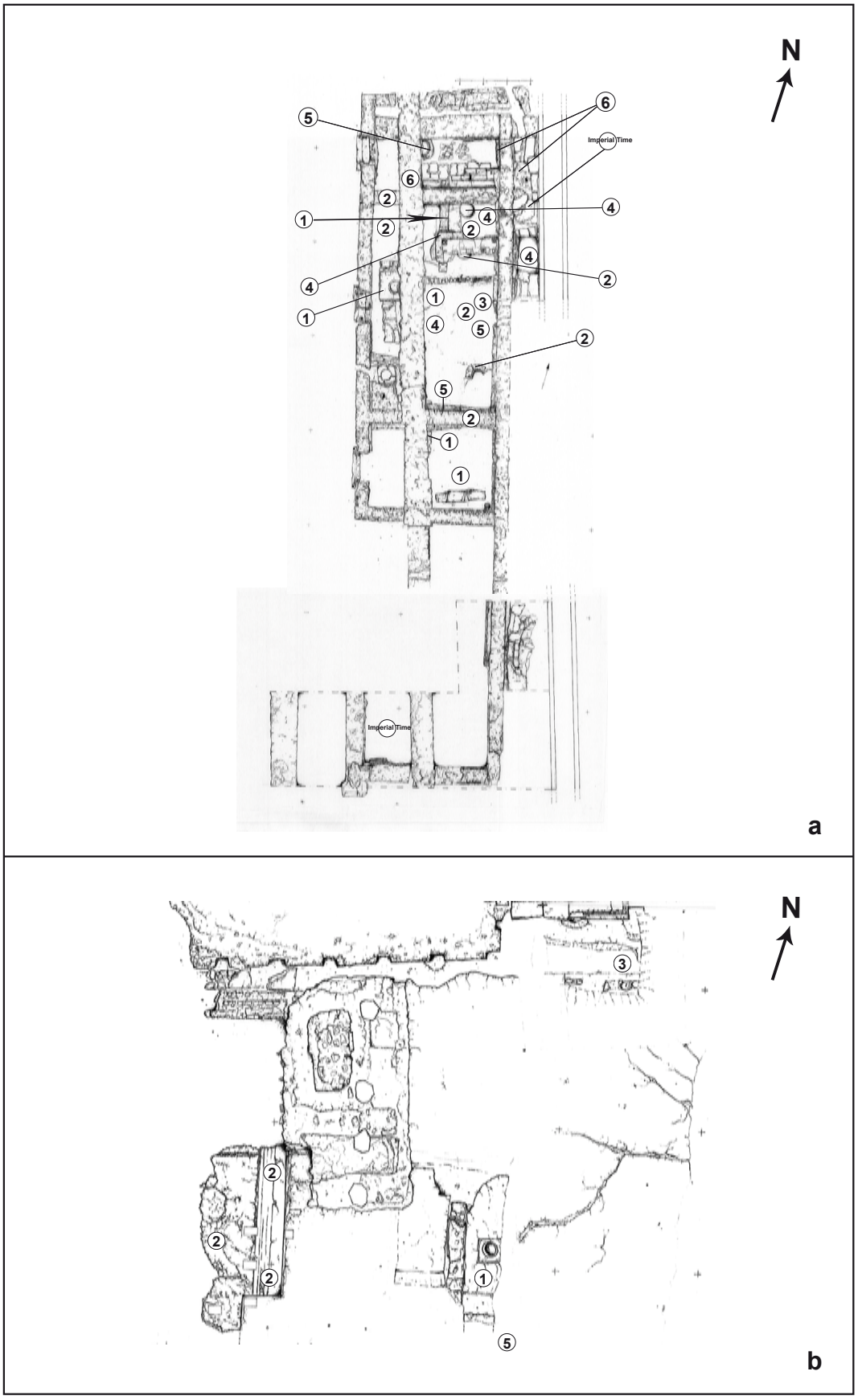

Figure 2. Details of northern (a) and southern (b) excavated areas of the Temple of Venus. Circles with number indicating points of sampling (1: end 4th-3rd century BC; 2: second half 2nd century BC; 3: 1st century BC; 4: Augustan age; 5: Julio-Claudian age; 6: Flavian age.)

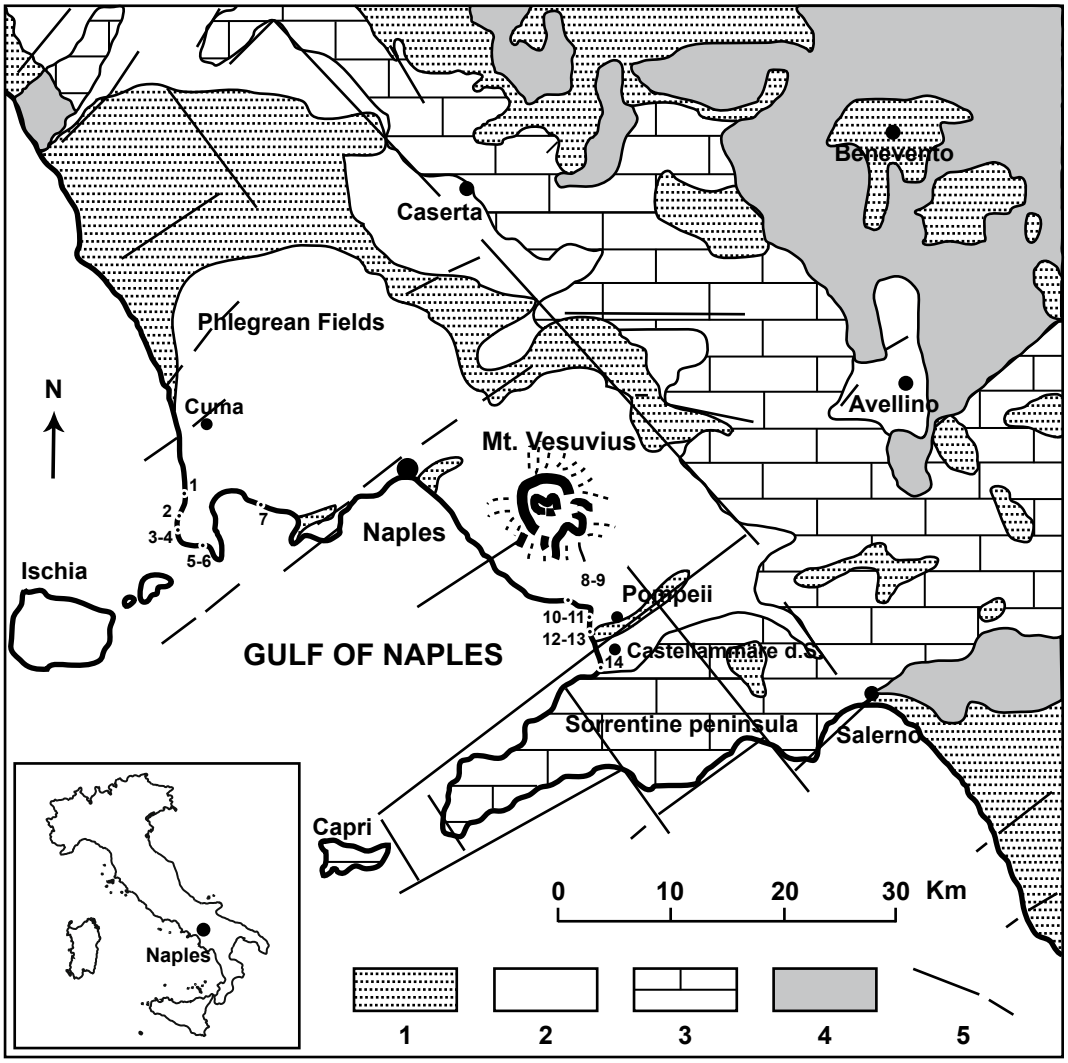

Figure 3. Geological sketch of Mount Vesuvius and surrounding areas. 1. Alluvial, lacustrine and coastal sediments; 2. Potassic to ultrapotassic lavas and volcaniclastic deposits; 3. Limestone and dolostone; 4. Silico-clastic and carbonate deposits, evaporates; 5. Faults.

Also sand samples were petrographically studied in thin section by optical microscopy (OM).

Selected samples representative of the main petrographic groups were also studied by scanning electron microscopy (SEM) for microtextural and microchemical characterisation. Concentrations of major elements Al, Fe, Si, Ca and Mg were also determined by analysis of selected areas of the binder by an energy-dispersive X-ray system (EDS). They define the hydraulicity of the mortar, measured by the hydraulicity index (HI), defined by Boyton (1966) as:

$$HI = \frac{Al_2O_3 + Fe_2O_3 + SiO_2}{CaO + MgO}.$$

The higher the index, the greater the property of the mortar to harden in a wet or water-saturated environment. HI should be lower than 1.2, which corresponds to the upper limit

for quick-setting limes. Higher HI values indicate the presence in the selected area of small silicate rock or mineral fragments, which increases Al_2O_3, Fe_2O_3 and SiO_2 in the analysis, without reflecting the real amount of hydraulic reaction products. HI was also determined for lumps of lime, which were interpreted as a measure of the purity of the limestone used for its preparation (Charola and Henriques, 2000). In situ EDS analyses were also performed on several crystals of characteristic minerals of the aggregate, to obtain their composition and better defined the provenance of the raw materials. Chemical compositions were also compared with unpublished data (Grifa, pers. comm.) of Somma-Vesuvius products.

Considering the recent evolution of the image-analysis approach to the quantification of mortar parameters (e.g. textural features of aggregate and aggregate:binder ratio) (Carò and Di Giulio, 2004; Carò et al., 2006; Mertens and Elsen, 2006; Carò et al., 2008), back-scattered SEM images of selected samples were analyzed with the Image SXM 1.75 software (Barrett, 2005). This allowed determining morphological and textural parameters of the aggregate, and obtaining objective quantification of the relative abundances of binder, aggregate and porosity. In the present work only preliminary results will be reported.

3. GEOLOGICAL AND VOLCANOLOGICAL SETTING OF THE SOMMA-VESUVIUS AREA

The Somma-Vesuvius volcanic complex is located in the centre of the so-called Piana Campana, a graben-like structure that formed in Pliocene times at the western border of the Appenines chain, presumably as a consequence of the opening of Tyrrhenian basin (De Vivo et al., 2001). This structural low is bordered on the north-eastern side by the north western-south eastern apenninic faults to the south and by the north eastern-south western antiapenninic faults to the north (Santacroce, 1987). The complex is probably located at the intersection of a system of conjugate extensional faults (Principe et al., 1987) and its base lies underneath the Campanian Ignimbrite deposits (Brocchini et al., 2001; Di Renzo et al., 2007), being therefore younger than ca. 39 ka (De Vivo et al., 2001). Mesozoic and Cenozoic carbonate rocks – limestones and subordinate dolostones – form the sedimentary basement of the Somma-Vesuvius and also constitute the structural highs that borders the Campanian plain, including Monte Massico, Monti Tifatini, Monti del Partenio, Monti di Nola and the Sorrento peninsula (Ippolito et al., 1975, Santacroce, 1987, Figure 3).

Mount Somma-Vesuvius volcano belongs to the Italian Potassic Magmatism and is comprised in the *Roman Province* – i.e. volcanic provinces of Latium and Campania (Conticelli et al., 2004). It consists of an older volcano dissected by a summit caldera, Monte Somma, and a recent cone, Vesuvius, which grew discontinuously, after the 79 A.D. Pompei pumice eruption, during periods of persistent activity (Cioni et al., 1999).

Volcanic products, ranging from effusive lava flows to explosive Plinian eruptions, have alkaline potassic affinity and they have been assigned to three main magmatic periods that according to Arnò et al. (1987) and Civetta and Santacroce (1992) (and references quoted

therein) are: an ancient period (25 ka – 11.4 ka) characterised by slightly undersaturated lavas (K-basalt to K-latite) and pyroclastic deposits; a second period (7.9 ka – 79 AD) characterised by phonotephrite to phonolite; and a youngest period (79 AD – 1944 AD) characterised by leucititic phonotephrite to leucititic phonolite.

Since 19 ka, Somma-Vesuvius activity has been characterized by peculiar eruptive cycles. After long periods of quiescence – from hundreds to thousands of years – in which the volcanic complex was in obstructed conduit conditions, new eruptive cycle begun with major plinian or subplinian eruptions. Usually, at this period followed an open-conduit, semi-persistent strombolian activity characterized by lava flows and low-energy explosive eruptions (Civetta and Santacroce, 1992). The most famous Plinian eruption is the 79 AD event that destroyed the towns of Pompeii and Herculaneum. This event was characterized by the explosion of a huge volume of pumice and ash in a very short period of time with a maximum extrusion rate exceeding 10^4 m^3/s (Sheridan, 1981). The eruptive sequence that summarizes the type section progress is constituted by rough pumice-fall, pumice-flow, ash-flow, pyroclastic surge and mud deposits (Santacroce, 1987).

The mineralogical composition of the Somma-Vesuvius volcanic products, according to Joron (1987), consist in strongly zoned clinopyroxene (diopside and Fe-rich diopside), plagioclase, sanidine, leucite, biotite, melanitic garnet with andradite content in the range of 50-85% and significant Ti proportions, extensively zoned olivine, ranging in composition from $Fo_{78\text{-}60}$ to $Fo_{66\text{-}48}$, and, less often, nepheline, amphibole, Fe-Ti oxides, scapolite and apatite.

4. Petrography and microstratigraphy

The definitions originally described by Vitruvius and reused again by Mora et al. (1984) were adopted to define different portions of the multi-layered plasters, normally composed of the following microstratigraphic sequence: scratch coat, *arriccio*, and *intonaco*. As defined by Mora et al. (1984) and Vitruvius, scratch coat is a very rough rendering applied to smooth the surface of a wall, *arriccio* is a sequence of "not less than three coats of sand and mortar, besides the rendering coat" (Vitruvius), and *intonaco* is a set of finishing layers made of limewash and a very fine sand, which may also be painted on (A in Figure 4). Floors and hydraulic structures also display a multi-layer structure, but generally with a simpler microstratigraphy, composed of a preparation layer and one or two finishing layers (B and C in Figure 4). The filler, including various types of rocks and minerals such as carbonate rocks, ground ceramic materials and volcanic sand, was chosen according to the required aesthetic and physical properties, such as colour and brightness, hydraulicity and weathering durability.

In all samples bearing silicate aggregate, that is always constituted by a volcanic sand composed of leucite-bearing volcanic rock fragments and volcanic scoria leucititic or trachytic

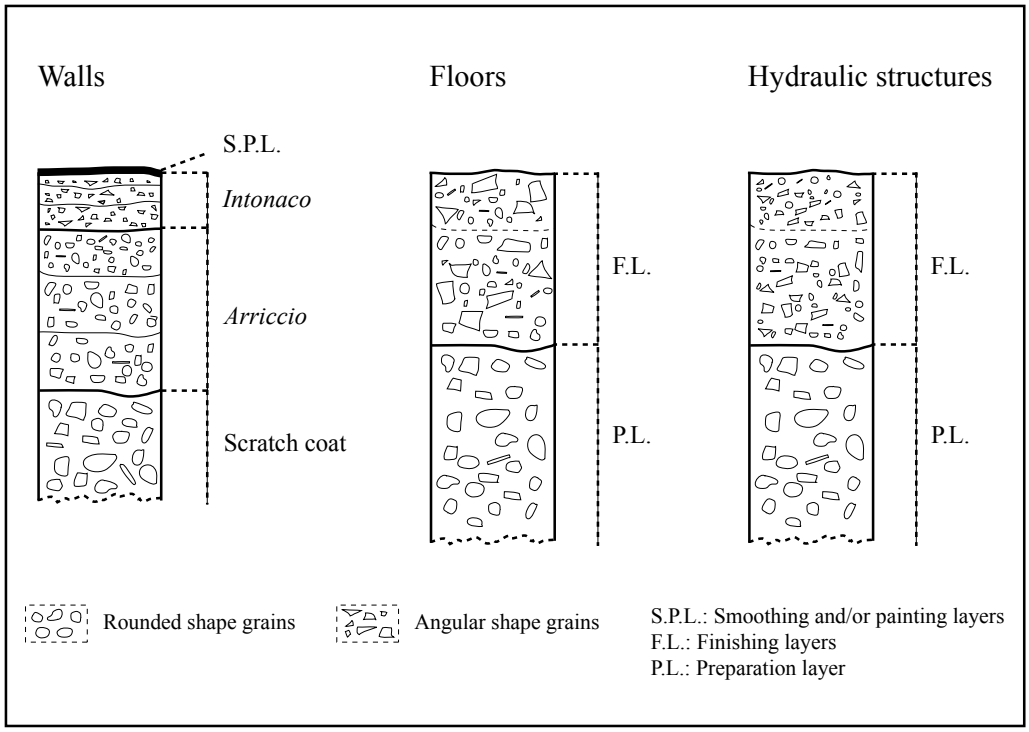

Figure 4. Microstratigraphy of walls, floors and hydraulic structures. Thicknesses of layers are not to scale.

in composition, associated with abundant crystals of green and colourless clinopyroxene, black and yellow fragments of altered volcanic glass, rare crystals of feldspar and flakes of mica, and very rare crystals of garnet. In situ EDS analyses were performed on several crystals of these mineral phases – i.e. clinopyroxene, feldspar, mica and garnet – and chemical data were compared with unpublished data (Grifa, pers. comm.) in order to better defined the provenance of the raw materials. Results of chemical analysis are discussed bellow and all the data are reported in Table 2.

Clinopyroxene: Chemical analysis on this crystals indicated that they are mainly composed by diopside and salite, as shown in Figure 5. Clinopyroxenes are often zoned (Figure 6a) and core to rim compositional profile showed enrichment in Fe and decrease in Mg (Table 2).

Feldspar: A minor amount of plagioclase feldspar is also present, which are characterized by high An content. Euhedral crystals occur either in the groundmass of the volcanic rock fragments and as large crystals or phenocrysts (Figure 6b), and usually display a bytownitic-labradoritic zoned composition (Figure 7). K-feldspar is also present as sanidine (Figure 7) both in the groundmass of volcanic rock fragments and separated crystals.

Mica: Rare brown crystals of Mg-rich biotite are also present (Table 2, Figure 6c) with MgO up to 17%.

Garnet: Very rare crystals of orange garnet have been identified in the aggregate. They are constituted by a Ti-rich andradite (melanite) (Table 2, Figure 6d).

The layers have different textural characteristics, aggregate compositions and matrix properties. The three classes of mortar-based building materials analysed here were found to have differing petrographic and microstructural features, and are described below.

Table 2
EDS analyses of clinopyroxene, biotite, garnet and feldspar crystals (wt.%).

Sample	SiO_2	TiO_2	Al_2O_3	FeO	MnO	MgO	CaO	Na_2O	K_2O	Cr_2O_3	Sum
Clinopyroxene											
Px1	47.30	1.08	8.30	9.95		11.10	22.28				100.01
Px2	38.37	3.64	18.21	12.57		17.53			9.68		100.00
Px3	50.15	0.76	6.53	7.91		13.98	20.67				100.00
Px4	48.52	1.00	7.12	6.48		12.78	24.09				99.99
Px5	48.44	0.82	7.60	7.59		12.38	23.17				100.00
Px6	51.45	0.93	5.51	8.37		13.00	20.75				100.01
Px7	50.97	0.87	5.47	7.50		13.98	21.21				100.00
Px8	48.3	0.92	7.65	9.84		11.37	21.92				100.00
Px9	49.95	0.62	6.49	5.11		14.45	23.38				100.00
Px10-a ring	46.95	1.03	8.48	11.01		10.45	22.09				100.01
Px10-b ring	46.51	1.23	8.60	11.68		9.72	22.27				100.01
Px10-c ring	46.96	1.11	8.31	11.08		9.74	22.79				99.99
Px10-d core	52.50	0.54	4.17	4.46		15.87	22.47				100.01
Px10-e core	52.35	0.45	4.56	4.68		15.46	22.49				99.99
Px10-f core	52.18	0.54	4.65	4.62		15.60	22.4				99.99
Px10-g core	52.16	0.48	4.66	4.59		15.53	22.58				100.00
Px10-h ring	46.54	1.27	8.59	10.67		10.07	22.87				100.01
Px11	43.90	0.80	6.14	19.64	1.99	5.04	20.96	1.54			100.01
Px12	52.80	0.47	5.75	6.03		16.48	17.2	1.27			100.00
Px13	51.88	0.39	3.48	3.86		15.01	23.66	1.08		0.65	100.01
Px14	49.65	0.87	7.02	5.91		13.82	21.35	1.39			100.01
Px15	45.15	1.17	9.02	13.94		7.95	22.78				100.01
Px16	44.8	1.64	9.83	12.45		9.23	22.06				100.01
Px17-a ring	45.52	1.23	10.05	10.79	0.40	9.79	22.23				100.01
Px17-b ring	47.71	0.93	8.45	10.38	0.59	10.69	21.25				100.00
Px17-c ring	44.57	1.21	8.15	12.73	0.56	8.91	23.86				99.99
Px17-d core	53.49	0.12	3.36	3.04		16.79	22.75			0.44	99.99
Px18	49.1	1.16	6.57	8.30		13.31	21.34			0.22	100.00
Px19	48.51	1.31	7.11	8.92		12.83	21.32				100.00
Px20	51.55		2.48	4.18		16.26	25.53				100.00
Px21	42.67	1.71	4.76	12.85		9.05	28.97				100.01
Px22	43.61	1.11	7.50	15.18		7.73	24.87				100.00
Px23	50.07	0.86	6.50	5.88		13.58	23.12				100.01
Px24	53.89		3.06	3.25		16.44	22.82			0.53	99.99
Px25	47.72	1.26	9.36	8.28		12.65	20.73				100.00
Px26	51.67	0.54	5.67	4.27		15.27	22.58				100.00
Px27	48.99	1.14	7.65	7.26		13.67	21.29				100.00
Px28	44.53	1.67	10.8	10.82		9.62	22.57				100.01
Px29	51.18	0.68	5.74	5.19		14.41	22.81				100.01
Px30	49.26	1.43	6.78	8.16		13.10	21.27				100.00
Px31	48.45	1.12	8.27	7.24		12.76	22.16				100.00
Px32	52.94		4.11	3.45		15.93	22.77			0.81	100.01
Px33	49.45	0.62	7.04	8.55		11.95	22.40				100.01
Px34	52.55	0.63	4.73	4.21		16.27	21.61				100.00
Px35	52.86	0.77	3.97	4.01		16.54	21.85				100.00
Px36	49.4	1.07	8.20	6.28		13.50	21.55				100.00
Px37	44.69	1.76	11.46	7.57		11.65	22.87				100.00
Biotite											
Bt1	36.57	5.50	18.36	15.12		14.74			9.71		100.00
Bt2	37.50	4.40	17.97	14.43		15.03		1.08	9.59		100.00
Bt3	38.23	4.57	18.00	11.94		17.09			10.17		100.00

(continued on next page)

Table 1 *(continued)*

Sample	SiO_2	TiO_2	Al_2O_3	FeO	MnO	MgO	CaO	Na_2O	K_2O	Cr_2O_3	Sum
Feldspars											
Plg1	49.45		32.73	0.59			12.88	3.21	1.14		100.00
Plg2	46.70		34.42	0.75			14.74	2.64	0.75		100.00
Plg3	42.79		35.19	0.67			19.12	1.59	0.64		100.00
Plg4	47.26		32.98	0.77			15.68	2.41	0.89		99.99
Plg5	45.25		33.68	1.10			17.22	2.11	0.63		99.99
Plg6	47.63		33.44	0.68			14.9	2.42	0.93		100.00
Plg7	48.53		33.50				14.59	2.59	0.78		99.99
Plg8	46.87		34.32	0.66			15.17	2.39	0.60		100.01
Plg9	49.82		31.70	0.85			13.53	3.13	0.97		100.00
Plg10	46.00		35.35	0.65			16.00	2.00			100.00
Sd1	64.81		20.22					1.54	13.44		100.00
Sd2	55.83	0.16	23.94	0.50					19.57		100.00
Garnet											
Gt1	24.28	2.27	9.62	45.19	2.85		15.78				99.99
Gt2	36.94	2.31	9.89	17.87	1.84	0.82	30.33				100.00
Gt3	37.54	2.37	9.50	18.00	1.77		30.81				99.99
Gt4	35.25	2.77	8.47	20.12	1.74		31.65				100.00

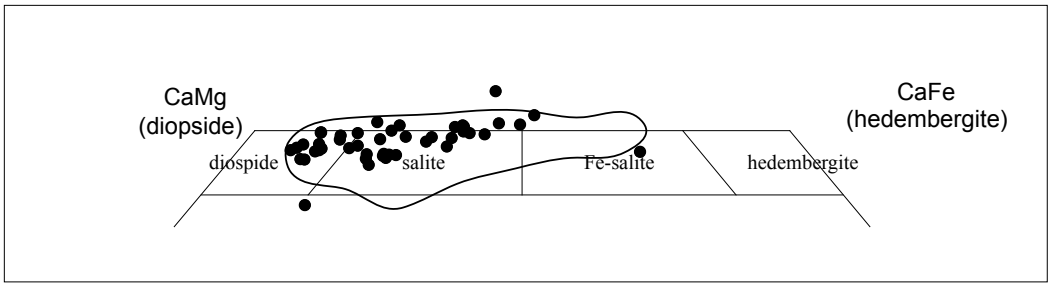

Figure 5. Clinopyroxene classification of the analysed crystals (solid circles), continue line delimits composition of clinopyroxene from Somma-Vesuvius volcanic deposits (unpublished data, Grifa, pers. comm.).

4.1. Walls

Most of the wall samples are composed of several layers of preparatory plaster *(arriccio)* covered by one or more poorly adherent *intonaco* layers. In some cases, smoothed and/or painted layers were also found, strongly adhering to the *intonaco* (A in Figure 4). The *arriccio* consists of strongly adherent grey plaster layers characterised by medium to fine sand-sized aggregate, high to medium porosity and low cohesion. The *intonaco* layers are composed of fine sand and limewash, and have low porosity and high cohesion. In some cases reed bundles imprints of yellowish hue have been recognised on the backside of the sample. These evidences, consistent with the description of Vitruvius, could be associated mostly with ceiling location although partition walls made of plastered wood should not be excludes (Maiuri, 1958). The same kind of imprints has been reported in findings at Zliten, Herculaneum (Maiuri, 1958), Bolsena, Strasbourg, and also Pompeii (Wallert and Elston, 1997 and references quoted therein).

On the basis of grain size, sphericity, roundness and composition of aggregate plus the aggregate:binder ratio, two types of *arriccio* and three types of *intonaco* were identified. Their petrographic and microstructural features are listed in Table 3.

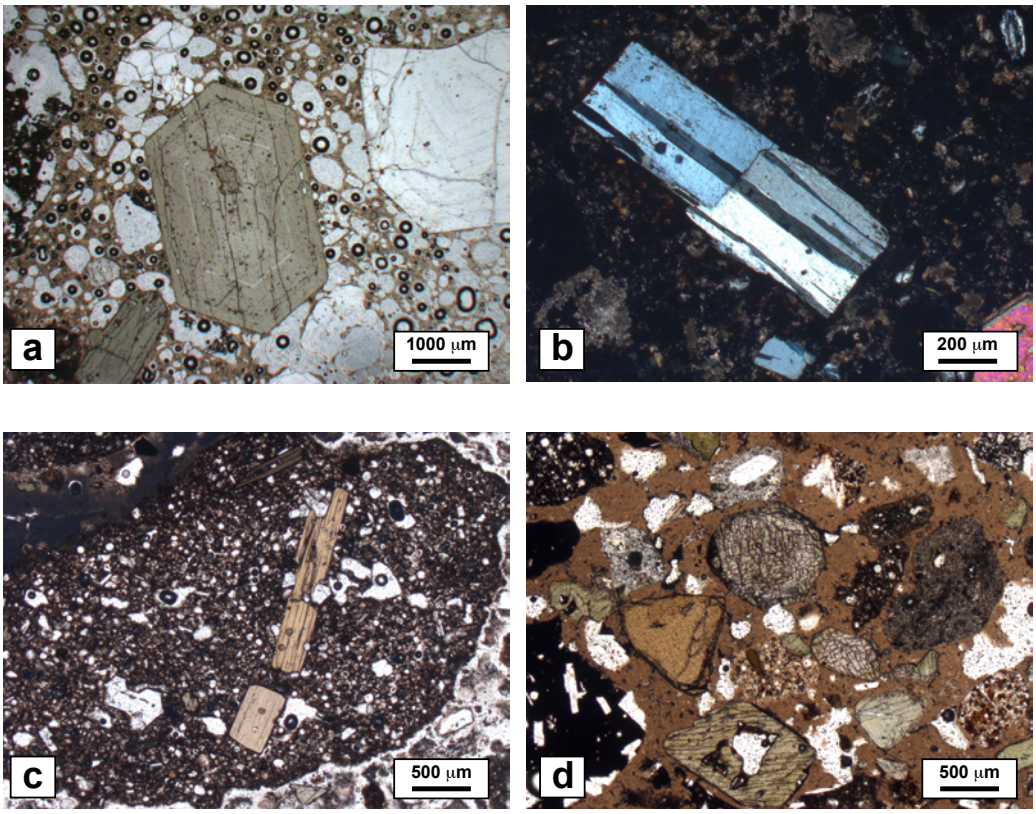

Figure 6. Polarising light micrographs of: a) clinopyroxene and leucite; b) plagioclase; c) biotite; d) garnet. Images a, c and d taken in PPL, image b taken in XPL.

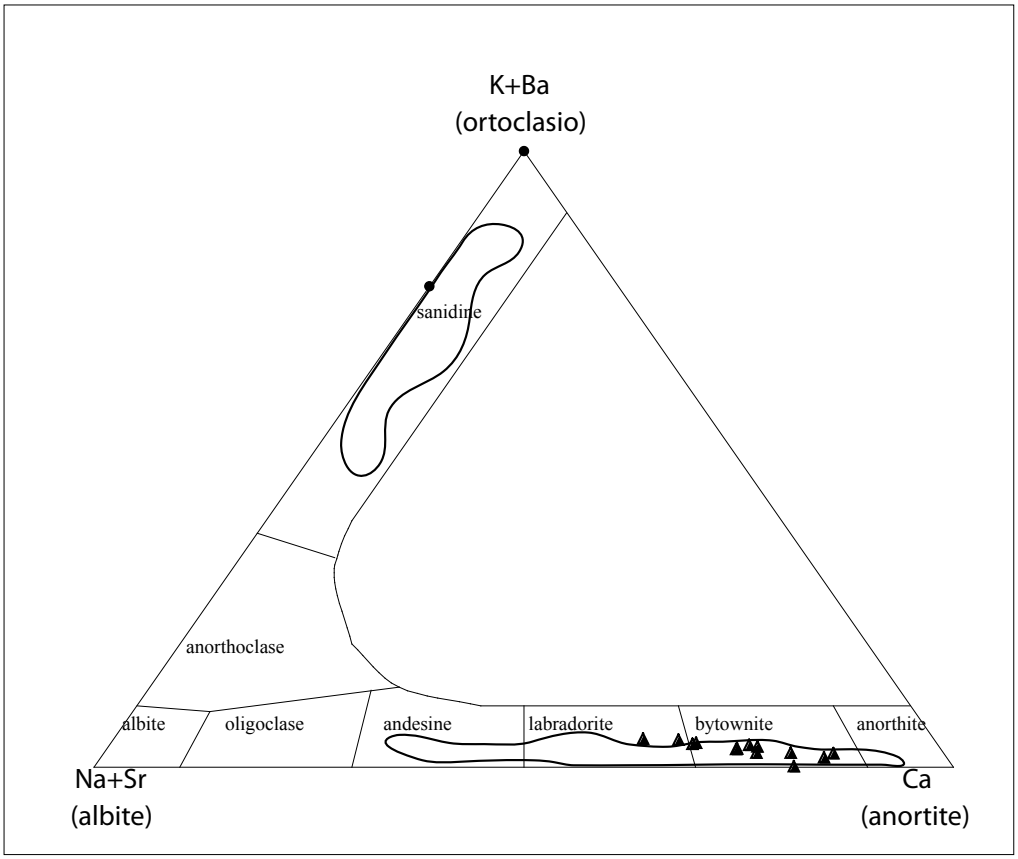

Figure 7. Feldspars classification of analysed crystals (solid circles: sanidine; solid triangles: plagioclase), continue line delimits composition of plagioclase and sanidine, respectively, from Somma-Vesuvius volcanic deposits (unpublished data, Grifa, pers. comm.).

Table 3
Classification of *arriccio* and *intonaco*. Grain size after Wentworth (1922).

		Arriccio	
		Volcanic scoriae-rich arriccio	**Clinopyroxene-rich arriccio**
	Aggregate to Binder	1:1	about 1:1
Aggregate	**Grain size**	Granules to very fine sand	Very coarse to very fine sand
	Main fractions	Coarse to medium sand	Coarse to medium sand
	Sphericity	High to medium	Medium
	Roundness	VS: well-rounded to rounded grains. Cpx and Bt: sub-angular to angular	Mainly sub-angular to sub-rounded
	Distribution	Homogeneous	Homogeneous
Matrix	**Matrix**	Micrite-like to spotted	Micrite-like to spotted
	Hydraulicity Index (HI)	From 0.08 to 3.36	From 0.14 to 4.10

		Intonaco		
		Intonachino	***Cocciopesto***	***Marmorino***
	Aggregate to Binder	about 1:1	1:1	about 1:1
Aggregate	**Grain size**	From granules to very fine sand	From granules to coarse silt	From granules to coarse silt
	Main fractions	Coarse to medium sand	Coarse to fine sand	Medium to very fine sand
	Sphericity	High to medium	High to low	From high (L) to very low (SC)
	Roundness	VS: well-rounded to rounded grains. Cpx and Bt: sub-angular to angular	Very angular to rounded	From strongly angular (SC) to sub-rounded (L)
	Distribution	Homogeneous	Homogeneous	Homogeneous
Matrix	**Matrix**	Micrite-like	Spotted	Micrite-like
	Hydraulicity Index (HI)	From 0.14 to 0.19	From 0.19 to 0.38	From 0.04 to 0.06

Cpx: Clinopyroxene; Bt: Biotite; VS: Volcanic Scoriae; L: Limestone; SC: Sparry calcite.

4.1.1. Arriccio

The two types of *arriccio* were distinguished, according to the composition and relative abundance of the various types of aggregate particles.

- Volcanic scoria-rich *arriccio*

Most *arriccio* layers in wall samples belong to this type. It has a homogeneous matrix,

consisting mostly of crypto- to microcrystalline calcite, with a high HI of 0.08 to 3.36, especially when the aggregate is medium silt-sized. In some cases, sub-millimetric lumps of lime, probably due to incomplete carbonation, were also identified. The aggregate:binder ratio is always about 1:1. The filler shows a wide grain-size distribution, ranging from granules to very fine sand, the coarse to medium sand fraction being most abundant. This fraction is mainly composed of rounded to well-rounded fragments of leucite-bearing volcanic rock, of leucititic or trachytic composition, and spherical scoria particles associated with abundant angular and sub-angular crystals of green and colourless diopside (Figure 8a), of medium sphericity. A few crystals of sanidine and plagioclase feldspar, black and yellow fragments of altered volcanic glass, rare flakes of biotite, and very rare crystals of garnet also occur.

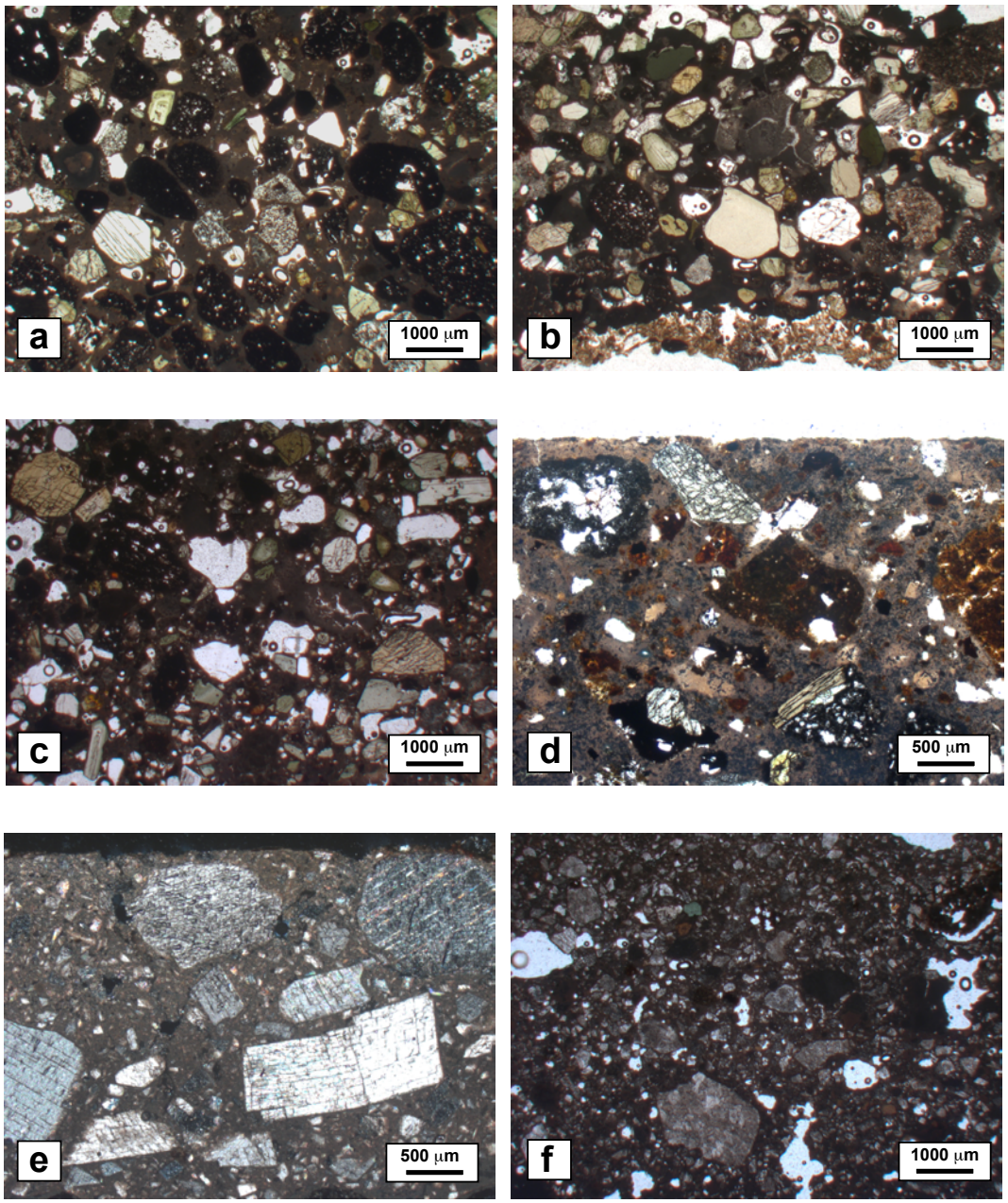

Figure 8. Polarising light micrographs of mortar samples. *Arriccio*: a) volcanic scoria-rich *arriccio* ; b) clinopyroxene-rich *arriccio*; *intonaco* c) *intonachino*; d) *cocciopesto*; e) *marmorino* with only sparry calcite; f) *marmorino* also with limestone. All images taken in PPL.

- Clinopyroxene-rich *arriccio*

This plaster is very similar to the former type as regards the composition and grain size of its aggregate. It differs in terms of its higher aggregate:binder ratio, which ranges from 1.5:1 to 1:1, as well as the higher relative abundance of clinopyroxene crystals compared with fragments of volcanic rock and scoriae (Figure 8b).

4.1.2. Intonaco

The three types of *intonaco* were detected in wall plaster samples, and were classified, according to the composition of their aggregate particles, as *intonachino* (siliceous minerals and rock), *cocciopesto* (crushed pottery or bricks) and *marmorino* (limestone and calcite).

- *Intonachino*

This type of *intonaco,* which is not common in wall samples, is characterised by an almost pure crypto- to microcrystalline calcite matrix, with sporadic lumps of lime, a low HI (0.14-0.19) and an aggregate:binder ratio of about 1:1. The filler shows homogeneous distribution, and grain size ranges from granules to very fine sand, coarse and medium sand granulometric classes being the most frequent. The filler is composed of fragments of volcanic scoriae and volcanic rock, frequently associated with sub-angular to angular crystals of diopside and, less often, sanidine, plagioclase, biotite and melanite (Figure 8c).

- *Cocciopesto*

Intonaco layers of *cocciopesto* are quite common in the wall samples analysed. They have a spotted matrix (Figure 8d), composed of cryptocrystalline calcite and hydrated calcium silico-aluminates, with a relatively high HI (0.19-0.38; Table 3) and an aggregate: binder ratio of about 1:1. The aggregate grain size ranges from granules to coarse silt, with modal values of coarse to fine sand. Angular fragments of ground ceramic materials (grog) are most common, with a few well-rounded fragments of rock, scoriae, and altered glass, all of volcanic origin (Figure 8d). Rare crystals of diopside, sanidine, plagioclase and garnet and flakes of biotite also occur.

Two types of grog were distinguished within the aggregate of the *cocciopesto intonaco*. The first contains rounded sand-sized inclusions of volcanic rock, volcanic scoriae, and relatively few angular crystals of diopside, plagioclase and opaque minerals; the second contains quartz, feldspars and rare opaque minerals.

- *Marmorino*

The third type of *intonaco, marmorino,* has a micrite-like matrix (Figure 8e,f) composed of crypto- and microcrystalline calcite, with a very low HI (0.04-0.06). The filler shows homogenous distribution within samples, and wide grain-size distribution, from granules to coarse silt, with maximum frequency in the medium to very fine sand classes. The aggregate consists of euhedral crystals of calcite, associated with occasional fragments of volcanic scoriae and rare crystals of diopside and feldspar (Figure 8e). In some cases, the carbonate fraction of the aggregate is composed of well-rounded fragments of micritic limestone rather than crystals of spathic calcite (Figure 8f).

4.2. Floors

Petrographic and microstratigraphic analysis of floor samples revealed that they consisted of preparatory and finishing layers with similar compositional and textural characteristics (B in Figure 4). According to the petrographic composition of the filler, two types of plasters were identified (Table 4).

Table 4
Classification of floor mortar. Abbreviations as in Table 3.

		Floors		
		Volcanic scoria-rich f.	**Ceramic-rich floors**	**Carbonatic layers**
	Aggregate to Binder	About 1:1	1:1	About 1:1
Aggregate	**Grain size**	From granules to coarse silt	Pebbles to very fine sand	From granules to coarse silt
	Main fractions	Coarse to fine sand	Medium to fine sand	Medium to very fine sand
	Sphericity	High to medium	Medium to low	High to medium
	Roundness	VS: well rounded to sub-angular grains Cpx and Bt: sub-angular to angular	Angular to sub-angular	Various
	Distribution	Homogeneous	Homogeneous	Homogeneous
Matrix	**Matrix**	Micrite-like to spotted	Micrite-like	Micrite-like
	Hydraulicity Index (HI)	From 0.16 to 1.60	From 0.10 to 0.17	From 0.01 to 0.07

- Volcanic scoria-rich floors

This type has a crypto- to microcrystalline calcite matrix, with an average HI lower than that of the preparatory layers of the walls, and an aggregate:binder ratio of 1.5:1 to 1:1. The aggregate grain size ranges from granules to coarse silt, with a maximum frequency in the fine sand class. It is predominantly composed of well-rounded, highly spherical, sand-sized grains of volcanic rock, scoriae and glass (Figure 9a); angular crystals of diopside are also common, and are associated with rare crystals of plagioclase, sanidine, biotite and garnet.

- Ceramic-rich floors

This type of plaster is characterised by an aggregate composed of angular, medium to fine sand-sized fragments of grog (Figure 9b). Two types of grog were identified, closely matching those observed in the *cocciopesto*. The fragments are embedded in a spotted matrix composed of cryptocrystalline calcite and hydrated calcium silico-aluminates, with HI between 0.10 and 0.17.

A finishing layer was also observed in two of the floor samples. It was characterised by a micrite-like calcite matrix with a low HI (0.01-0.07), an aggregate:binder ratio of 1.5:1-1:1,

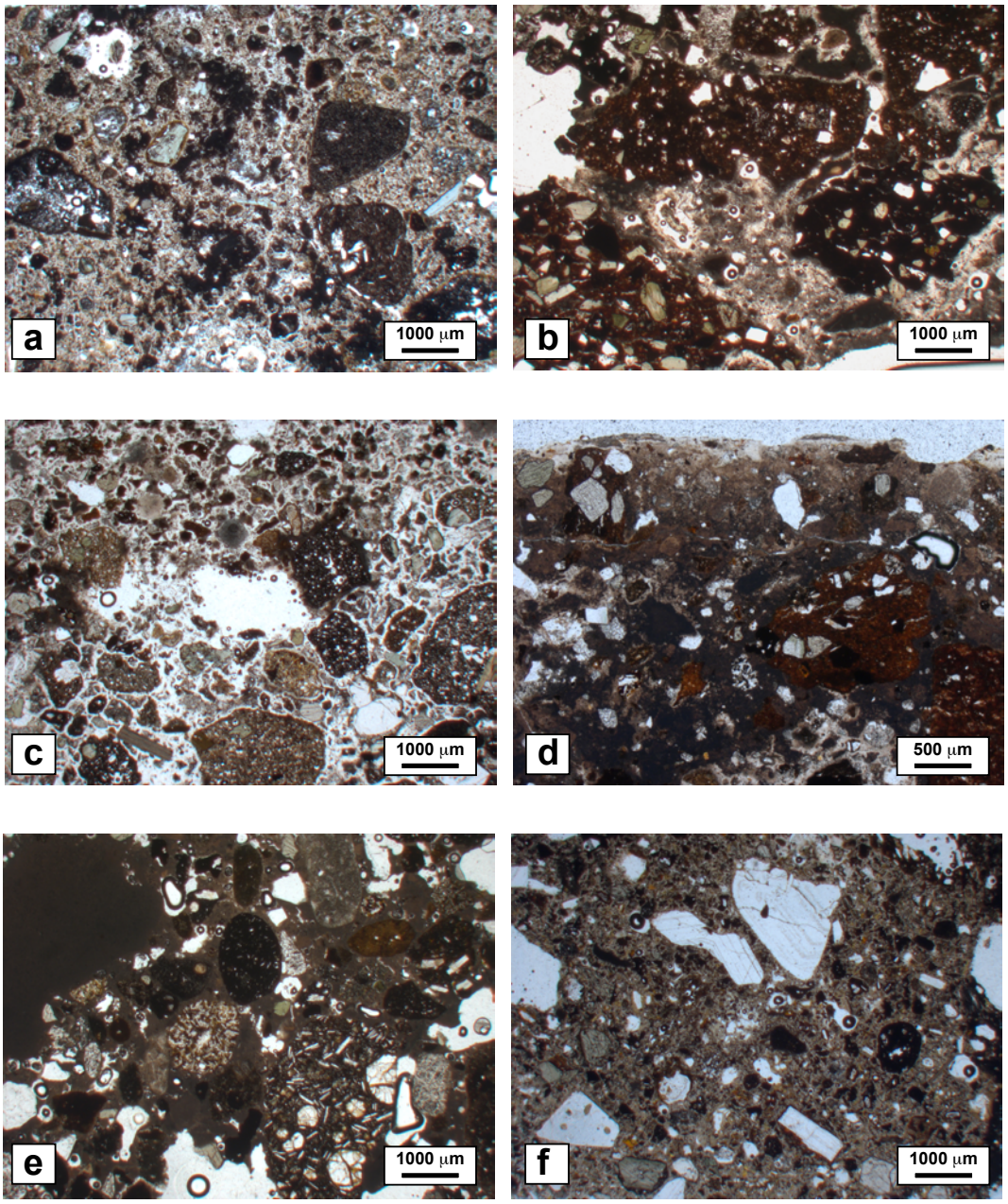

Figure 9. Polarising light micrographs of mortar samples. Floors: a) volcanic scoria-rich floors; b) ceramic-rich floors; hydraulic structures: c) volcanic scoria-rich hydraulic structures; d) ceramic-rich hydraulic structures; e) micrite-like matrix with lime lumps; f) spotted matrix. All images taken in PPL.

and aggregate composed of predominant spathic crystals of calcite and subordinate rounded fragments of micritic limestone.

Mostly the ceramic-rich floors type of mortar was also used as support for floor decorations in which a variety of materials, such as gravel, stone and very coarse ceramic fragments were arranged (*opus signinum*) (Figure 10a,b,c,d). The pattern would be extremely rough, or no pattern would exist at all. Specifically in our samples squared stone fragments constituted by dolomitic limestone (Figure 10e,f) and pebbles of various carbonate rocks have been recognised.

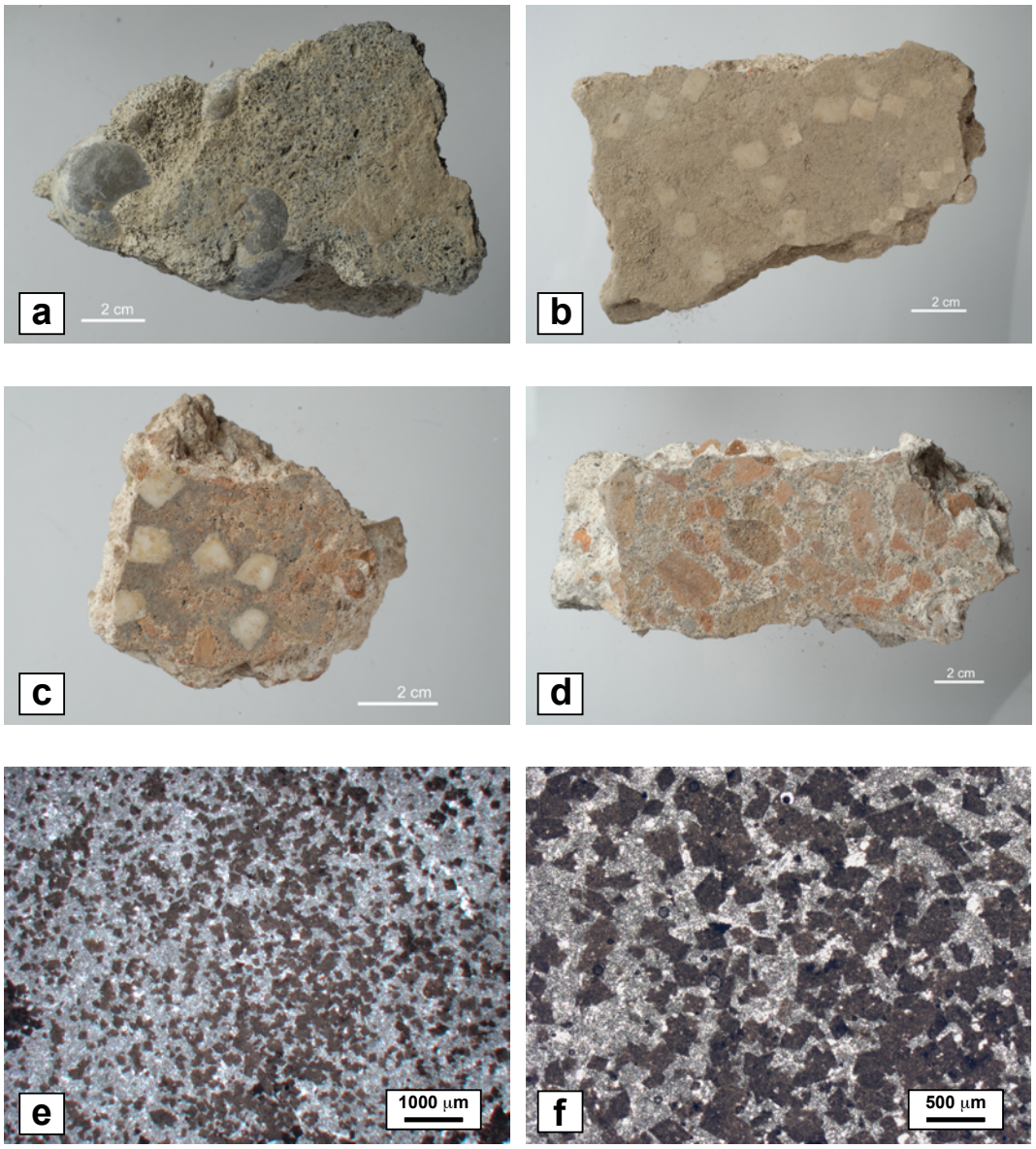

Figure 10. Types of Opus signinum from the Temple of Venus in Pompeii characterised by: a) carbonate pebbles embedded into a volcanic scoria-rich mortar; b) squared fragments of carbonate rocks embedded into a volcanic scoria-rich mortar; c) squared fragments of carbonate rocks and very coarse ceramic fragments embedded into a ceramic-rich mortar; d) very coarse ceramic fragments embedded into a ceramic-rich mortar. e,f) Thin section polarising light micrographs of squared fragments of dolomitic limestone, both images taken in PPL under different magnifications.

4.3. Hydraulic structure

Within the conduit, well and cistern samples, two types of plaster were identified: one rich in volcanic scoriae and a second characterised by grog (Table 5; Figure 9c,d). These mortars show strong textural and compositional similarities to those used in the construction of the floors, but with a higher HI. These two types of plaster were used for both preparatory and finishing layers in the hydraulic structures. However, volcanic scoria-rich plaster was used more frequently for preparatory layers, and ceramic-rich plaster mostly but not exclusively for the finishing layers.

Table 5
Classification of mortar in hydraulic structures. Abbreviations as in Table 3.

		Hydraulic structure	
		Volcanic scoria-rich hydraulic structure	**Ceramic-rich hydraulic structure**
	Aggregate to Binder	About 1.5:1	About 1:1
Aggregate	**Grain size**	From pebbles to coarse silt	From pebbles to coarse silt
	Main fractions	Coarse to medium sand	Medium to fine sand
	Sphericity	High to medium	Medium to low
	Roundness	VS: well rounded to rounded grains. Cpx and Bt: sub-angular to angular	Angular to sub-angular
	Distribution	Homogeneous	Homogeneous
Matrix	**Matrix**	Spotted	Spotted
	Hydraulicity Index (HI)	From 0.59 to 2.68	From 0.22 to 2.31

4.4. Sands

Petrographic analysis of the recent beach sands from the Neapolitan coastline and of the drilled ancient sands showed moderate variability both in composition and in grain-size distribution. Petrographic composition and textural features of the analysed sands are list in Table 6.

As regards textural features, although the sands show a wide grain-size distribution ranging from granules to medium silt, the coarse to medium fraction are surely the most abundant. This fraction is mainly composed of rounded to well-rounded fragments of leucite-bearing volcanic rock leucititic or trachytic in composition, and spherical scoria particles associated with angular and sub-angular crystals of green and colourless diopside, of medium sphericity. A few crystals of sanidine and plagioclase feldspar, black and yellow fragments of altered volcanic glass, rare crystals of leucite and flakes of biotite, and very rare crystals of Ti-rich andradite (melanite) also occur. In sample CM1, FS1 and FS2 carbonate fragments, constituted by spathic and micritic limestone, are also present. Two main petrographic compositions have been identified in both samples from beaches and from drillings; samples TA3, S1 and S2, indeed, displayed a clinopyroxene-rich composition (Figure 11a, c), while the other showed less clinopyroxene and abundant volcanic scoriae (Figure 11b, d).

5. IMAGE ANALYSIS

Image-analysis software (Image SXM) was used to treat the BSE images captured by SEM. The aim of image processing is to obtain evidence of specific characteristics of the

Table 6
Schematic description of sands studied microscopically.

Sample	Provenance	Grain Size	Main fractions	Sphericity	Roundness	Components													
						Cpx	Sd	Pl	Lc	Ol	Bt	Grt	Qt	Op	VS	VG	SLim	MLim	Sh
CM1	Castellammare di Stabbia	CSl-VCS	FS	M	A	x	x	x	+		x	+		+	xxx	x	x	x	x
TA1	Torre Annunziata	CS-G	VCS	HM	SR-R	x	+	x	x	x	+				xxx	x			x
TA2	Torre Annunziata	FS-VCS	MS-CS	HM	SR-R	x		+	x				+		xx	+			
TA3	Torre Annunziata	CSl-CS	FS	LM	A	xxx	x	x	x		+	+		+	xx	+			
TA4	Torre Annunziata	VFS-CS	MS	HM	SA	xx	x	x	x		+	+			xxx	+			
FS1	Foce Sarno	FS-VCS	MS	HM	SR	x	x	x	x			+			xxx	+	x	x	
FS2	Foce Sarno	FS-VCS	CS	H	SR-R	xx	x		x						xx	x	x		
S1	Drilling 1 (11,00-11,80 m deep)	FS-G	MS	HM	SA	xxx	x	x				+	+		x	x			
S2	Drilling 2 (13,80-14,50 m deep)	FS-VCS	CS	HM	SA-SR	xx	x	x	x						xxx	x			
S3	Drilling 3 (10,70-11,80 m deep)	MSl-VCS	CS	M	SA-SR	x	x	x					x	x	xxx				
S4	Drilling 4 (12,00-13,00 m deep)	MSl-VCS	MS	M	SA	xxx	+	x	+			x	x	x	x	x			

Grain size and main fractions: MSl: medium silt; CSl: coarse silt; VFS: very fine sand; FS: fine sand; MS: medium sand; CS: coarse sand; VCS: very coarse sand; G: granules. Sphericity: H: high; MH: from medium to high; M: medium; LM: from medium to low. Roundness: A: angular; SA: sub-angular; SR: sub-rounded. Composition of sands (components): Cpx: clinopyroxene; Sd: sanidine; Pl: plagioclase; Lc: leucite; Ol: olivine; Bt: biotite; Grt: garnet; Qt: quartz; Op: opaque minerals; VS: volcanic scoria; VG: volcanic glass; SLim: spathic limestone; MLim: micritic limestone; Sh: fragments of shell. Relative quantity: xxx: very abundant, xx: abundant, x: scarce, +: rare.

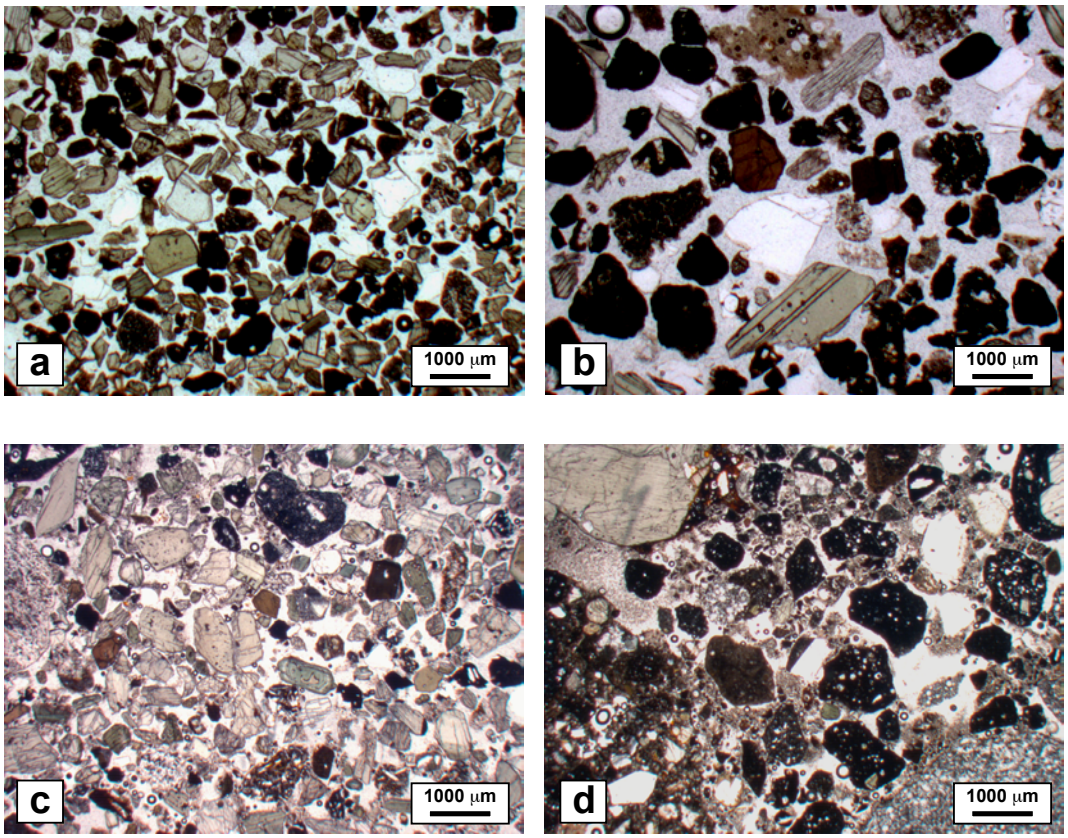

Figure 11. Polarising light micrographs of sands samples. Recent beach sands from the Neapolitan coastline: a) TA3 (clinopyroxene-rich); b) FS1 (volcanic scoria-rich). Drilled ancient sands: c) S1 (clinopyroxene-rich); d) S3 (volcanic scoria-rich). All images taken in PPL.

mortar such as binder:aggregate ratio and percentage of the porosity. During the elaboration of the images became evident that the discrimination of silicate aggregates was simpler that the carbonate ones (Figure 12). The inaccuracy of the discrimination of carbonate aggregate from the binder, which displays the same mineralogical composition, invalidated every further measurement on mortar with this type of aggregate. On the contrary, silicate aggregates were well discriminated and their textural features parameters easily obtained – i.e. perimeter length, major and minor axis and area. A quantification of the total area of the aggregate was then possible. To measure the porosity the total amount of black pixels (grey level 255) was considered. Finally, the area of the binder was obtained subtracting at the total pixels of the image those of aggregate and porosity. Consequently these data allowed calculating the binder:aggregate ratio. As we can see in Table 7 the aggregate:binder ratios vary from 0.30 to 1.70 while the porosity percentages go from 0% up to 15%. The comparison with literature data show that normally in mortars the aggregate:binder ratio is never below 1 (1:1) and that the porosity, particularly in an ancient mortars, ranges from 20% to 40% (Moropoulou et al., 2003; Moropoulou et al, 2005). Probably, while macro-porosity is very well discriminated, this approach fails in detecting part of the micro-porosity, causing underestimation of the total porosity. Consequently, also the aggregate:binder ratios result to be underestimated. Nevertheless, this approach gives a useful preliminary indication of the relation among the different elements of a mortar. Other methodology, such as mercury intrusion porosimetry,

will be more accurate for the measurement of micro-porosity (Moropoulou et al., 2003), but happens to be destructive.

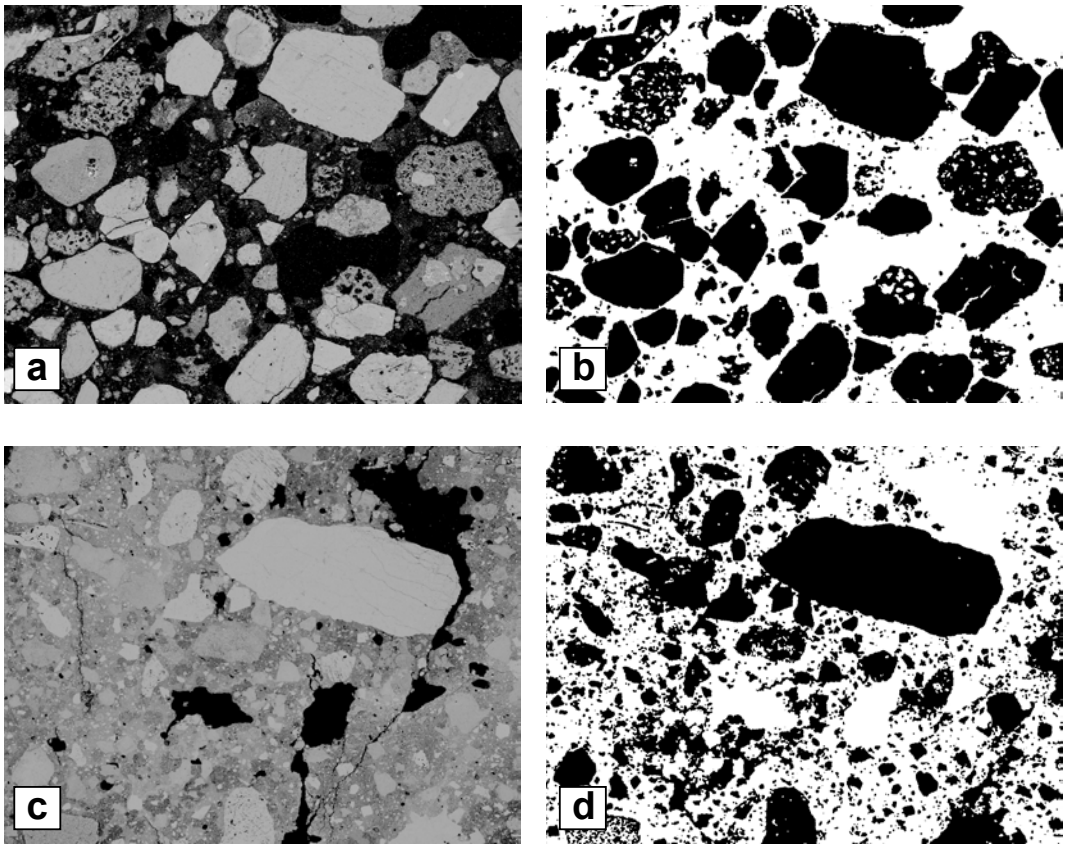

Figure 12. Image analysis: a) SEM-BSE images of a silicate aggregate-bearing mortar and b) relative elaborated image; c) SEM-BSE images of a carbonate aggregate-bearing mortar and d) relative elaborated image.

6. Discussion

In this section considerations will be exposed concerning raw materials and production techniques, derived from the data described above.

6.1. Binders

Petrographic analysis of the various mortar-based building materials from the Temple of Venus revealed that they have a lime-based matrix. HI values and the micrite-like (Figure 9e) vs. spotted (Figure 9f) microscopic aspect of the matrix suggest differing contents of hydrated calcium silico-aluminates, implying either the use of a lime prepared from impure limestone, or pure lime which underwent hydraulic reactions with a pozzolanic aggregate. The use of impure limestone in the preparation of the mortars is not supported by the chemical analysis of the lime lumps, which generally have a high degree of purity and low chemical variability, with very low HI values (mostly about 0.02), even when they are found in mortars with a spotted matrix and high HI, suggesting that pure limestone was selected and ignited

Table 7
Percentage of pores, aggregate and binder, and aggregate:binder ratio obtained by image analysis on selected samples of mortars representing the main studied petrographic type. Abbreviations as in Table 1.

Sample	Group	% Porosity	% Aggregate	% Binder	Aggregate/Binder ratio
LF006-a	VSRA	15	49	36	1.36
LF006-b	VSRA	8	28	64	0.44
LF017-a	VSRA	2	57	41	1.39
LF020-a	VSRA	5	56	39	1.44
LF038-a	VSRA	8	50	42	1.19
LF041-b	VSRF	8	45	47	0.96
LF042-a	VSRF	0	61	39	1.56
LF042-b	VSRF	5	57	38	1.50
LF043-b	VSRF	11	55	34	1.62
LF046-a	CRH	0	59	41	1.44
LF046-b	CRH	7	38	55	0.69
LF046-c	CRH	6	27	67	0.40
LF047-a	VSRH	11	51	38	1.34
LF047-b	CRH	5	23	72	0.32
LF053-a	VSRF	10	44	46	0.96
LF053-b	CRF	5	27	68	0.40
LF057-a	CRA	0	53	47	1.13
LF057-b	I	3	33	64	0.52
LF060-a	VSRH	4	49	47	1.04
LF060-b	CRH	3	31	66	0.47
LF090-a	VSRF	0	23	77	0.30
LF090-b	VSRF	14	52	34	1.53
LF090-c	CRF	0	22	78	0.28
LF091-a	VSRF	0	42	58	0.72
LF091-b	VSRF	0	58	42	1.38
LF099-a	VSRA	1	57	42	1.36
LF099-b	VSRA	1	54	45	1.20
LF099-c	C	0	32	68	0.47
LF103-b	CRA	0	44	56	0.79
LF118-b	VSRH	2	32	66	0.48
LF120-a	VSRA	0	63	37	1.70
LF120-b	I	0	40	60	0.67

to produce lime. Pozzolanic aggregates such as those containing volcanic scoriae, volcanic glass and ground fragments of ceramic materials (Elsen, 2006), must therefore have been involved in hydraulic reactions. Lime lumps in hydraulic structures have higher HI, with values between 0.08 and 0.27, indicating that true hydraulic lime was probably used only to construct these architectural features. The use of pure lime in most of the applications is also confirmed by the observation that mortars with a carbonate aggregate such as *marmorino* and the carbonate layers of floors always have a micrite-like matrix with low HI (< 0.07), whereas samples from hydraulic structures are always characterised by a spotted matrix and high HI values (> 0.22).

The systematic differences observed in the matrix of *cocciopesto intonaco* and ceramic-

rich floors – i.e., spotted matrix and high HI vs. micrite-like matrix and relatively low HI, respectively – may be related to the grain size of the aggregate, the former including the fine-grained fraction which was hydraulically reacted with lime, and the latter the sifted coarse-grained fraction, thus causing the different chromatic effects.

All the other types of mortars show very variable HI, suggesting that varying amounts of the fine-grained pozzolanic fraction were originally present in the raw material used as aggregate, rather than added intentionally to modulate hydraulicity.

The occurrence of lime lumps in a large number of samples indicates that some of the lime often did not react completely with water during slaking or with atmospheric CO_2 (Hughes et al., 2001) after application. This provides strong evidence that lime, water and aggregate were mixed without due attention, perhaps because of workers' lack of technological skills or acceptance by buyers of such wares.

6.2. Aggregates

The composition of the aggregates in the mortars analysed shows that three types of filler were commonly used: volcanic rock, crushed ceramic material (grog), and carbonate rock.

The mineralogy and petrography of the volcanic aggregate is compatible with the products of the Somma-Vesuvius volcano (Santacroce, 1987), and matches the composition of the sand collected from beach deposits relatively close to Pompeii (samples TA1, TA2, TA3, TA4, FS1, FS2) (Figure 3), as well as that of the sand samples derived from borehole cores (S1, S2, S3, S4) (Figure 1a), suggesting that local materials was used for the aggregate. Differences in the composition of the volcanic aggregate in volcanic scoria-rich *arriccio* and clinopyroxene-rich *arriccio* may be due to differing sources of local sand.

Petrographic analysis of the grog inclusions in the crushed ceramic plaster (*cocciopesto*) suggests that the two types of ceramic were used indiscriminately. The presence of volcanic inclusions compatible with the Somma-Vesuvius complex in one type of grog, and the quartz and feldspar inclusions in the other, suggests that both locally produced and imported ceramic were used as fillers.

The carbonate-bearing plasters contain filler composed of euhedral spathic crystals of calcite. This material may have been ground from crystalline calcite veins occurring in limestone. As such, its origin is not easy to determine.

7. Conclusions

Archaeometric study of mortar-based building materials from the Temple of Venus at Pompeii allowed several distinct mortar recipes to be identified, according to their microstratigraphy, the petrographic features of the aggregate, and their matrix. These various types were deliberately prepared for specific applications, due to their different hydraulicity

or for aesthetic purposes. *Cocciopesto* plaster containing crushed ceramic was used in hydraulic structures, perhaps because of its better hydraulic performance with respect to other types of plaster. It may have been used as *intonaco* on walls, due to its warm hues and resistance to damp.

The recipes used to construct the various mortar-based features at the Temple of Venus remained constant from the 4th century BC to the 1st century AD, suggesting the persistence of technological tradition (Table 1).

The ubiquitous presence of grains of volcanic origin, consistent with the volcaniclastic deposits of Somma-Vesuvius in many different types of plaster clearly indicates that the raw materials were local in origin. This is also confirmed by the comparison between chemical compositions of the mineral phases in the aggregate and unpublished data (Grifa, pers. comm.) on the same mineral phases from the Somma-Vesuvius deposits, that showed good agreement for clinopyroxene (Figure 5), feldspars (Figure 7), garnet and biotite. The source of the raw materials may have been alluvial or beach deposits in the Vesuvian area and particularly in the area of Pompeii. The small grain size, high sphericity and roundness of the volcanic aggregate in many samples indicate great standardisation in the selection of the raw materials, which were probably quarried from identified sources as early as the 4th century BC.

Mortars used in hydraulic structures, where specific performance was required, or in surfaces with specific aesthetic features such as *intonachino*, *cocciopesto*, *marmorino* and ceramic-rich floors, were produced by careful mixing of good-quality raw materials, and generally display relatively homogeneous textural features and hydraulicity. Other mortars, such as those used in *arriccio* and volcanic scoria-rich floors, generally covered by a finer finishing layer and a floor decoration (i.e., *opus signinum*), respectively, display a greater variability in aggregate grain-size distribution, microscopic aspect of the matrix (i.e., micrite-like vs. spotted) and HI, suggesting less attention paid to their preparation. The finding of lime lumps in all types of mortars suggests that production was not sufficiently checked or that skilled workers were not readily available.

As regards the *marmorino* filler and the stone fragment in *opus signinum*, the occurrence of carbonate sequences of pure limestone and dolostone outcropping near Pompeii (Figure 3) indicates that these raw materials were locally available, although specific provenance markers are missing.

As regards image analysis, the approach adopted in this study allowed the computation of silicate aggregate textural parameters. This approach resulted to be a powerful tool for the determination of the mortar specific characteristics – i.e. aggregate:binder ratio, porosity – although the total porosity resulted to be underestimated. Nevertheless, further investigation is required to improve and test this approach before making it a routine in the study of mortars.

REFERENCES

Arnò, V., Principe, C., Rosi, M., Santacroce, R., Sbrana, A. and Sheridan M.F., 1987. Eruptive history. In: Santacroce R. (Ed.), Somma Vesuvius - CNR, Quaderni de "La Ricerca Scientifica", Roma, vol. 8: 53 – 103.

Barrett, S. 2005. Image SXM 1.75, software. http://reg.ssci.liv.ac.uk/~sdb/ImageSXM.

Brocchini, D., Principe, C., Castradori, D., Laurenzi, M.A. and Gorla, L., 2001. Quaternary evolution of the southern sector of the Campanian Plain and early Somma-Vesuvius activity: insights from the Trecase 1 well. Mineralogy and Petrology, 73: 67–91.

Boynton, R.S., 1966. Chemistry and technology of lime and limestone. 2nd edition. John Wiley & Sons Inc., New York.

Carò, F. and Di Giulio, A., 2004. Reliability of textural analysis of ancient plasters and mortars through automated image analysis. Materials Characterization, 53: 243–57.

Carò, F., Di Giulio, A. and Marmo, R., 2006. Textural analysis of ancient plasters and mortars: reliability of image analysis approaches. In: (M. Maggetti and B. Messiga eds.) Geomaterials in cultural heritage, Special Publication, Geological Society, London, 257: 337–45.

Carò, F., Riccardi, M.P. and Mazzilli Savini, M.T., 2008. Characterization of plasters and mortars as tool in archaeological studies: the case of Lardirago castle in Pavia, northern Italy. Archaeometry, 50: 85-100.

Charola, A.E. and Henriques, F.M.A., 2000. Hydraulicity in lime mortars revisited. In: Bartos, P., Groot, C. and Hughes, J.J. (Eds.) Proceedings of the International RILEM-workshop "Historic Mortars: Characteristics and Tests", Paisley, 2000, RILEM Publications: 5-105.

Cioni, R., Santacroce, R. and Sbrana, A., 1999. Pyroclastic deposits as a guide for reconstructing the multi-stage evolution of the Somma-Vesuvius Caldera. Bullettin of Volcanology, 60:207-222.

Civetta L. and Santacroce R., 1992. Steady state magma supply in the last 3400 years of Vesuvius activity. Acta Volcanologica, Marinelli volume 2: 147-159.

Conticelli S., Melluso L., Perini G., Avanzinelli R. and Boari E., 2004. Petrologic, geochemical and isotopic characteristics of shoshonitic to potassic and ultrapotassic alkalic magmatism in Central-Southern Italy: inferences on its genesis and on the nature of its mantle source. Periodico di Mineralogia, 73: 135-164.

Curti, E., 2007. La Venere Fisica trionfante: un nuovo ciclo di iscrizioni dal santuario di Venere a Pompei. In: Il filo e le perle. Studi per i 70 anni di Mario Torelli, Venosa: 57-71.

Curti, E., 2008. Il tempio di Venere Fisica e il porto di Pompei? In: Guzzo, P.G. and Guidobaldi, M.P. (Eds.) Nuove ricerche archeologiche nell'area vesuviana (scavi 2003-2006)", Roma: 47-60.

De Vivo, B., Rolandi, G., Gans, P.B., Calvert, A., Bohrson,W.A., Spera, F.J. and Belkin, H.E., 2001. Newconstraints on the pyroclastic eruptive history of the Campanian volcanic plain (Italy). Mineralogy and Petrology. 73: 47–65.

Di Renzo, V., Di Vito, M.A., Arienzo, I., Carandente, A., Civetta, L., D'antonio, M., Giordano, F., Orsi, G. and Tonarini, S., 2007. Magmatic history of Somma-Vesuvius on the basis of new geochemical and isotopic data from a deep borehole (Camaldoli della Torre). Journal of Petrology. 48 (4): 753-84.

Elsen, J. 2006. Microscopy of historic mortars – a review. Cement and Concrete Research, 36:1416-1424.

Hughes, J.J., Leslie, A. and Callebaut, K., 2001. The petrography of lime inclusions in historic lime based mortars. In: Proceedings of the 8th Euroseminar on Microscopy Applied to Building Materials. Athens, Greece, September 2001: 359-364.

Ippolito, F., D'Argenio, B., Pescatore, T. and Scandone, P., 1975. Structural stratigraphic units and tectonic framework of south-ern Appenines. In: Squyres, C.H. Ed., Geology of Italy, 2: 317–328.

Joron J.L., Metrich N., Rosi M., Santacroce R. and Sbrana A., 1987. Chemistry and Petrography. In: Santacroce R. (Ed.), Somma Vesuvius - CNR, Quaderni de "La Ricerca Scientifica". Roma, volume 8: 105–174.

Maiuri, A., 1958. Ercolano: i nuovi scavi, 1927-1958, Roma.

Mora, P., Mora, L. and Philippot, P., 1984. Conservation of wall paintings, Butterworth & Co., London.

Mertens, G. and Elsen, J., 2006. Use of computer assisted image analysis for the determination of the grain-size distribution of sands used in mortars. Cement and concrete research, 36: 1453-1459.

Moropoulou, A., Bakolas, A. and Anagnostopoulou, S., 2005. Composite materials in ancient structures. Cement & concrete composites, 27: 295-300

Moropoulou, A., Polikreti, K., Bakolas, A. and Michailidis, P., 2003. Correlation of physicochemical and mechanical properties of historical mortars and classification by multivariate statistics. Cement and concrete research, 33: 891-898.

Prentice, J. E., 1990. Geology of construction materials, Chapman and Hall, London.

Principe C., Rosi M., Santacroce R. and Sbrana A., 1987. Explanatory Notes to the Geological Map. In: Santacroce R. (Ed.), Somma Vesuvius - CNR, Quaderni de "La Ricerca Scientifica", Roma, vol. 8: 11 – 51.

Santacroce, R. (Ed.).1987. Somma-Vesuvius, Quaderni de "La Ricerca Scientifica". Progetto finanziato "Geodinamica". Monografie finali, 8. CNR Roma.

Sheridan, M.F., Barberi, F., Rosi, M. and Santacroce, R., 1981. A model for Plinian eruptions of Vesuvius. Nature, 289: 282-285.

NORMA UNI EN 11176. 2006. Cultural Heritage - Petrographic description of a mortar. Milano.

Vitruvius, 1999. The ten books on architecture. I.D. Rowland trans., Cambridge University Press.

Wallert, A. and Elston, M., 1997. Fragments of Roman wall painting in the J. Paul Getty Museum: a preliminary technical investigation. In: Béarat, H., Fuchs, M., Maggetti, M., and Paunier, D. (Eds.) Roman wall painting: materials, techniques, analysis and conservation: Proceedings of the International Workshop on Roman Wall Painting, Fribourg, 7-9 March 1996. Institute of Mineralogy and Petrography Fribourg University: 93-104.

Wentworth, C.K., 1922. A scale of grade and class terms for clastic sediments. *Journal of Geology*, 30: 377-392.

CHAPTER 2

Fresco and *mezzofresco*: experimental study and analytical procedure for the determination of the painting technique

INTRODUCTION

Raw materials and painting technique used to realized a wall painting, represent fundamental issue for the history of art and during restoration action. Effectiveness in conservation depends upon accurate characterisation of the raw materials and precise evaluation of type and degree of degradation whereas knowledge on painting techniques, type of pigments and binder are essential information for the history of art. These observations are particularly relevant when wall paintings are considered, since both raw materials and painting techniques are numerous, and painters may have used them with different combinations. In particular, distinction of *fresco* from *mezzofresco* techniques is often problematic, as they only differ for the time and way of application, being the binder composed of lime and pictorial effects very similar in both cases.

Painting on a wall requires adequate preparation, in order to obtain a uniformly flat, smooth and white surface. For this reason, at least two preparation layers are generally applied on the wall before painting: 1) a medium-fine plaster directly applied to the water-wetted rough surface of the wall; 2) a fine plaster made up of fine-grained sand and lime. According to Vitruvius, the Romans, which used a large gamut of wall painting techniques, used up to six preparetion plaster layers before the paint (three medium-fine grained layers called *arriccio* and three more fine-grained layers called *intonaco*). In the case of *fresco* technique, elsewhere also define as *buon fresco*, a very fine-grained pigment diluted into water, is spread on a damp fine-grained plaster. Plasters have optimal characteristics to be used as a background in the fresco painting only for a short period (about eight hours), called "golden period", during which they have high degree of humidity. For this reason, the plaster is applied only on the portion of the wall, which is supposed to be painted within the same day. Calcite formed for reaction between slacked lime ($Ca(OH)_2$) and atmospheric CO_2 in the plaster, guarantee the binding of the pigment to the surface (Rosati, 1991). In the case of *mezzofresco*, lime-resistant pigments are mixed with slaked lime and spread on dry plaster (Botticelli, 1992; Pesenti, 1973). These two main painting techniques can be integrated with different dry-finishing paintings to make retouching and details.

The definition of the painting technique is commonly based to mere macroscopic

observations and on the experience of art historians, archaeologists and restorers, although in a few cases diagnostic microtextural and microstratigraphic features have been described (Daniilia et al. 2000; Edreira et al. 2003; Ajò et al. 2004; Paternoster et al. 2005) supported by historical data. (Perardi et al. 2003; Felici et al. 2004). Nevertheless, standardised analytical criteria and procedures are missing for distinguishing *fresco* from *mezzofresco*. In order to fill this gap, in this paper we present the results of an experimental study, in which we reproduced *fresco* and *mezzofresco*, and propose an analytical protocol for their recognition. The same protocol was then applied to the analysis of five fragments of wall paintings sampled from "Annunciation" (half of the c. XIV) by Stefano Fiorentino and from "Saints of the tribune" (end of the c. XIV) by a lombard anonymous (end of the c. XIV) in the Chiaravalle Abbey, Milan (Italy) Here the use of *fresco*, dry-finish and *mezzofresco* is well documented by Bandera et al., 2005.

1. SAMPLE PREPARATION AND ANALYTICAL PROCEDURE

In order to contribute to the definition of criteria and analytical procedures for the identification of the painting technique used in wall paintings, two 20 cm by 40 cm hollow building bricks were painted at the "Accademia delle Belle Arti – Aldo Galli" (Como, Italy), adopting both *fresco* and *mezzofresco* techniques, and using for each of them fourteen traditional natural pigments provided by the Kremer Pigmente GmbH & Co. KG (Aichstetten, Germany), and white lime. These pigments differ in mineral composition, grain size and texture. Earths such as Verona green, Bavarian green earth, burnt umber, Italian burnt Sienna and Italian raw Sienna, are rich in clay minerals and fine grained oxyhydroxides, and contain minor quantities of other silicates. Additional pigments are basically made of single mineral phases such as carbonates (azurite), oxides (yellow ochre, Spanish red ochre, lead-tin yellow), sulphides (cinnabar), and silicates (lapis lazuli). Moreover, blue smalt is a grinded Co-rich glass, furnace black is produced by hydrocarbon combustion, vine black is made up of calcined vine wood (Matteini and Moles, 1989), and white lime is a lime such as that used for the plaster.

The painting techniques were reproduced applying an about 1 cm thick preparation plaster, defined as scratch coat, composed of coarse-grained quartz-rich sand and slaked lime with a 2:1 ratio, on the bricks to smooth the surface. Once dried, it was wetted with water and covered by fine plaster (*Intonaco*), made of fine-grained quartz-rich sand and slaked lime with 2:1 ratio. In the case of *fresco*, pigments were then diluted with water and fifteen strips (one for each pigment) were painted on the surface about four hours after the application of the plaster. In the case of *mezzofresco*, pigments were mixed with slaked lime and painted in strips after about a week from the application of the plaster (Figure 1). A polished section was then prepared for each of the coloured strips of the two painted bricks, as well as for the five wall paintings fragments from the Chiaravalle Abbey, kindly provided

by the "Soprintendenza al patrimonio storico artistico ed etnoantropologico di Milano". These historical samples are respectively fragments of *fresco* (sample VI4836-1, VI4836-2, VI4836-5) and *mezzofresco* (VI4836-9, VI4836-10).

Preliminary analyses on Chiaravalle Abbay (Bandera et al., 2005) paintings indicate the presence of a *sinopia* at the base of most of the paintings, where the *sinopia* is a sketch prepared according to the *fresco* technique using a reddish-brown earth pigment (from which the name).

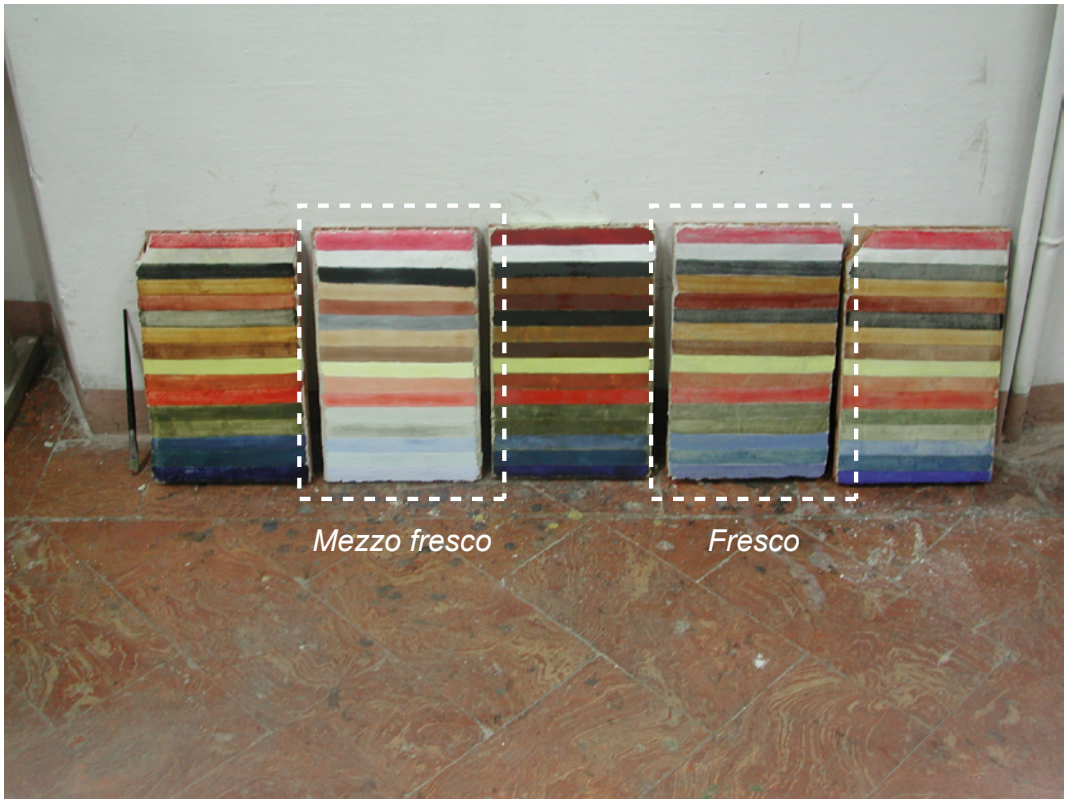

Figure 1. Wall paintings obtained with different pictorial technique. In the present work are considered only fresco and mezzofresco ones.

Microstratigraphy and microtextural features were studied on polished sections by optical (OM) and scanning electron microscopy (SEM), using a Camscan MX 2500S microscope at the Dipartimento di Geoscienze (DGS, University of Padova), carrying out both backscattered electron (BSE) images and distribution maps of major elements.

In order to better characterised the starting materials all the pigments were analysed and their mineral and chemical composition determined. Mineral phases were determined by X-ray diffraction (XRD), using a Philips PW 3710 diffractometer equipped with a CuKα radiation, at the DGS and by Fourier transform infra-red spectroscopy (FT-IR), using a Jasco FT-IR 300E at the C.S.G. Palladio s.r.l. (Vicenza). Chemical analyses were carried out by atomic absorption spectrophotometry (AAS) with a Perkin-Elmer AAS 5000. C, H, N and S were also determined on cinnabar, furnace black and vine black by gas chromatography, using a CE Instruments EA 1110 CHNS elemental analyser (EA) at the Istituto di Geoscienze e Georisorse (IGG, Padova). Hg in cinnabar was calculated on the basis of measured S.

2. RESULTS

Mineral assemblages of the pigments are reported in Table 1. Although each of the pigments is dominated by a specific mineral phase which also determines its colour (colouring agent), they generally contain numerous mineral phases, as expected in pigments prepared by grinding a natural raw material. This causes differences in the bulk chemical composition of the pigments as determined by AAS and EA (Table 1) with respect to theoretical composition of the relative pigmenting mineral phase. Only blue smalt, furnace black and vine black pigments are composed by a glass or an amorphous phase.

Table 1

Chemical composition determined by AAS (expressed in oxides) and EA (C, H, N, S) and mineral assemblage obtained by XRD and FR-IR.

	Azurite	**Blue smalt**	**Cinnabar**	**Lapis lazuli**	**Furnace black**	**Vine black**	**Yellow ochre**	**Spanish red ochre**	**Lead-tin yellow**	**Italian burnt Sienna**	**Italian raw Sienna**	**Burnt umber**	**Bavarian green earth**	**Verona green**
SiO_2	4.77	69.75	0.45	45.02	0.00	8.41	18.13	50.56	0.00	18.86	22.81	19.77	69.61	31.01
TiO_2	0.19	0.04	0.00	0.42	0.00	0.10	2.99	0.15	0.00	0.36	0.30	1.39	0.09	1.96
Al_2O_3	1.88	0.30	0.10	13.86	0.10	4.05	15.33	22.30	0.10	2.57	5.64	8.21	4.26	8.90
Fe_2O_3	0.83	0.00	0.00	1.41	0.00	1.85	19.48	11.45	0.00	48.19	36.05	30.10	7.30	8.62
FeO	0.31	0.15	0.00	0.54	0.00	0.00	0.44	0.35	0.31	0.28	0.22	0.24	2.46	3.72
MnO	0.01	0.00	0.00	0.01	0.00	0.01	0.07	0.01	0.00	0.30	0.45	0.79	0.01	0.18
MgO	0.11	0.03	0.02	12.08	0.00	0.40	0.60	0.11	0.00	5.36	1.34	2.04	1.81	11.04
CaO	0.04	0.11	0.07	13.18	0.00	0.29	18.33	0.29	0.00	8.41	12.51	14.71	4.42	9.73
Na_2O	0.00	0.45	0.00	6.17	0.01	0.16	0.07	0.79	0.00	0.35	0.33	0.23	0.08	0.43
K_2O	0.02	11.55	0.00	2.89	0.02	0.75	0.08	1.95	0.00	0.42	0.63	0.71	2.28	0.94
Cu_2O	21.50	-	-	-	-	-	-	-	-	-	-	-	-	-
CuO	38.60	-	-	-	-	-	-	-	-	-	-	-	-	-
CoO	-	16.45	-	-	-	-	-	-	-	-	-	-	-	-
PbO	-	-	-	-	-	-	-	-	83.12	-	-	-	-	-
SnO_2	-	-	-	-	-	-	-	-	11.95	-	-	-	-	-
P_2O_5	0.12	0.03	0.00	0.40	0.00	0.00	0.43	0.22	0.07	0.87	0.64	0.83	0.12	0.76
P.F.	32.04	1.13	-	2.63	-	-	24.43	11.16	4.38	14.64	18.43	19.13	7.22	22.80
C	-	-	0.16	-	96.44	82.85	-	-	-	-	-	-	-	-
H	-	-	0.19	-	0.26	1.07	-	-	-	-	-	-	-	-
N	-	-	0.02	-	0.43	0.00	-	-	-	-	-	-	-	-
S	-	-	13.49	-	0.00	0.00	-	-	-	-	-	-	-	-
Hg*	-	-	84.89	-	-	-	-	-	-	-	-	-	-	-
Totale	100.42	99.99	99.39	98.61	97.26	99.94	100.38	99.34	99.93	100.61	99.35	98.15	99.66	100.09
	Az Qtz Mal	Am	Cn	Sod Bt Cpx San Ne Py	Am	Am Qtz Ms Chl Ank	Cc Gth Kln Ant	Qtz Ill Hem Kln	PS Css Crs	Qtz Dol Hem Ank Cc	Gy Qtz Cc Gth Smc Anr	Cc Gy Qtz Gth Hem Ank Kln	Qtz Cc Chl Ank Cel	Cc Qtz Smc Chl

Abbreviations: Am = amorphous phase; Qtz = quartz; Az = azurite; Mal = malachite; Cn = cinnabar; Sod = sodalite; Cpx = clinopyroxene; Bt = biotite; San = sanidine; Ne = nepheline; Ill = illite; Chl = chlorite; Ank = ankerite; Cc = calcite; Gth = goethite; Knl = kaolinite; Ant = anatase; Hem = hematite; PS = Pb_2SnO_4; Css = cassiterite; Crs = cerussite; Dol = dolomite; Gy = gypsum; Smc = smectite; Anr = anhydrite; Cel = celadonite. (*) calculated on the basis of S content.

These relatively low-cost analytical techniques are efficient for identifying the type of pigment but do no give any hint on the painting technique adopted, which implies specific timing and sequence of materials applied rather then compositions. Instead, the analysis of microstratigraphy and microtextural features on polished sections under OM and SEM seems to be more suitable for distinguishing *fresco* and *mezzofresco* painting techniques. But, since different and numerous pigments were used in this study, microscope analysis were firstly address to discriminate among textural peculiarities related to the nature of a specific pigment and features actually related to the painting technique adopted.

In the case of *fresco*, significant differences, although not always very marked, were observed between earths, ochres, and other pigments. Under reflected light, coarse-grained particles in earths and ochres display smooth surface and are generally well incorporated into the binder, which perfectly adheres to their surface forming a uniform film several microns thick and assuming a hazed aspect (Figure 2a). Other pigments such as blue smalt, cinnabar, azurite, lapis lazuli, furnace back and vine black are made of grains, which display sharp surfaces and are surrounded by transparent binder paste (Figure 2b). SEM-BSE images show that layers of binder surrounding single grains of pigment are thicker in the case of earths and ochres (Figure 3a) then for other pigments (Figure 3b). These differences may be related to the presence of clay minerals in earths and ochres, increasing pigment hygroscopicity and

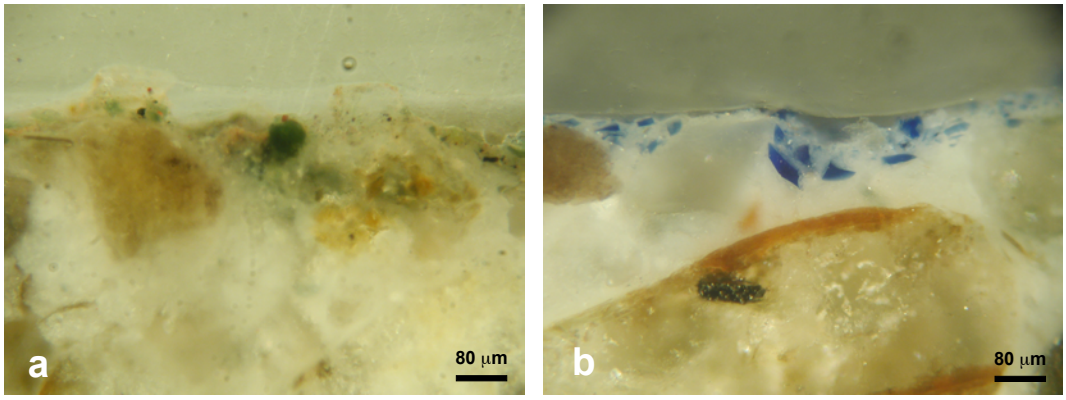

Figure 2. a) Reflected light image of the Bavarian green earth pictorial surface (*fresco*); b) Reflected light image of the blue smalt pictorial surface (*fresco*).

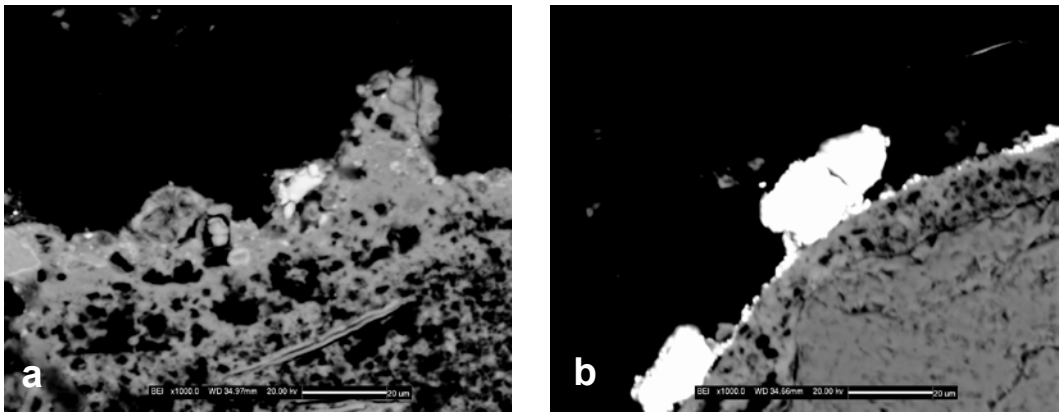

Figure 3. a) SEM-BSE image of the burnt umber pictorial surface (*fresco*); b) SEM-BSE image of the cinnabar pictorial surface (*fresco*).

therefore allowing a greater amount of water and lime to be adsorbed from the underlying plaster during setting. Moreover, fine-grained particles are better dispersed, causing a high paucity of the binder and making the painted surface more uniformly coloured. In addition, they better adhere to the painted surface, resulting more uniformly and smoothly distributed with respect to coarser grains, generally isolated each other, protruding from the external plaster surface, and often being only partially coated by the binder.

In the case of the *mezzofresco*, pigments are generally homogeneously distributed within a clear-aspect binder, independently from their nature and grain size. Systematic differences between *fresco* and *mezzofresco*, allowing defining objective criteria for their discrimination were observed under OM and SEM in terms of microstratigraphy ad microtextural features.

Microstratigraphy and discrimination among three main layers – from the surface inwards, paint, fine plaster (*intonaco*) and scratch coat, respectively was defined on the basis of microtextural features, grain-size and mineral composition of aggregate. The three layers show under OM sharp boundaries and relatively constant thickness. In the case of *fresco*, the pigment-bearing layer resulted to be relatively thin (generally below 180 μm), the surface being rough and irregular. Coarser grains of pigment do not penetrate into, but remain over the surface of the plaster, bound by a thin film of calcite (Figure 4a). In the case

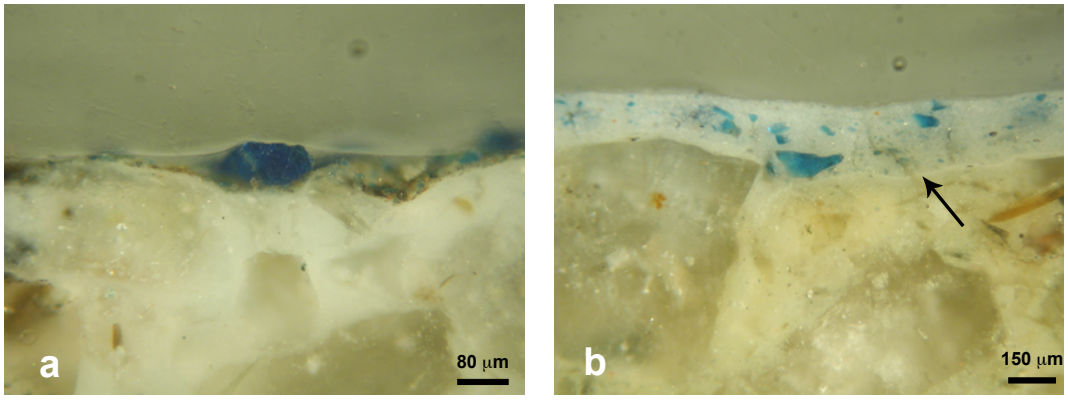

Figure 4. Reflected light images of azurite lied on according to a) *fresco* and b) *mezzofresco* technique, respectively. The white level marked by the arrow represent the carbonation layer in the plaster at the contact with the painted layer.

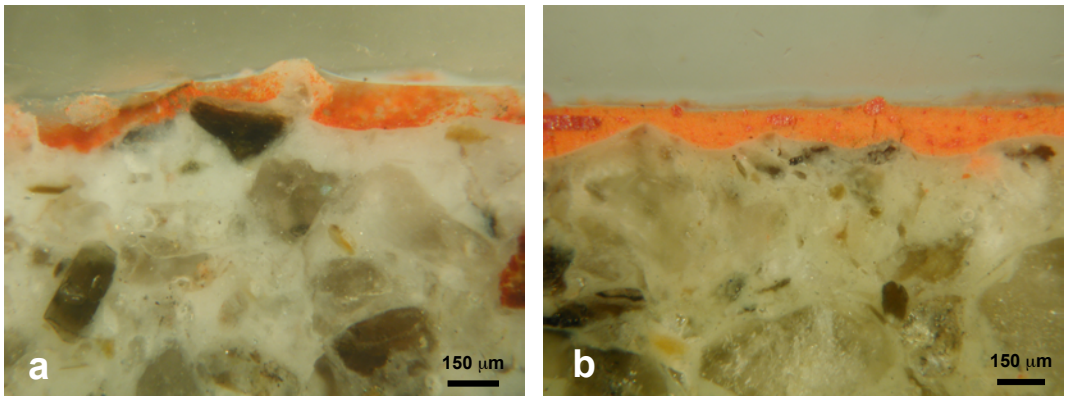

Figure 5. Reflected light images of cinnabar spread on according to a) *fresco* and b) *mezzofresco* technique, respectively.

of *mezzofresco*, the pigment-bearing layer is systematically thicker (up to 650 μm), and displays a smooth surface. Grains are always regularly and completely distributed within a uniform layer of calcite (Figure 4b). Nevertheless, when pigments are very fine grained, such as in the case of cinnabar (Figure 5) and burnt Sienna (Figure 6), the differences between *fresco* and *mezzofresco* become less evident, suggesting that these microtextural features should be used with care as discriminating criteria. Furthermore, thickness of the paint might vary according to painter wishes and skill.

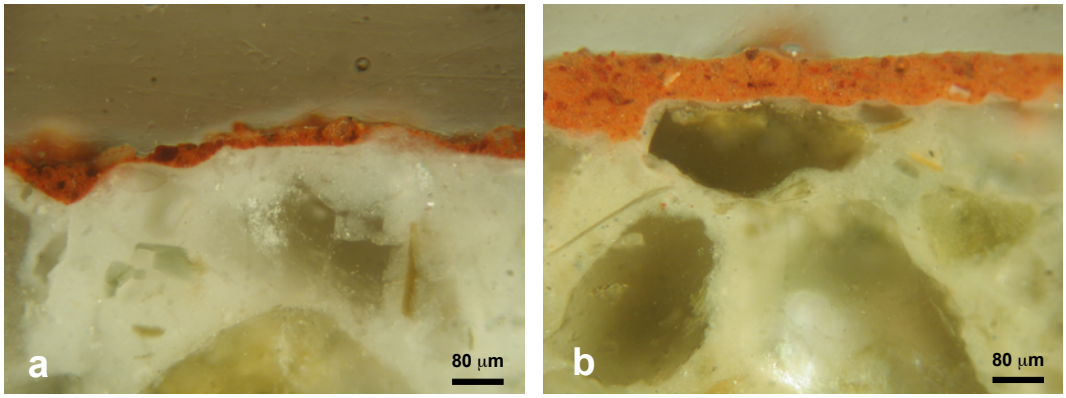

Figure 6. Reflected light images of burnt Sienna spread on according to a) *fresco* and b) *mezzofresco* technique, respectively.

These features are probably related to the different modality of preparation of the paint. In the case of *mezzofresco*, pigment is mixed with slaked lime which well adhere to the pigment grains, providing a thick and viscous paint which remains coherent also after its application to the wall, making the external surface smooth and regular. In the case of *fresco*, the suspension of pigment in water provides a rather liquid media. After application to the wall, water is adsorbed by the underlying plaster and pigment particles tend to concentrate and adhere to each other, producing a thin dense paint film in which coarser-grained pigment particles tend to lean out from a rough surface.

The distinction between the two painting techniques resulted to be more evident at SEM. In the case of *mezzofresco*, elemental distribution maps show a high-density layer, few ten micron thick, Ca-rich layer. Which typically occurs on the more superficial portion of the plaster, as show in Figure 7. This Ca-rich layer is very sharp at the contact with the painted layer and gradually haze towards the plaster. This evidence is more pronounced when SEM-BSE image of *fresco* and *mezzofresco* paints are compared (Figure 8). Moreover, pores progressively decrease toward the plaster surface and increase dramatically within the painted layer, clearly remarking the thin dense layer between the two of them (Figure 9). Sometimes, this Ca-rich level is also visible under reflected light microscope, showing a very bright halo at the base of the painted layer (Figure 4b). An analogous Ca-rich and scarcely porous layer, is also present on the surface of the painted layer (Figure 8), both in the case of *fresco* and *mezzofresco* techniques.

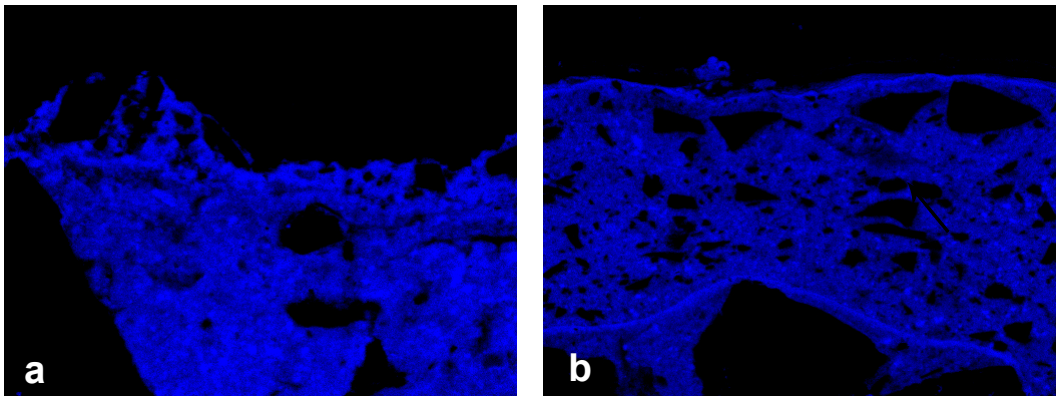

Figure 7. Ca elemental map of blue smalt, spread on according to a) *fresco* and b) *mezzofresco t*echnique, respectively.

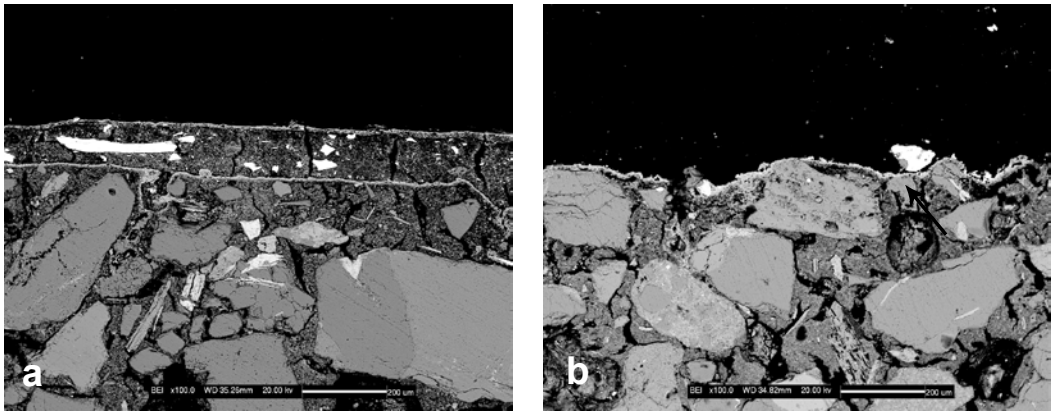

Figure 8. SEM-BSE images of azurite paint spread on according to a) *mezzofresco* and b) *fresco* technique, respectively.

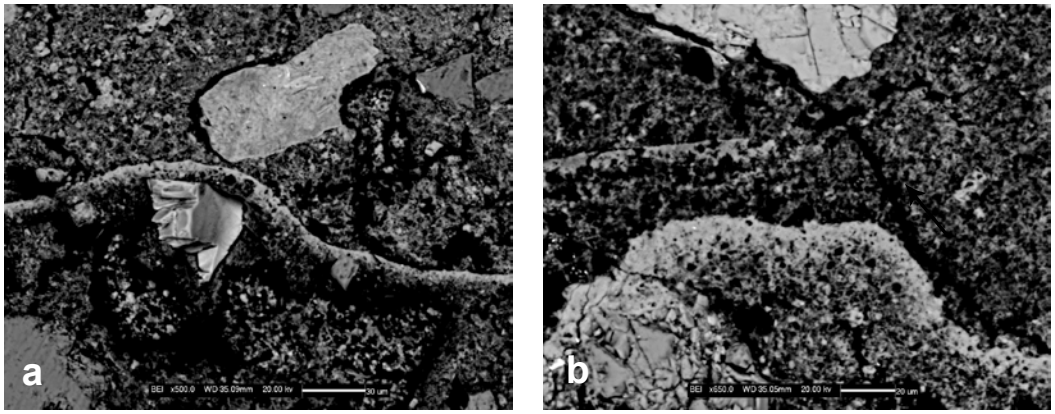

Figure 9. SEM-BSE images of carbonation layer in the plaster immediately underneath the painted layer in a mezzofresco a) Bavarian green earth and b) white lime paint.

All the studied *fresco* paints show a different miscrostratigraphy, in which the painted layer is always thinner than that in the *mezzofresco,* and the Ca-rich and low porosity layer occurs only on the surface (Figure 8a), being thicker and including the whole painted layer and part of the underneath plaster.

Microstretigraphic and microstructural study on wall painting fragments from Chiaravalle Abbey gave very reassuring results. In terms of the distinctive features observed

between the two painting technique. All the samples are composed of two or three overlapped painted layers (Figure 10). Samples VI4836-1, VI4836-2, VI4836-5 and VI4836-9 are all characterised by the presence of a *sinopia*, which appear at the OM as a very thin layer (5 to 20 μm thick) composed of red/yellow ochres, spread on a fine-grained plaster (Figure 10). SEM-BSE images of *sinopia* layers always show the occurrence of a Ca-rich, low porous level including the *sinopia* pigment and part of the underneath plaster. It represents the first *fresco* level of the wall paintings. In the case of samples obtained with *fresco* technique, the Ca-level is always located on the painting surface, whereas in *mezzofresco* painting samples, it is also present at the base of the painted layer (Figure 11,12). Particolarly interesting is the case of sample 9, in which no carbonation layer is present in the third painted layer. FT-IR analysis indicate the presence of an organic binder for this dry finishing painting layer. The fore feature and the location of Ca-rich levels identified in the Chiaravalle Abbey's in *fresco* and *mezzofresco* technique samples are consistent with that recognised in the experimental samples.

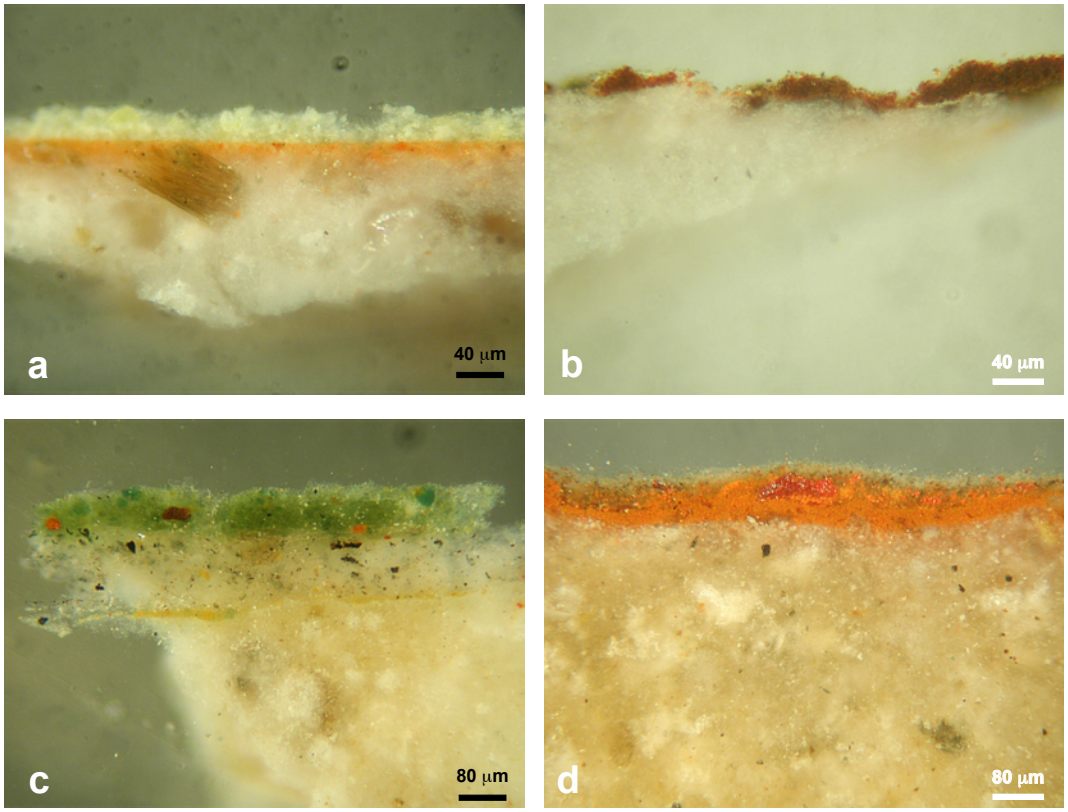

Figure 10. Reflected light images of: a) sample VI4836-1; b) sample VI4836-5; c) sample VI4836-9; d) sample VI4836-10.

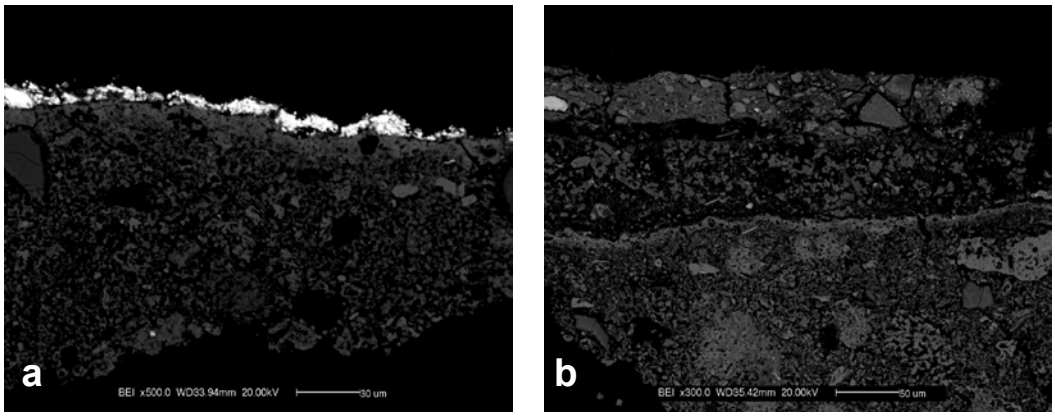

Figure 11. SEM-BSE images of carbonation layer in sample a) VI4836-5 and b) VI4836-9.

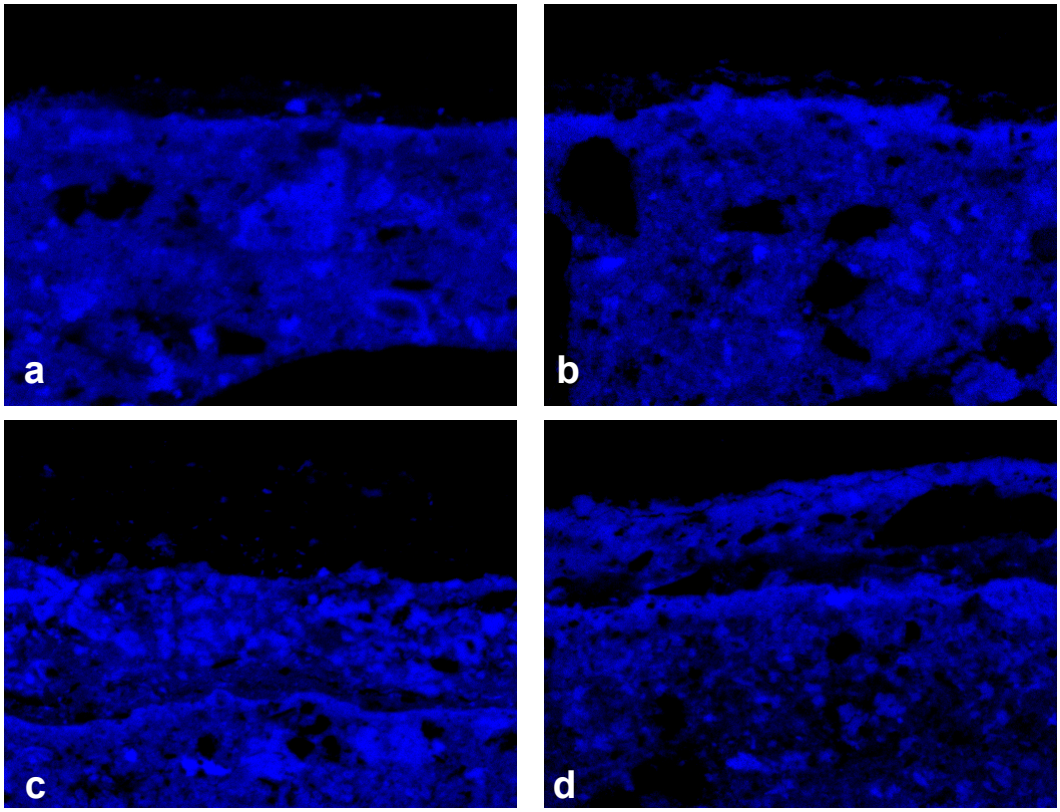

Figure 12. Ca elemental maps of a) sample VI4836-2; b) sample VI4836-5; c) sample VI4836-9; d) sample VI4836-10

3. CONCLUSIONS

The microstratigraphic evidence in the *fresco* and *mezzofresco* wall painting is strictly related to the carbonation process, taking place during the drying of plaster the painted layers. The plaster gripping depends on the reaction of the Ca hydroxide, constituting the binder, with the atmospheric CO_2, producing Ca-carbonate and releasing water. This process is more efficient on the surface, where CO_2 concentration is higher and water evaporation more effective, and determines superficial hardening and porosity reduction, which inhibited

and retard the carbonation process in the more inner portion of the underneath plaster. In the *mezzofresco* technique drying and carbonation processes can take place before the application of the pigment, since the painted layer is spread on the plaster after many hours. This producing a low porous carbonated crust on the plaster surface exposed to the air. When Ca-hydroxide mixed with the pigment is then applied to this layer, a new process of drying and carbonation starts on the surface of the paint. For this reason, the contact between the plaster and the painted layer result very sharp and a second low-porous carbonated level is formed on the surface of the painted layer. In this case draying is limited to the painted layer and consequently the water moves in the intergranular pores, transporting a modest quantity of carbonate to the surface, and forming a thinner carbonation layer.

In the case of *fresco* painting, a mixing of water and pigment is applied on a damp plaster, which has not yet undergone drying and carbonation process. In this situation, the water guarantees a good initial adhesion of the pigment to the plaster surface. Subsequently, the water evaporation and the carbonation process cause calcite precipitation in the painted layer and in the more superficial portion of the plaster, so that the painted layer shows a continuity solution with the upper portion of the underneath plaster. In this technique the use of water to apply the pigment, slow the plaster drying process, producing Ca migration and its precipitation to the surface. For this reason in *fresco* technique, the superficial carbonation layer is thicker and includes all the pigment grains, which are completely wrapped into a thin calcite film. Moreover, no second and deeper carbonation level can form, since layers were continuosly spread, without any interruption.

On the basis of these pieces of evidence, microstratigraphic analysis of a wall painting can provide useful information for defining weather a *fresco* or *mezzofresco* technique was used. This method also allows to identify more complex situations, recording possible retouching, second though and adding of details, of the painter. The validity of this method and the criteria identify to distinguish the *fresco* from the *mezzofresco* technique is clearly supported by the microstratigraphic data obtain by the study of some wall painting fragments from the Chiaravalle Abbey, produced according to different and several documented techniques.

In conclusion the results here presented indicate that a standard analytical procedure for the characterisation of wall lime-based paints can be advanced, with particular reference to the discrimination between *fresco* and *mezzofresco* techniques. This procedure has to include a complete series of analysis to characterise the pigments, and to define the possible presence of organic binders or theirs derivates by XRD, FT-IR, micro-ATR for mulilayered paints, and elemental maps, and to identify microstratigraphic features by reflected light and electronic microscopy and Ca elemental map on SEM, which also allow to distinguish the different painting techniques.

REFERENCES

Ajò, D., Casellato, U., Fiorin, E. and Vigato, P.A., 2004. Ciro Ferri's frescoes: a study of painting materials and technique by SEM-EDS microscopy, X-ray diffraction, micro FT-IR and photoluminescence spectroscopy, *Journal of Cultural Heritage*, **5**, 333–348.

Bandera, S., Nicola, A.R., Parodi, V., Frezzato, F., and Monni, E., 2005. Gli affreschi trecenteschi dell'Abbazia di Chiaravalle milanese: Il primo maestro a confronto con il cantiere giottesco, restauro in corso, Scienze e beni culturali XXI. 2005, Sulle pitture murali, Edizioni Arcadia Ricerche, 793-811.

Botticelli, G., 1992. Metodologie di restauro delle pitture murali, Centro Di, Firenze.

Daniilia, S., Sotiropoulou, S., Bikiaris, D., Salpistis, C., Karagiannis, G., Chryssoulakis, Y., Price, B.A. and Carlson, J.H., 2000. Panselinos' Byzantine wall paintings in the Protaton Church, Mount Athos, Greece: a technical examination, Journal of Cultural Heritage, 1, 91–110.

Edreira, M.C., Feliu, M.J., Fernández-Lorenzo, C. and Martín, J., 2003. Spectroscopic analysis of roman wall paintings from Casa del Mitreo in Emerita Augusta, Mérida, Spain, Talanta, 59, 1117–1139.

Felici, A.C., Fronterotta, G., Piacentini, M., Nicolais, C., Sciuti, S., Venditelli, M. and Vazio, C., 2004. The wall paintings in the former Refectory of the Trinità dei Monti convent in Rome: relating observations from restoration and archaeometric analyses to Andrea Pozzo's own treatise on the art of mural painting, Journal of Cultural Heritage, 5, 17–25.

Mattini, M. and Moles, A., 1989. La chimica nel restauro. I materiali dell'arte pittorica. Nardini editore, Firenze.

Paternoster, G., Rinzivillo, R., Nunziata, F., Castellucci, E.M., Lofrumento, C., Zoppi, A., Felici, A.C., Fronterotta, G., Nicolais, C., Piacentini, M., Sciuti, S. and Venditelli, M., 2005. Study on the technique of the Roman age mural paintings by micro-XRF with Polycapillary Conic Collimator and micro-Raman analyses, Journal of Cultural Heritage, 6, 21–28.

Perardi, A., Appolonia, L. and Mirti, P., 2003. Non-destructive in situ determination of pigments in 15th century wall paintings by Raman microscopy, Analytica Chimica Acta, 480, 317–325.

Pesenti, F.R., 1973. L'affresco, La tempera. In: Le tecniche artistiche, strumenti per la nuova cultura, guide e manuali, (Ed. C. Maltese), 314-326, Mursia U.& C, Milano.

Rosati, C., 1991. Tecniche pittoriche e restauro dei dipinti, Edizioni Scientifiche A. Cremonesi, 57-69.

Vitruvius, 1999. The ten books on architecture. I.D. Rowland trans., Cambridge university press.

CHAPTER 3

The pigments of the Temple of Venus (Pompeii)

INTRODUCTION

Italian Roman pigments, particularly from Rome and Pompeii, have been extensively but not completely studied using various analytical techniques and recognising a great variety of pigments and mixtures (Augusti, 1967; Walsh et al, 2003). Scientific research on paintings and fragments of paintings has been also performed Switzerland, Greece and England (Fuchs and Béarat, 1997; Meggiolaro et al, 1997; Edwards, 2002). Currently we have a good knowledge on the Roman palette, but further investigations are still needed especially to understand the recipes of mixtures of pigments.

One of the most important questions in the study of ancient paintings is the identification of pigments and recipes, which can give useful information about the material knowledge of a culture and helps in identifying lines of communication and trades. However, also the comprehension of techniques for colour preparation and application is an interesting topic for understanding technological level.

The site of Pompeii is probably the most studied site of the Roman Age, but many areas of research are still unexplored, and the Temple of Venus is one of those. Venus, indeed, is the main and polyad divinity of Pompeii and her temple is one of the most important buildings in the town, located in south-west side of Pompeii (Figure 1). This site had a complex and long history of building and reconstructions. The present building itself underwent numerous reconstructions and renovations until the eruption of Mount Vesuvius in 79 AD. The area was probably a place of worship since archaic time and was occupied by the Sannites from the late 4^{th}-3^{rd} centuries BC. Redesigned during definitive Romanisation in 130 BC and renovated during the Julian and Claudian ages, the building was completely destroyed during the earthquake of 62 AD. At the time of the Mount Vesuvius eruption in 79 AD, it was still under renovation, as attested by the findings of building elements (Curti, 2007; Curti, 2008).

The main aim of this work is the characterisation of the paintings from the Temple of Venus with a multi-analytical approach (including OM, ESEM, XRPD, FT-IR and Mössbauer spectroscopy) and to derive information about the artistic knowledge, technology, and probable trade lines of the Sannitic and the Roman in Pompeii. Within the frame of this research, we also had the possibility to test a new Mössbauer portable apparatus.

The palette from the site shows a great variety of pigments, with carbon, calcite, ochre (iron oxides and hydroxides), cuprorivaite, green earth, cinnabar, and an uncommon

yellow glass. Samples showed very simple recipes (i.e. adding of calcite to lighten colours) as well as some interesting and unusual mixtures. Data allow also some remarks about the manufacturing of artificial pigments although evidence for possible provenance of the raw materials is missing.

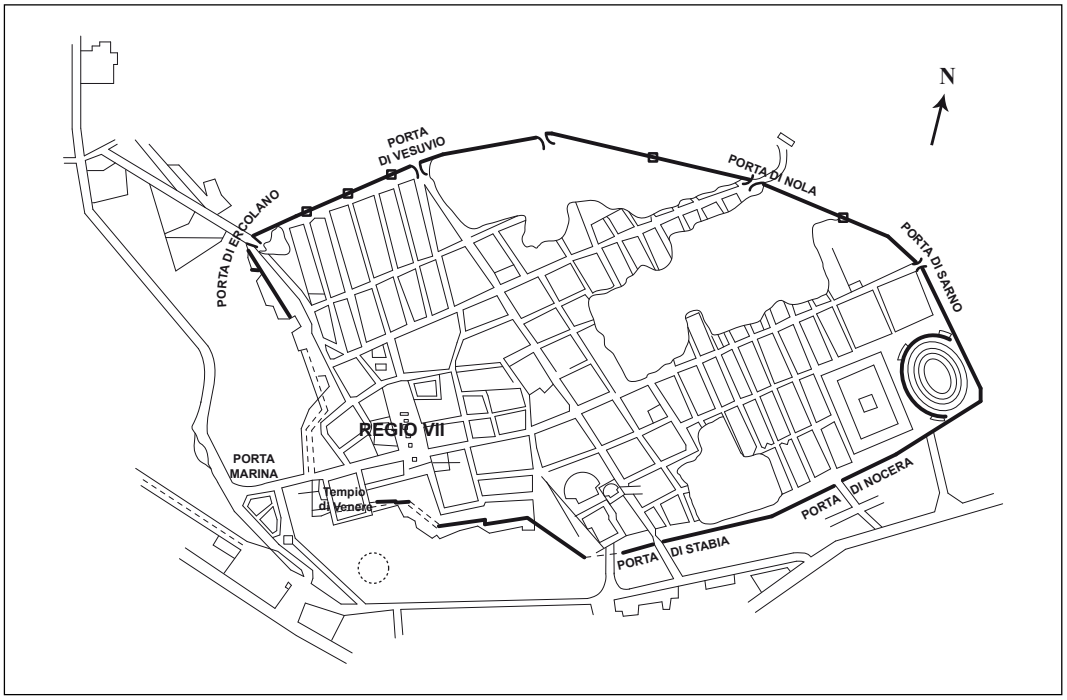

Figure 1. Map of the archaeological site of Pompeii with the location of the temple of Venus.

1. SAMPLE PREPARATION AND ANALYTICAL APPROACH

A set of 68 coloured fragments of wall paintings was collected prevalently from debris and floor filling material belonging to five different chronological units from Republican to Imperial times (Table 1). In two cases (samples LF057, LF117) samples were also collected from their primary location, i.e. from walls of the 3rd century AC and the end of the 2nd century AC respectively. They represent the main colour palette (Figure 2), used for the wall paintings of the Temple of Venus. The dimension of the fragments analysed ranged from 1 cm^2 to 10 cm^2. Due to the fragmentary nature and in most of the cases secondary location of the samples, it was not possible to make any technological remark about the wall paintings as a whole, nevertheless the analyses of these samples are is a useful method for the identification of pigments and recipes used in the temple.

The samples were observed under an optical microscope both in thick and standard petrographic thin section. Thick sections were polished and studied under optical microscope using the inclined reflected light of a movable fibreglass system (RL-OM). This type of observation allowed determining microstratigraphy and the main microtextural features of the pigments, such as grain-size, shape, roundness and degree of dispersion of the fragments of pigment in the matrix. A small quantity of each pigment was then reduced to powder by

scraping the surface of the sample with a scalpel, and mounted on a glass using Cargille Meltmount as mounting media with a refractive index of n_d 1.662 (at 25°C). These sections were then analysed by transmitted light optical microscopy (TL-OM) both in parallel (PPL) and crossed polarised light (XPL). Petrographic thin sections of plasters were also prepared and used for the study of the white painted layers and the preparation layers.

Table 1.
Time distribution of the recipes used for the preparation of the paints. Boxes filled with a pale colour refer to samples of uncertain age.

		Black 1	Black 2	Black 3	Red 1	Red 2	Red 3	Yellow 1	Yellow 2	Yellow 3	Yellow 4	Light Blue	Green 1	Green 2	Green 3	Grey	White 1	White 2
Republican times	End 4th-3rd BC				■					■					■			
	Second half 2nd BC					■		■										□
	1st BC	■		■	■				■									
Imperial times	Augustan age	▯				▯	▯	▯				▯				▯		
	Julio-Claudian age	▯	■						▯		▯							
Unknown age		1	-	-	5	-	2	-	-	-	-	1	3	1	-	1	3	1

Samples with a painted surface wider than 1 cm^2 were also analysed by colorimetry, using a CR-400 Chroma Meter Minolta portable colorimeter with a circular measuring area of 8 mm in diameter. This instrument returns the L^*, a^* and b^* parameters, the three coordinates of the CIELAB colour space, a colour system which more closely represents human sensitivity to colour defined in 1976 by the International Commission on Illumination (CIE, formerly *Commission Internationale d'Eclairage*). Within the CIELAB colour space, L^* indicates the lightness of the colour from black ($L^* = 0$) to white ($L^* = 100$), a^* represents the position of the colour with respect to magenta (positive values) and green (negative values), and b^* with respect to yellow (positive values) and blue (negative values) (Fairchild, 2005). Colorimetric data were standardised according to procedures designed by Vitali and Franklin (1986) and Baxter (1999), and elaborated statistically performing a principal component analysis (PCA) with the Minitab© (version 13.20) commercial software package.

Secondary electron images were acquired using a Fei Quanta 200 environmental scanning electron microscope (ESEM) at the C.S.G. Palladio s.r.l. of Vicenza (CSGP), equipped with an EDAX Falcon EDS microanalysis detector. Images were taken under low vacuum conditions, to avoid gold or graphite coating of the samples. Semi-quantitative EDS microanalyses were also performed to obtain information on the elemental composition of the pigment particles.

Chemical composition of one of the yellow pigments made of glass fragments was determined with a Cameca SX 50 electron probe (EPMA) at the Institute of Geosciences and Georesources, CNR, Padova, with an acceleration voltage of 15 KV and a beam current of 10 nA, and using natural mineral phases as standards. In order to minimise volatile loss and alkali (especially Na) migration, analyses were performed using a defocused beam (30 mm in diameter), and moving the specimen during the analysis. The counting time on the

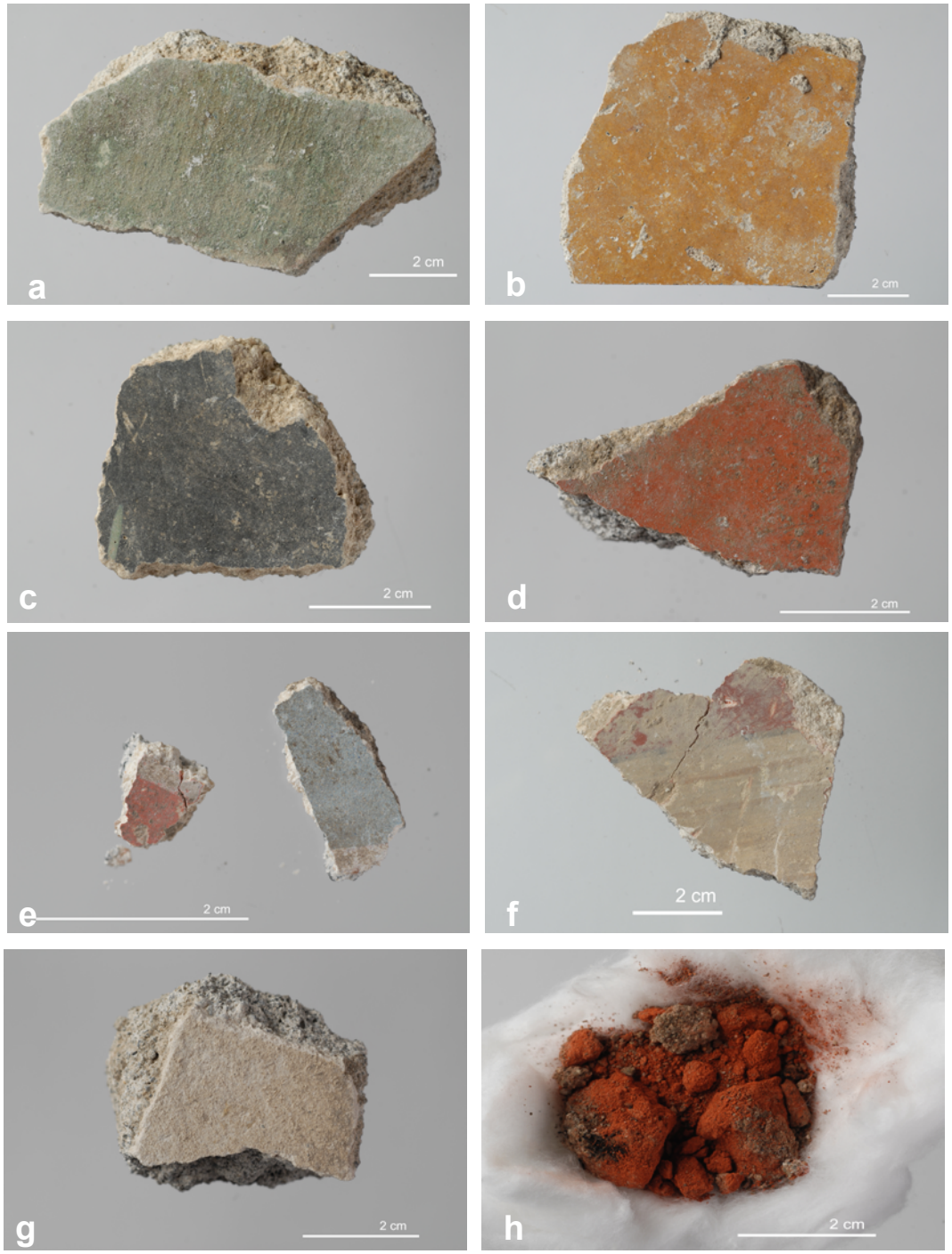

Figure 2. Hand specimens of the paintings: a) green; b) yellow; c) black; d) red; e-f) multi-layered colour painting; g) white and h) bunch of a red pigment powder.

element peak and background was 10 s and 5 s, respectively.

The identification of the different crystalline phases present in some of the pigments was carried out by X-ray powder diffraction (XRPD). Analyses were performed by means of a Philips X'Pert powder diffractometer at the Department of Geosciences (DG), with Ni-filtered Ka radiation of Cu from a graphite monochromator. Measurements were performed at 40 kV and 40 mA.

Absorption spectra in the IR region (between 4000 and 400 cm^{-1}) were collected at the

(CSGP) using a Thermo-Nicolet Avatar 370 Fourier transform infrared spectrophotometer with the aid of a diamond cell for the powdered samples and a Thermo-Nicolet Continuum micro-spectrometer for the study of thick sections (m-ATR), both of these instruments working in attenuated total reflection (ATR) mode. Infrared spectroscopy was useful both for the determination of pigments and for the identification of possible organic binders. When applicable, the m-ATR method has been preferred to the analysis on powder with the diamond cell. However, in sampled with too thin pictorial layers, the second method was the only way to obtain a useful spectrum. In these cases a small amount of painting has been collected from the surface with a scalpel. Since the two approaches returned the same results, I will indifferently refer to as FT-IR analyses hereafter.

Three red and two yellow pictorial layers were also analysed by Mössbauer spectroscopy in order to better identify their mineralogical composition. This is a nuclear technique that provides information about the interactions between a specific nuclide – most commonly ^{57}Fe – and its surroundings in a solid matrix. Mössbauer spectrum is characterised by the number, shape, position and relative intensity of the various absorption lines. These features result from the nature of the various hyperfine interactions that characterize the nucleus-electron interaction and can be summarized in the Table 2.

Mössbauer spectroscopy generally requires a considerable amount of sample to be prepared in a powder and analysed. This may represent a problem when studying wall paintings. For this reason a new non-destructive portable ^{57}Fe Mössbauer spectrometer was tested in this study. This instrument is made of a standard constant acceleration spectrometer equipped with four proportional counters controlled by a specific electronics that allows the simultaneous collection and summation of four spectra that will be fitted with the usual methodology by dedicated software. Spectra were collected for a relatively long time (5 days or more) in order to improve spectrum statistics.

Table 2
Hyperfine parameters and their significance.

Hyperfine Interactions	**Description and Information obtained**
Isomeric shift, *d*	Representative of the interaction between nucleus and electron density, it gives information mainly on the oxidation state of the Mössbauer nucleus
Quadrupole splitting *D*, or quadrupole shift, *e**	Representative of the interaction between nucleus and electric field gradient, it gives information mainly on the coordination number of the Mössbauer nucleus
Magnetic Field, *H***	Representative of interaction between the nuclear magnetic moment and the magnetic field. It give information on the nature of the magnetic ordering and details of the electronic structure of the Mössbauer nucleus

In addition, the composition of selected samples was determined by X-ay fluorescence (XRF) spectrometry, using a Bruker® ARTAX portable μXRF, equipped with a Mo tube, able to analyse an area of 0.79 mm^2 acquiring for 500 s using a voltage of 20 kV and an intensity of 1550 mA.

2. WALL PAINTINGS MICROSTRATIGRAPHY

All the considered wall painting samples of the Temple of Venus were initially examined under a microstratigraphic viewpoint. To this aim, petrographic thin sections have been analysed under a polarizing light microscope with transmitted-light. ESEM-EDS analyses were also performed to better define the sequence of layers.

Microstratigraphy revealed a sequence of layers which differ for grain size and nature of inclusions, constituting mortar and plaster supporting the painted layer. According to Prentice (1990), mortar is a material composed of a carbonate binder and an aggregate with grain size up to 5 mm. With the term "plaster" here we refer to a multi-layered fine-grained mortar that provides a smooth coat to a wall or other surface. According to Vitruvius the covering of a wall that has to receive a painting, must to be constituted of a plaster normally composed by scratch coat, *arriccio*, and *intonaco*, where scratch coat is a rough rendering coat applied to smooth the surface of the wall, *arriccio* is a sequence of at least three coats of sand and mortar, spread on the scratch coat, and *intonaco* is a set of finishing layers made of lime and a very fine-grained sand, that receives the painting. In this chapter only the different types of *intonaco* will be considerate and briefly described. I refer to chapter 1 for the complete description of all the mortars collected in the area of the Temple of Venus.

The following three classes of *intonaco* were recognised and classified based upon the petrographic composition of the aggregate:

Marmorino

Marmorino is the most abundant *intonaco* in the painting samples (72%). Under petrographic analysis in thin section, *marmorino* displays a micrite-like matrix (see chapter 1 in this volume) composed of crypto- and microcrystalline calcite and filler, with an aggregate: binder ratio of about 1:1. Aggregate shows a wide grain-size distribution, from granules to coarse silt, with maximum frequency in the medium to very fine sand classes. The aggregate consists of euhedral crystals of calcite and dolomite, occasionally associated to volcanic scoriae and rare crystals of diopside and feldspar (Figure 3a). In some cases, the carbonate fraction of the aggregate is composed of well-rounded fragments of micritic limestone rather than crystals of spathic calcite. This type of *intonaco* often appears composed of two or three layers, only distinguished by the change of granulometry among the different coats, although clear discontinuities have not been recognised between the various layers, both from OM and BSE images (Figure3b). This suggests that each coat has been spread one when the underlying one was still partially wet (see chapter 2 in this volume).

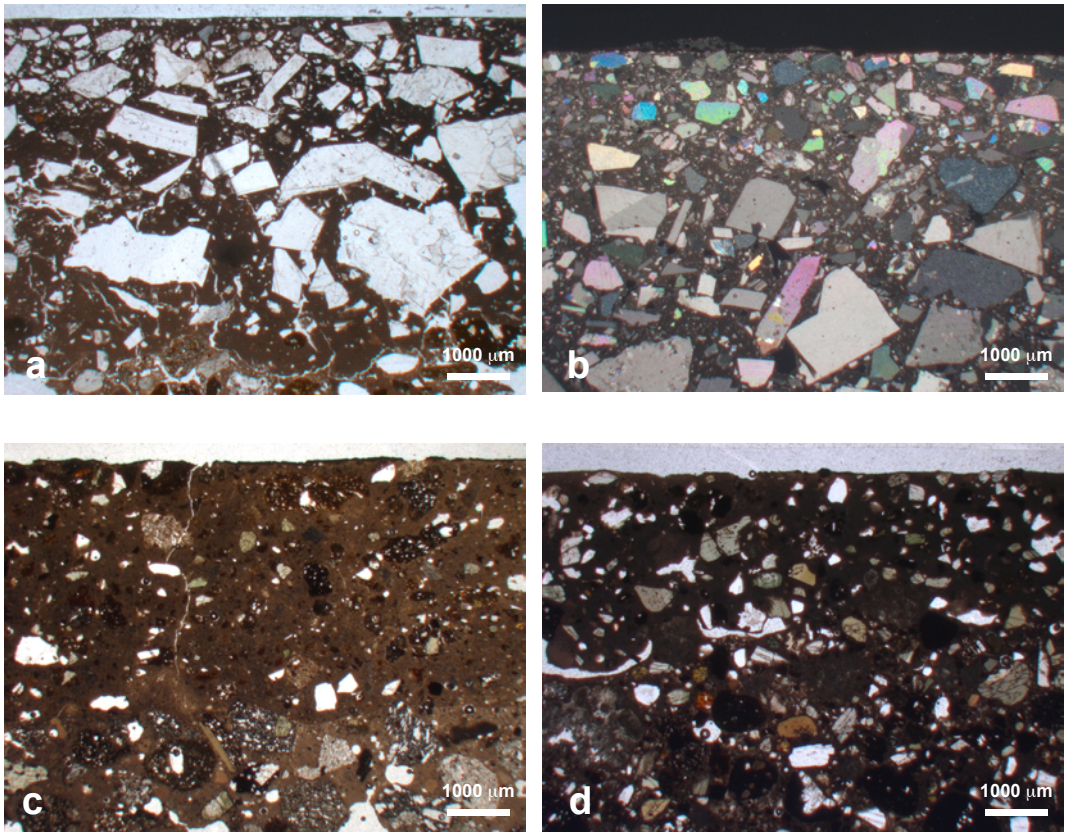

Figure 3. Microscope images of the plasters analysed in this study: a-b) *marmorino*; c) *cocciopesto*; d) *intonachino*. All images were taken in PPL with the exception of (b), which was shoot in XPL.

Cocciopesto

Few *intonaco* layers of *cocciopesto* have been identified among the analysed samples (19%). It shows a spotted matrix (see chapter 1 in this volume) composed of cryptocrystalline calcite and hydrated calcium silico-aluminates, with an aggregate:binder ratio of 1:1. Grain size of the aggregate ranges from granules to coarse silt, with a maximum frequency of coarse to fine sand. The aggregate is mainly composed of angular fragments of ground ceramic materials (grog). Few well-rounded fragments of rock, scoriae and altered glass of volcanic origin are also present (Figure 3c). In few cases crystals of diopside, sanidine, plagioclase, garnet and flakes of biotite have been also observed. *Cocciopesto* only occurs in red and yellow painting layers from second half of the 2nd century BC, 1st century BC and Julio-Claudian age units.

Intonachino

This type of *intonaco* is rarely used as preparation layer of a painting and it is present in only 6 samples (9%). *Intonachino* is characterised by an almost pure crypto- to microcrystalline calcite matrix, with sporadic lime lumps and an aggregate:binder ratio of about 1:1. The filler shows homogeneous distribution and grain size ranges from granules to very fine sand, with coarse and medium sand granulometric classes being the most frequent. The filler is composed of fragments of volcanic scoriae and volcanic rocks, frequently associated with

sub-angular to angular crystals of diopside and, less often, sanidine, plagioclase, biotite and melanite (Figure 3d). In three cases (LF057, LF027.R, LF027.G) this *intonaco* resulted to be the preparation layer for yellow, red and grey painting respectively; while in other three cases (LF014, LF101, LF108), belonging to units from the second half of the 2nd century, it lies under a smoothing layer.

The mineralogy and petrography of the volcanic sand individuated as the main constituent of the aggregate in the *intonachino*, and also present in minor amounts in *marmorino* and *cocciopesto*, are compatible with the products of the Somma-Vesuvius volcano (Santacroce, 1987). Furthermore, the same type of sand is also present in grog in *cocciopesto* as inclusions. This suggests that grog derived from the grinding of ceramic materials of local production.

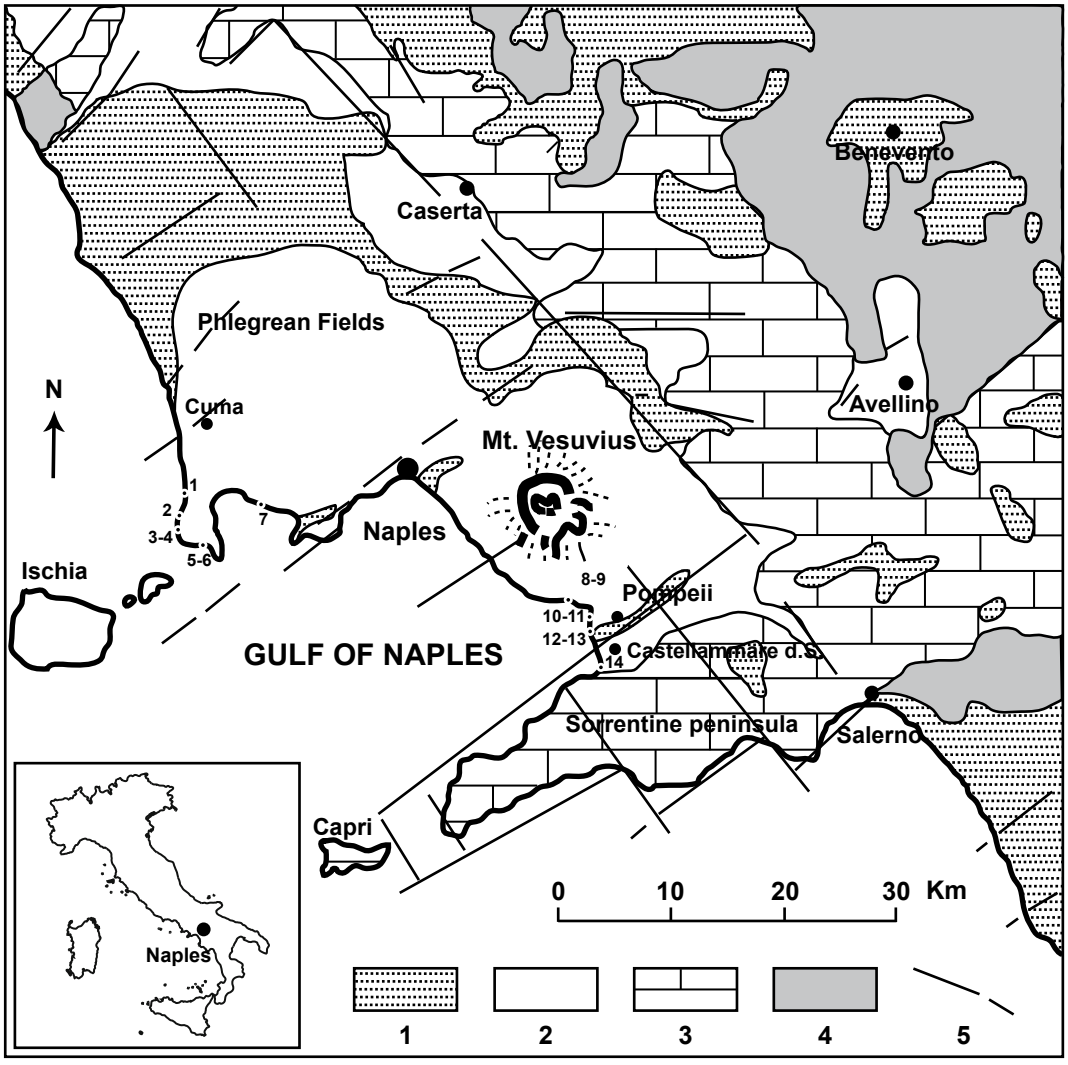

Figure 4. Geological sketch of the Mount Somma-Vesuvius and surrounding areas. 1. Alluvial, lacustrine and coastal sediments; 2. Potassic to ultrapotassic lavas and volcaniclastic deposits; 3. Limestone and dolostone; 4. Silico-clastic and carbonate deposits, evaporates; 5. Faults.

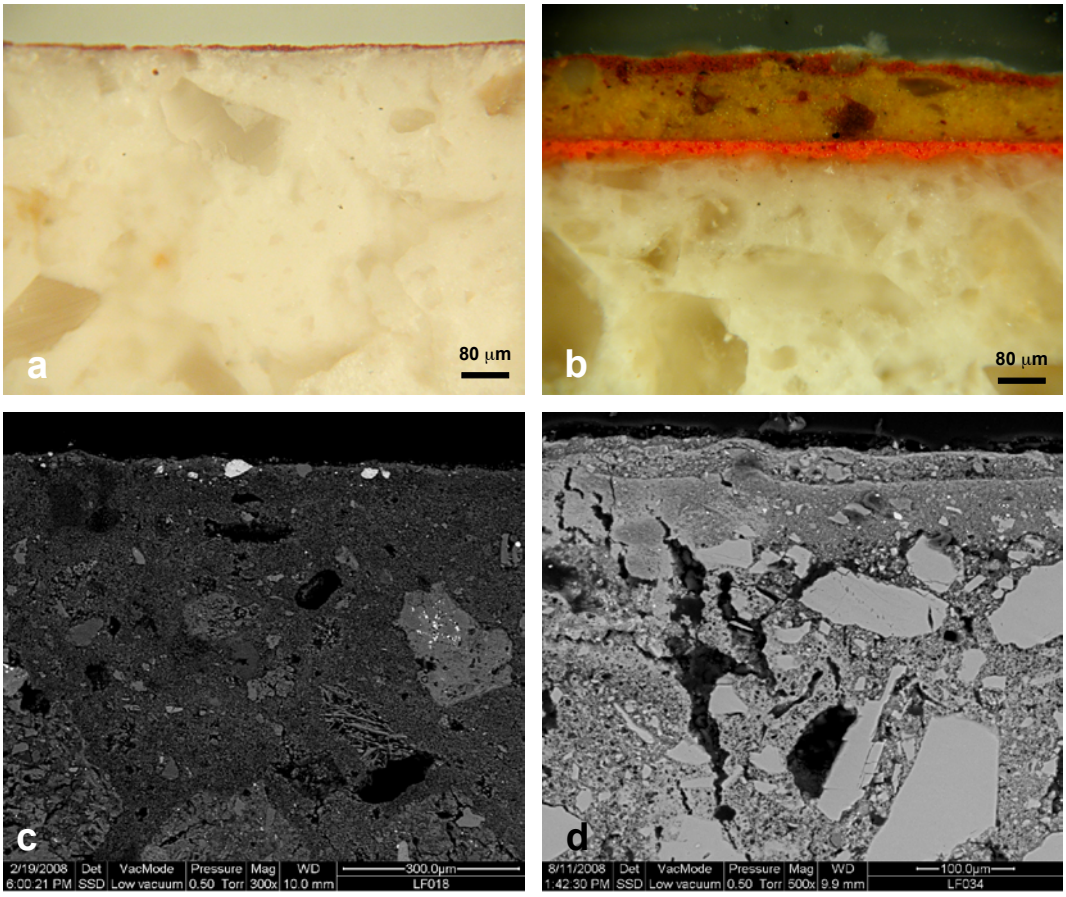

Figure 5. Reflected light micrographs of wall painted samples considered in this study. a) single-layer painting; b) multi-layer colour painting. BSE images of wall paintings analysed in this study: c) *fresco* paint; d) *mezzofresco* paint.

The provenance of the aggregate used in *marmorino* is not unequivocally recognizable. A local origin for these raw materials is also possible, considering that limestone and dolostone formations are common in the area south and east of Pompeii (Figure 4 – Sorrentine peninsula).

At the top of the microstratigraphic sequence one or more painting layers have been recognised. Among the samples considered for the present study single-layer paintings are predominant (Figure 5a); but some cases of multilayer paintings are also present, with a maximum of three coloured layers (Figure 5b). The superimposition of different colours is generally connected to the presence of drawings or decorations such as colour strips or geometrical figures (Figure 2e and f). Usually, a homogeneous colour was spread as a preparation layer, followed by the decoration, generally painted with a different and often more precious colour. Most of the samples here considered, showed continuity between the *intonaco* layer and the fist painting layer when observed under BSE (Figure 5c). On the contrary, all the second or third painting layers, and rarely some single-painted layers (e.g. sample LF035.V), display a clear discontinuity with the underlying painted layer (Figure 5d). In lime-based materials this discontinuity is constituted by a higher concentration of calcite and a lower porosity. This feature, as demonstrated in chapter 2, is one of the most powerful tools for the distinction of two of the most common lime-based painting techniques of the

fresco and *mezzofresco*, both widely utilized by the Romans artists. In paintings executed with the *fresco* technique, pigment is applied as a suspension in water onto a wet plaster. Consolidation occurs during carbonation of lime, so that only one layer of carbonation is formed on the surface. With the *mezzofresco* technique, pigment is mixed with a binding materials such as limewash (lime and water), and then applied on a dry lime plaster. In this case, a carbonation layer is observed on the surface of the plaster, and a second one on the top of the painted layer, derived from the limewash.

3. PIGMENTS AND RECIPES

The colour palette used in the buildings in the area of the Temple of Venus was determined by a combination of optical and electronic microscopy, colorimetry, FT-IR and Mössbauer spectroscopy. A list of the different colours, the related mineral composition and the set of analytical techniques used for their identification, is reported in Table 3. An estimate of the costs of the pigments per *libra* (almost 327 g) is also reported and discussed, on the basis of the study of Augusti (1967) who reported the prices described by Pliny in his "Naturalis Hystoriae", considering that one *denarius* was valued four *sestertii* and one *sestertius* four *asses*, and that in the first century AD the value one *denarius* corresponded to about 8 €.

Table 3
Preparation recipes. Number of samples, constituting pigments and list of samples for each recipe.

Recipes	N° of samples	Identified pigments		Samples
		Major components	Minor components	
Black 1	4	Coal black	-	LF022.N, LF026.N, LF033.N, LF125
Black 2	1	Burnt ochre	-	LF005
Black 3	1	Red ochre, coal black	-	LF126.N
Red 1	13	Red ochre	Yellow ochre	LF013, LF030.R, LF033.R, LF034.R, LF038, LF040, LF044.R, LF116, LF117, LF124, LF126.R, LF127.R, LF128.R
Red 2	4	Red ochre, yellow ochre	Clays, green earth, yellow glass	LF023.R, LF025, LF027.R, LF106
Red 3	4	Cinnabar	Red ochre	LF022.R, LF024.R, LF031.R, LF032
Yellow 1	3	Yellow ochre	Red ochre	LF015, LF028, LF102
Yellow 2	8	Yellow ochre and red ochre	Yellow glass, clays	LF008, LF010, LF018, LF099, LF107, LF126.G, LF127.G, LF128.G
Yellow 3	1	Red ochre, yellow glass	-	LF057
Yellow 4	1	Yellow and brown glass	Yellow ochre	LF007
Light blue	2	Egyptian blue	Yellow ochre, yellow glass	LF024.V, LF035.V
Green 1	3	Celadonite	Red and yellow ochre, Egyptian blue	LF030.V, LF031.V, LF034.V
Green 2	1	Red and yellow ochre, Egyptian blue, celadonite	Brown glass	LF036
Green 3	1	Celadonite, Egyptian blue	Red and yellow ochre	LF128.V
Grey	3	Yellow, red and brown ochre, Egyptian blue	Brown glass, cinnabar, glauconite	LF026.G, LF027.G, LF044.G
White 1	16	Lime, calcite	-	LF004, LF006, LF012, LF014, LF016, LF017, LF020, LF021, LF023.B, LF030.B, LF031.B, LF035.B, LF123, LF126.B, LF127.B, LF128.B
White 2	4	Lime	-	LF037, LF097, LF101, LF108

Colorimetric data were statistically treated, and the principal component analysis (PCA) indicates that the different hues are statistically well distinguished as shown by the PCA diagram (Figure 6) in which six populations of data clearly plot in different areas. PCA diagram was obtained plotting the principal components PC1 and PC2, which explained 51% and 40% of total variance, respectively. All the colorimetric data are listed in Table 4.

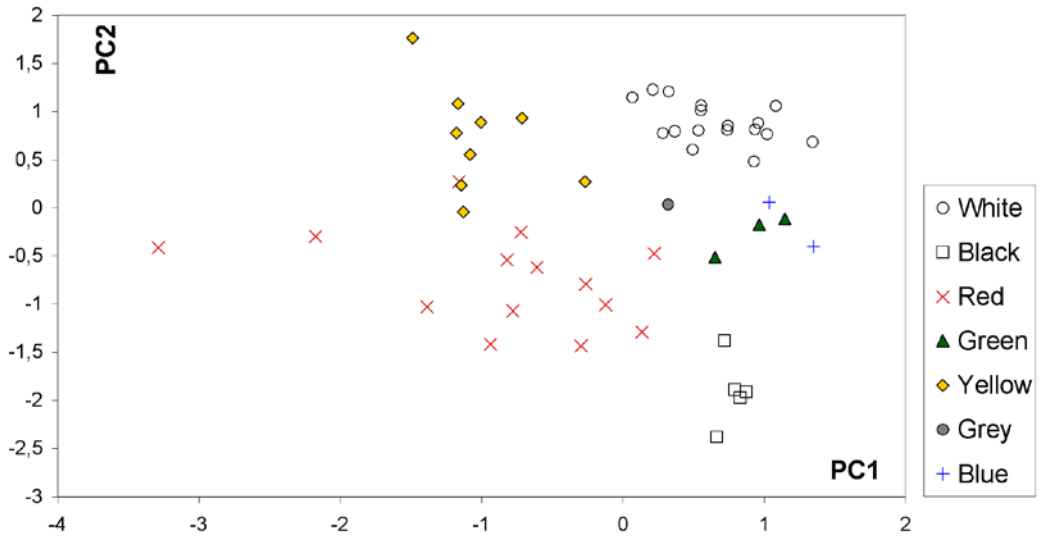

Figure 6. Plot of principal components PC1 and PC2 explaining 51% and 40% of total variance, respectively.

3.1 Black colour

The majority of the black paintings demonstrated to be made of a very fine-grained and black pigment which resulted to be opaque under TL-OM (Figure 7a), associated with rare colourless aggregates of fine-grained particles with high birefringence (interference colours of the third order or greater) (black 1 in Table 3). This second component resulted to be calcite, which may either represent a pigment used to correct the hue – see also section 3.7 – or be part of the binder. The above mentioned features are also confirmed by observation under RL-OM in thick section that always showed a homogeneous, opaque and thin black layer (in the range 0.02-0.07 mm) made by indistinct fine-grained particles (Figure 7b). Also BSE images did not allow distinguishing pigment particles, while EDS semi-quantitative analyses performed on selected areas showed a higher concentration of C with respect to the underlying preparation layers, the absence of P – which is present when bone black is used – and the absence of dark metal oxides (Figure 8). Other elements such as Ca, Al, Si, Na and K are also present in minor amounts, the first one related to the binder and the others are probably due to impurities. FT-IR analysis only revealed the presence of calcite, which is clearly the main constituent of the carbonate binder, and is characterised by the bands centred at 1400, 875 and 712 cm^{-1}, assignable to CO_3^{2-}. Also XRPD analysis only identified calcite, indicating the absence of any crystalline phase in the black paint (Figure 9).

Microtextural features, composition and spectroscopic data are consistent with the use of a pigment composed of amorphous carbon, such as flame carbon or lampblack

Table 4
Colorimetric analysis parameters.

Sample	Recipe	L*	a*	b*
LF026.N	Black 1	37.84	0.10	1.11
LF033.N	Black 1	45.68	1.68	3.70
LF125	Black 1	38.40	1.11	1.24
LF005	Black 2	37.44	0.90	0.64
LF126.N	Black 3	28.41	0.70	1.24
LF013	Red 1	50.29	24.72	22.57
LF038	Red 1	52.54	12.82	12.88
LF044.R	Red 1	47.11	15.43	10.63
LF117	Red 1	55.03	15.88	12.90
LF124	Red 1	43.49	11.49	6.86
LF126.R	Red 1	54.38	12.00	8.56
LF127.R	Red 1	41.79	16.99	9.74
LF128.R	Red 1	50.46	10.08	7.74
LF023.R	Red 2	48.13	8.58	4.79
LF025	Red 2	43.68	19.17	14.94
LF106	Red 2	55.53	12.42	16.25
LF022.R	Red 3	49.20	36.89	24.39
LF031.R	Red 3	60.47	7.76	7.80
LF015	Yellow 1	60.72	9.83	29.36
LF028	Yellow 1	69.66	10.16	36.53
LF102	Yellow 1	61.89	6.64	18.22
LF008	Yellow 2	62.38	12.84	23.74
LF010	Yellow 2	62.83	9.09	27.80
LF018	Yellow 2	66.43	7.96	25.36
LF107	Yellow 2	63.40	9.28	30.46
LF127.G	Yellow 2	57.91	13.68	22.42
LF057	Yellow 3	57.71	16.09	18.70
LF024.V	Light blue	65.09	-1.75	3.03
LF035.V	Light blue	68.08	-0.95	8.12
LF031.V	Green 1	59.89	3.25	6.59
LF036	Green 2	61.23	-4.95	9.93
LF128.V	Green 3	61.06	-2.56	9.68
LF044.G	Grey	63.00	3.48	12.83
LF004	White 1	83.13	2.11	8.23
LF006	White 1	85.98	1.37	4.49
LF012	White 1	80.27	2.81	11.30
LF014	White 1	77.72	3.38	13.37
LF016	White 1	73.81	3.15	13.26
LF017	White 1	78.31	5.30	18.85
LF020	White 1	83.57	1.96	9.64
LF021	White 1	82.56	2.22	9.42
LF023.B	White 1	74.73	4.34	15.56
LF123	White 1	87.84	1.70	9.03
LF126.B	White 1	79.46	3.80	18.82
LF127.B	White 1	76.09	1.23	9.11
LF128.B	White 1	81.57	3.16	14.38
LF037	White 2	81.54	3.15	11.11
LF097	White 2	75.67	3.87	14.99
LF101	White 2	80.43	2.89	14.48
LF108	White 2	80.44	3.45	17.66

(*atramentum*), a pigment constituted by fine-grained particles formed by the combustion of coal, wood, oil or other fuel (Eastaugh et al., 2004). Small quantities of this type of pigment were also used recognised in pictorial layers of different colour, such as some red and yellow ones, probably added to produce darker hues. Lampblack was commonly used all over the world from ancient times to present. The use of lampblack during Roman times is also documented by Bugini and Folli (1997) for the 1st century BC Roman wall paintings of the Capitolium in Brescia, Italy.

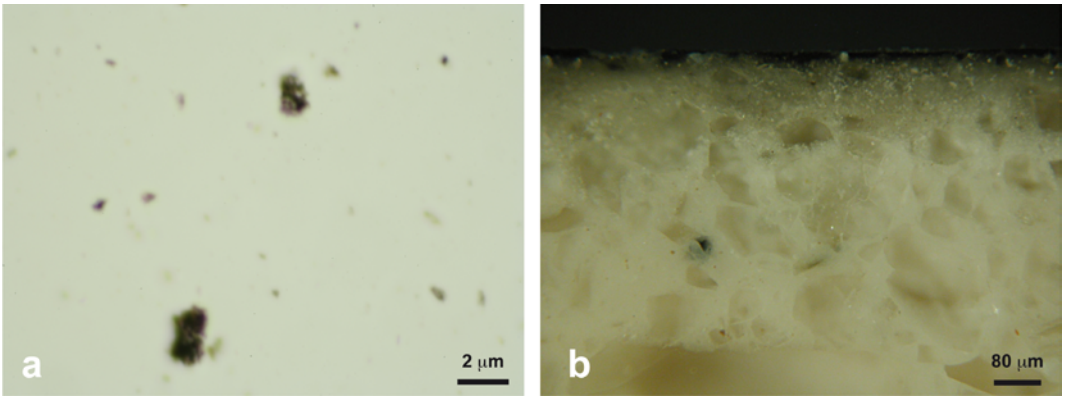

Figure 7. Black samples: a) PPL micrographs of carbon particles; b) XPL micrographs of black painting layer.

Three of the samples of black paint were collected from units of uncertain age, although two of them are (LF022.N, LF026.N) from the Imperial Age l.s., while a fourth one (LF125) belongs to a 1st century BC unit, the same age of the samples described by Bugini and Folli (1997).

Two additional black samples were also analysed. The first one (black 2 in Table 3, sample LF005) belongs to a Julio-Claudian Age unit. RL-OM and TL-OM displayed a relatively thick black layer (up to 0.40 mm) made of fine-grained particles with rare coarse grains of brown ochre. The presence of this pigment was also confirmed by the XRPD, which showed the typical reflections of partly hydrated iron oxide and haematite phases constituting the burnt ochre (Figure 10). Also in this case the binder is constituted by calcite as shown both by FT-IR and XRPD analyses. BSE images and EDS analysis showed that Fe-rich particles (burnt ochre) are rare but well distributed in the painted layer.

The last black sample (black 3 in Table 3, sample LF126.N) belongs to a stratigraphic unit of the 1st century BC, and under RL-OM displays a homogeneous black layer composed of flame black and very small amounts of homogeneously distributed dark red ochre fragments in a carbonate binder, as also indicated by XRPD, FT-IR and EDS analyses.

3.2 Red colour

Red colours are the most commonly used (Table 3). The RL-OM analysis showed that red layers are characterised both by indistinct small red and medium in size deep-red particles. Thickness of the layers ranges from 0.01 to 0.30 mm and the pigment appears unevenly

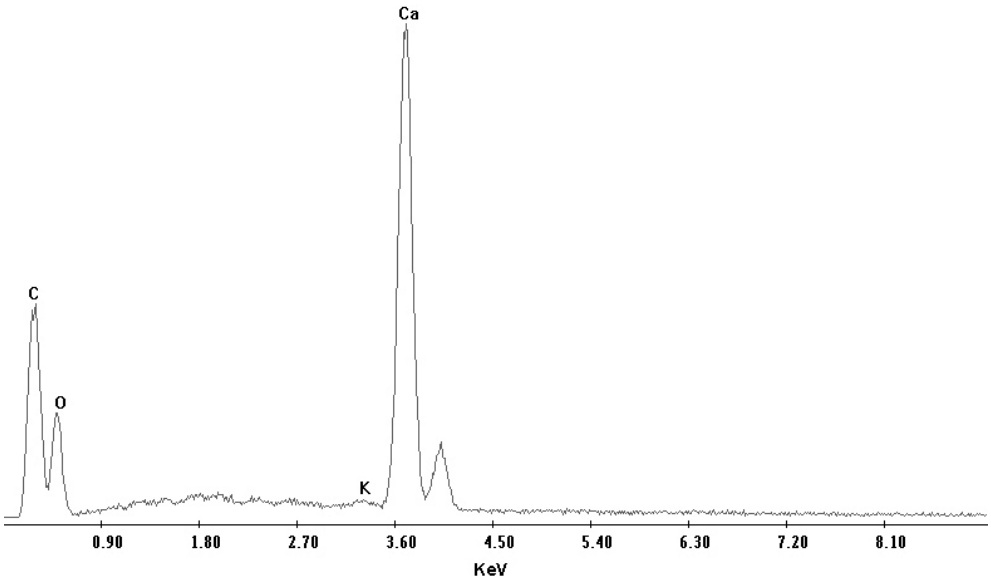

Figure 8. EDS spectrum of a black layer.

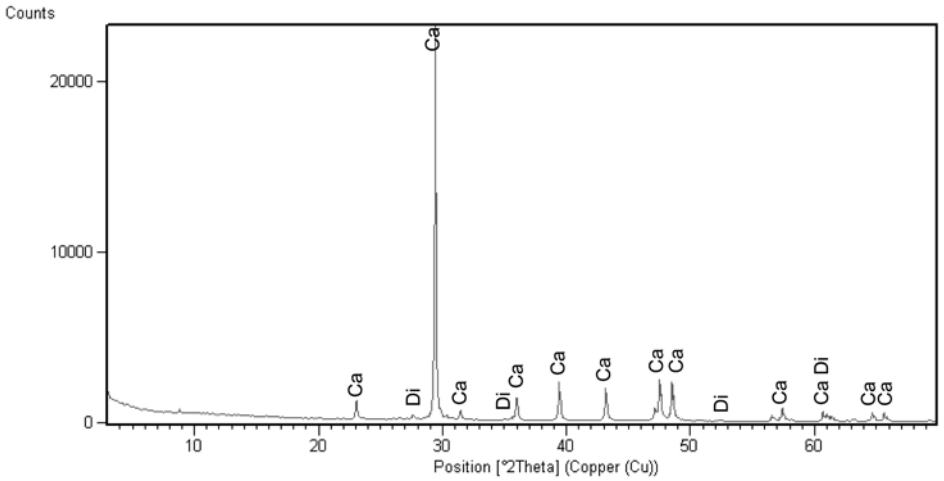

Figure 9. XRD pattern of a black sample with identified mineral phases: calcite (Ca) and diopside (Di).

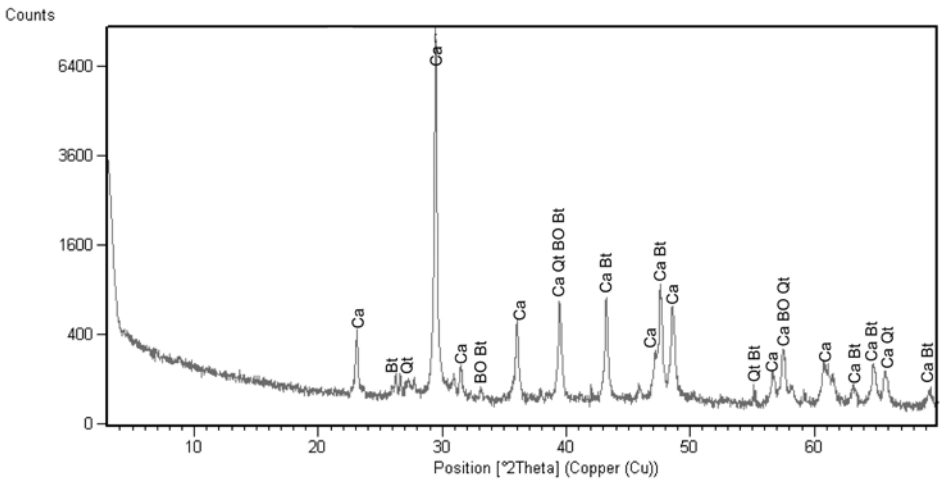

Figure 10. XRD pattern of a black sample with the following mineral phases: calcite (Ca), biotite (Bt), quartz (Qt) and burnt ochre (BO).

distributed, sometimes particles are scanty, sometimes they are abundant (Figure 11a, b). TL-OM study under plane-polarised light identified translucent to opaque red, orange and brown particles of various sizes, from very fine- to medium-grained, or more frequently aggregates of high relief fine-grained crystals (Figure 11e). Under crossed polars the interference colours are typically masked by the strong body colour. BSE images revealed the presence of several mineral phases with high atomic number (bright grains in the BSE image), which display high amounts of Fe (20-50 wt%) (Figure 12a, 13). All these data suggest that the colouring agent is a red ochre. XRPD analysis confirmed this evidence identifying haematite as the main mineral phase. FT-IR spectra showed the characteristic bands of the carbonate at 1400, 875 and 712 cm^{-1}, and the presence of Fe oxide and hydroxide, marked by the weak signals between 3600 and 3400 cm^{-1} (Figure 14).

All the analyses revealed, in the majority of the red samples, very low amounts of other minerals such as calcite, quartz, yellow ochre and particularly pure dark red ochre. A red powder discovered within the area of the temple (LF040), displayed the same composition and purity. Under TL-OM, XRPD and FT-IR this material appeared only composed by haematite with a very low amount of calcite (Figure 15), indicating that it probably represent an abandoned bunch of pigment. Samples with lighter red hue display smaller quantities of haematite (Figure 11a), whereas darker ones are made of pure haematite (Figure 11b). Orange-red hue was obtained by adding 20-30% of yellow ochre (which will be described in sections 3.3) to the same red ochre. The same recipe was identified in three orange-red samples (red 2 in Table 3). These samples also contain small amounts of the same impurities, such as clay minerals, green earth and yellow glass fragments (Figure 11c).

Red ochres form in the oxidised, weathered portions of iron-rich mineral deposits, especially those associated with so-called volcanic massive sulphide (VMS) deposits where they are derived from the breakdown of minerals such as iron pyrite and chalcopyrite and also from the direct weathering of haematite (Eastaugh et al., 2004). Ochres may also form in many environments as soils, concentrating haematite derived from the underlying bedrock. Red ochres may be also artificially produced by roasting yellow, brown or red ochres in air which will convert iron oxide hydroxides and iron oxides to the stable iron(III) oxide; in some cases it may be difficult to distinguish these burnt ochres from naturally occurring red ochres (Eastaugh et al., 2004). Washing, levigation and grinding natural or artificial red ochres produce red ochre pigments with various red shades.

The samples here analysed suggest that the majority of the red colours were prepared using an extremely pure starting material, which was selected and deliberately mixed by the artists with other pigments, in order to obtain the desired hues. In order to confirm this statement, three samples of red colour made of pure haematite (LF013, LF126.R, LF127. R) were studied also under Mössbauer spectroscopy. The spectra present the typical signal of oxide/oxyhydroxide species (Figure 16a, b); the parameters of haematite have been compared to literature data of pure phases recorded by transmission experiments in Murad

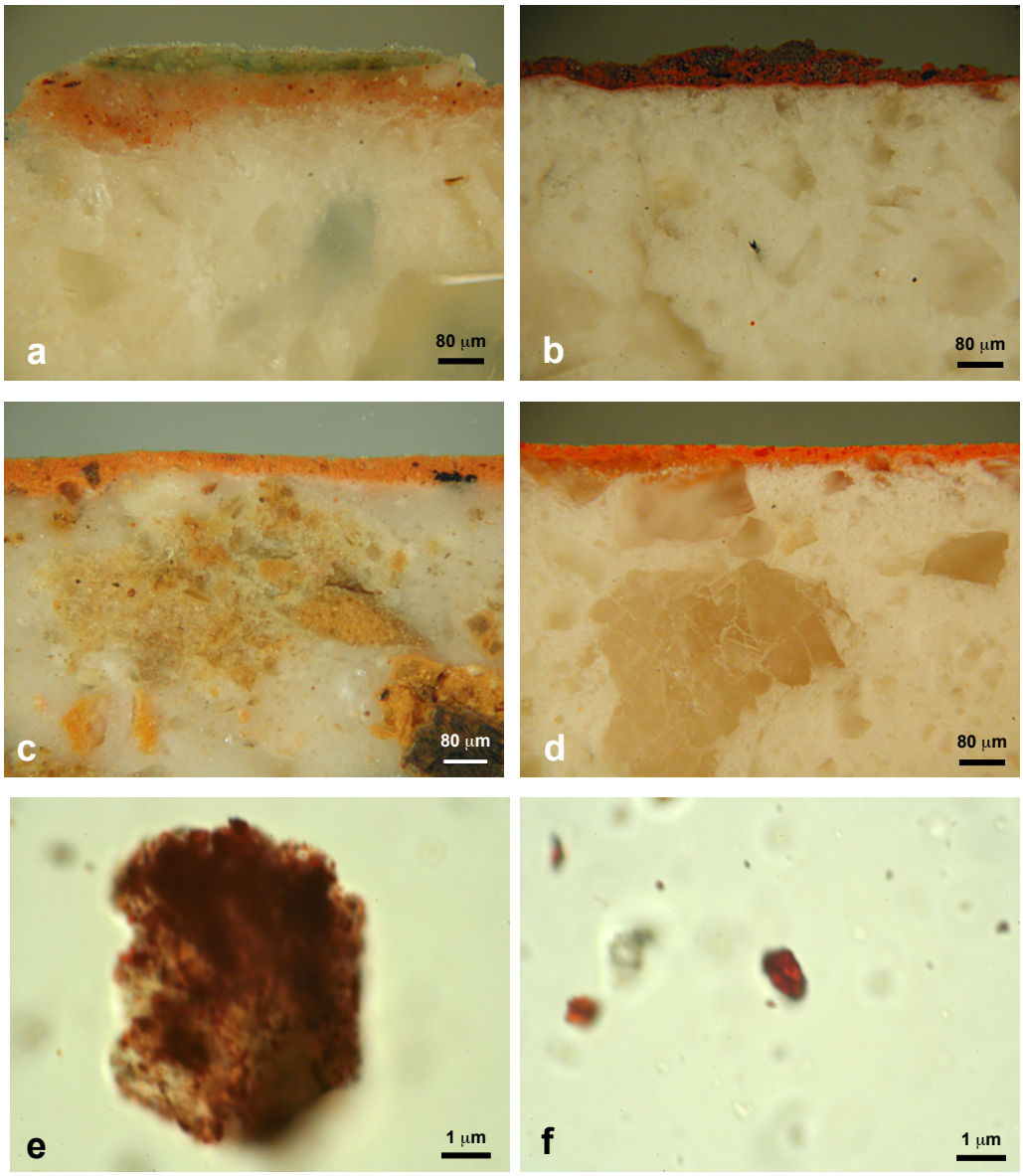

Figure 11. Red samples. Reflected light micrographs of: a) multi-layer painting with pale red paint under a thin green paint; b) single-layer dark red; c) orange-red layer on a *cocciopesto* preparation layer; d) orange-red (cinnabar) layer on a *marmorino* preparation layer. PPL micrographs of: e) red ochre; f) cinnabar. All images taken in PPL.

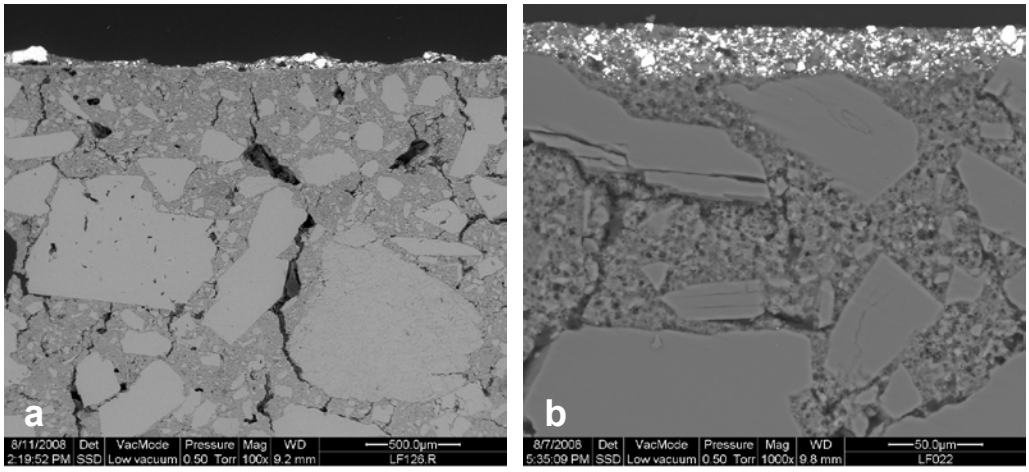

Figure 12. BSE images of the following wall painting samples: a) red ochre; b) cinnabar.

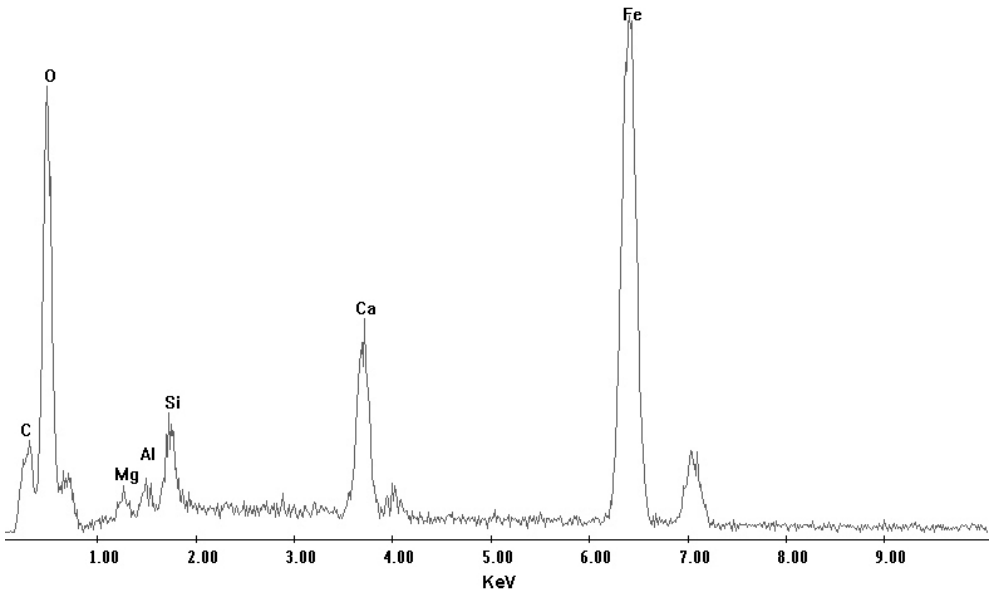

Figure 13. EDS spectrum of a red particles in a red layer (red ochre).

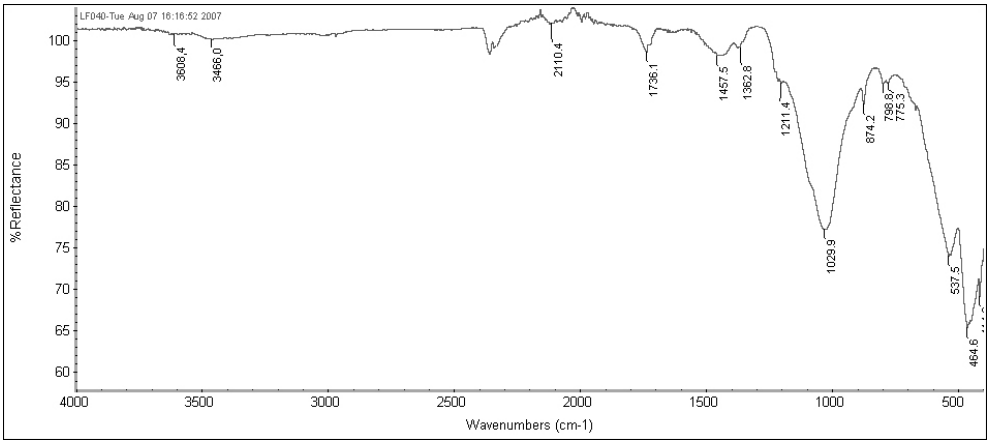

Figure 14. FT-IR spectrum of a red layer.

and Johnston (1987). The high value of B (magnetic field) in the haematite is representative of high purity and well-crystallized haematite (Table 3). Only one of the analysed samples (sample LF013) shows a doublet attributable to silicate and/or nanosized oxide/oxyhydroxide particles. Considering that Si content as measured by non-destructive XRF performed on the surface of the painting resulted to be extremely low and that, with the exception of rare crystals of quartz, silicates are completely absent, the doublet observed in the spectrum of sample LF013, is more probably to be ascribed to nanosized oxide/oxyhydroxide. The hyperfine parameters relative to the studied sample are reported on Table 5.

The evaluation of the original colour of samples which now appear red and are made of red ochre is often difficult to ascertain in Pompeii. There is evidence that many yellow wall paintings turned into red during the Mont Vesuvius eruption in 79 AD when coming in contact with the pyroclastic flow. At 230-280°C goethite (FeOOH) turns into haematite with disordered structure releasing water (Eastaugh et al., 2004). These temperatures are realistic

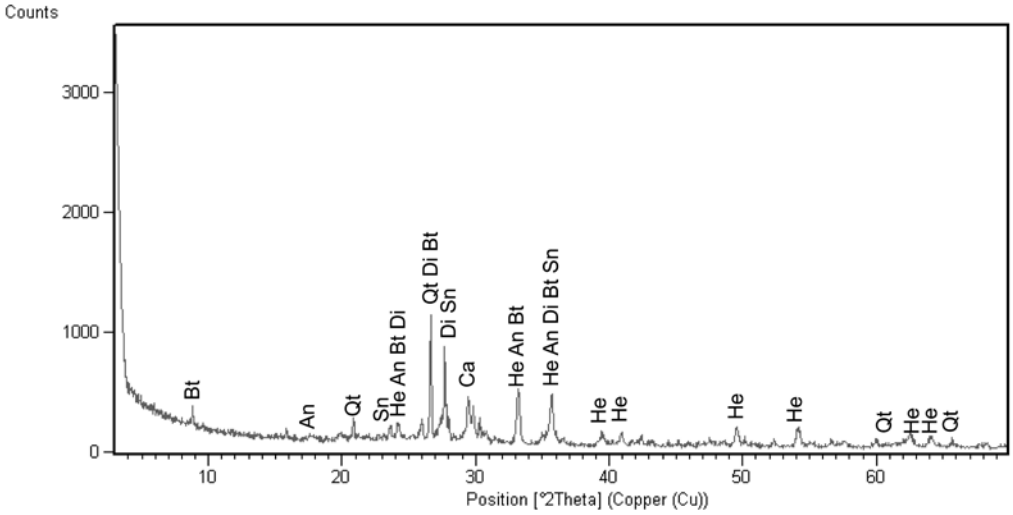

Figure 15. XRD pattern of a red sample with the following mineral phases: calcite (Ca), haematite (He), biotite (Bt), analcime (An), quartz (Qt), diopside (Di) and sandine (Sn).

for a pyroclastic flow. In particular, Cioni et al. (2004) estimated temperatures in the range 180-380°C – with maximum frequency between 240 and 340°C – by measuring the thermal remanent magnetization of lithic clasts and tiles carried by the pyroclastic flow. The samples analysed in this work were all collected from buried units and therefore they did not come into contact with the pyroclastic flow of the 79 AD eruption, suggesting that the observed colour is related to the original red ochres paintings.

Table 5
Mössbauer parameters of the analyzed samples. The d values refer to a Fe calibration collected at room temperature.

Sample	d (mm/s)	D/e (mm/s)	G (mm/s)	H_{int} (T)	Area (%)	Attribution
LF013	0.37	-0.17	0.50	50.4	75	Haematite
	0.35	0.82	0.94		25	Nanosized haematite
LF126.R	0.37	-0.18	0.40	51.0	100	Haematite
LF127.R	0.36	-0.19	0.41	51.8	100	Haematite
LF015	0.38	-0.30	0.50	37.2	68	Goethite
	0.36	0.96	0.90		32	Nanosized goethite
LF128.G	0.37	-0.26	0.53	37.74	100	Goethite

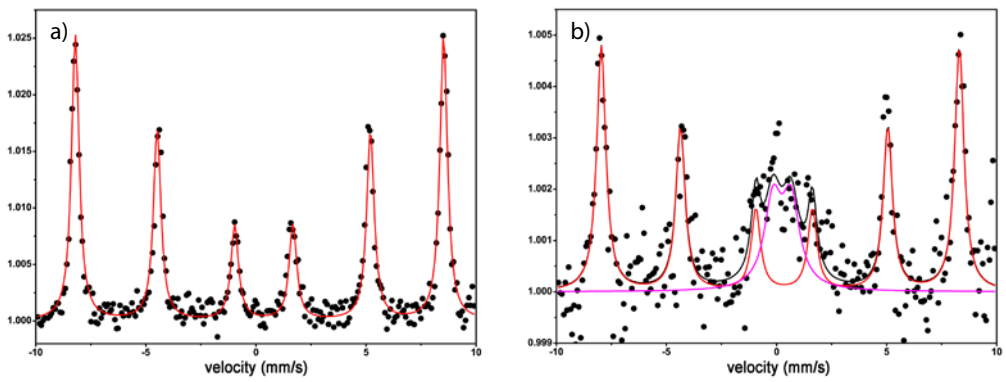

Figure 16. Backscattering Mössbauer spectra of: a) LF127-R, b) LF013. Red line represents haematite, ciano lines nanosized oxide/oxyhydroxide particles.

According to Augusti (1967) Pliny reported that red ochre (*cicerculum*) is a relatively inexpensive pigment (8 *asses* per *libra*). Red ochres were widely used in Roman art (i.e. see Bèarat, 1997, Meggiolaro et al., 1997, Bugini and Folli, 1997; Kakoulli, 1997; Fuchs and Bèarat, 1997; Varone and Bèarat, 1997; Edwards et al., 2002; Damiani et al., 2003 and Villar and Edwards, 2005).

Four of the red samples resulted to bear cinnabar pigment (red 3 in Table 3). Under RL-OM they showed a very thin and brilliant-red painted layer from 0.02 to 0.04 mm thick made of very fine-grained red particles (Figure 11d). Under TL-OM in PPL these particles exhibited very strong red-orange body colour weakly pleochroic from pale to deep red-orange and extremely high relief. Particles sometime display rectangular or columnar shape due to the prismatic habit with perfect cleavage but predominantly the shape is irregular with conchoidal fracture (Figure 11f). Under XPL particles grow a deep red due to high interference colours masked by the body colour and the strong internal reflections. XRPD and FT-IR identified traces of cinnabar, which are still relevant, considering that only small amounts of this pigment are necessary to obtain a deep red painting. However, ESEM-EDS analysis showed several particles with high mean atomic number, which resulted to be rich in Hg and S (Figure 12b and 17), confirming the presence of cinnabar, while the presence of C, O and Ca are due to the carbonate binder.

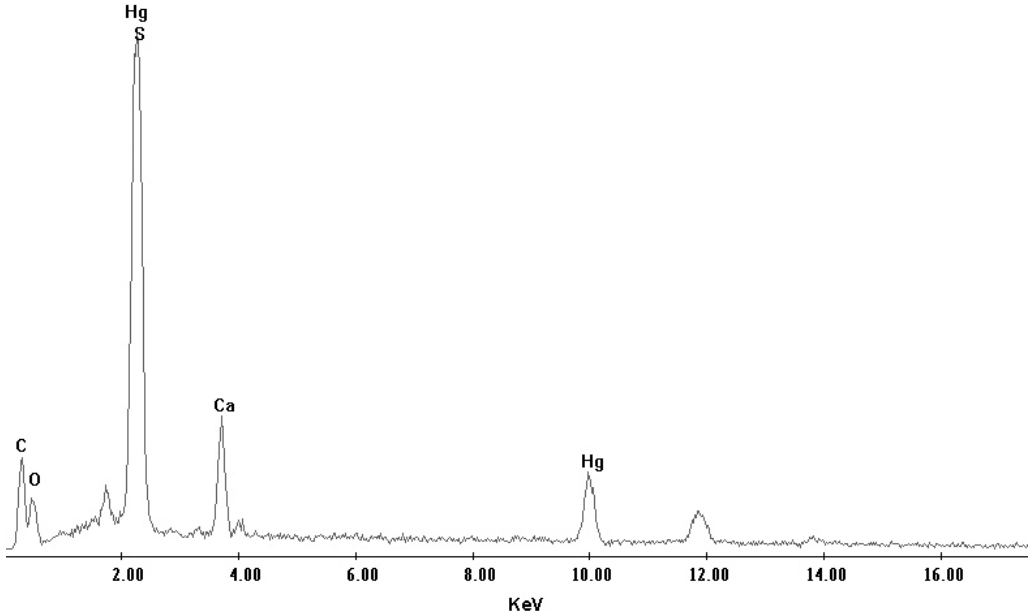

Figure 17. EDS spectrum of a red particle in a red layer (cinnabar).

BSE images revealed the absence of discontinuity between the preparation layer and the painting, suggesting that paint was applied using the *fresco* technique (see chapter 2 in this thesis for more details). It is worth reporting that in two of these cases (LF022.R, LF031.R) cinnabar occurred as the only pigment, if we exclude the presence of few particles of calcite and lime observed by TL-OM, which are probably derived from the underlying

plaster. There are only few cases in the literature describing the use of cinnabar as a pure pigment (Fuchs and Béarat, 1997; Wallert and Elston, 1997; Mazzochin et al., 2004; 2003). In the other two cases, cinnabar was used in conjunction with haematite presumably to both save this valuable pigment and brighten haematite red. The same recipe was also identified by Rozemberg (1997) in Israel, Meggiolaro et al. (1997) in Greece and Kakoulli (1997) in Cyprus.

Despite the presence of significant sources of the mineral cinnabar, much of the mercury sulphide used historically as a pigment in post-Classical times seems to be synthetic (Eastaugh et al. 2004). The term for the synthetic cinnabar is *vermilion*, which unfortunately is generally indistinguishable from the natural one. In Roman times this pigment was also named *minium*, though now this term exclusively refers to lead tetraoxide, and was considered both by Vitruvius and Pliny as one of the most precious pigments, with a cost of about 70 *sestertii* per *libra* (Augusti, 1967).

Although the exact age of the cinnabar-bearing paintings is unknown, the archaeological excavation context clearly indicates that they derive from buildings of the Imperial Age l.s. (Table 1). On the contrary the red paintings exclusively made of haematite display a chronological distribution from the 4th-3rd centuries BC to the 1st BC, indicating that they were probably used only in Republican times. As regards paints obtained by mixing red and yellow ochres (red 2 in Table 3) one sample (LF106) has been archaeologically dated to the second half of the 2nd century BC, and the other three samples have an Imperial age l.s., suggesting that in Imperial times red ochre was mainly used for orange-red paintings.

3.3 Yellow colour

Four different recipes have been recognised for the yellow colour (Table 3). The majority of the yellow paintings appear under RL-OM as a thin pale yellow layer from 0.02 to 0.05 mm thick (Figure 18a), although in some cases (samples LF107, LF0126.G) the painted layer is rather irregular, with thickness up to 0.3 mm (Figure 18b). Sometimes the limit between the paint and the *intonaco* may be difficult to distinguish, especially when this is made of *cocciopesto* (Figure 18c, d). TL-OM analysis under PPL showed that the pigment is made of translucent yellow particles with predominantly fine and medium grain size and moderate relief (Figure 18e), associated with few scattered medium grain-sized orange particles. Under XPL pigment grains display high birefringence, and interference colours are strongly masked by the body colour. XRPD analysis identified calcite, goethite and other iron hydroxides (Figure 19). FT-IR spectra also showed the characteristic bands of carbonate (1400, 875, 712 cm^{-1}) and the presence of oxide and hydroxide (weak signals between 3600 and 3400 cm^{-1}). EDS microanalyses performed on particles with a high mean atomic number (i.e. brighter in BSE images) revealed high concentration of Fe (between 15 and 35 wt%) (Figure 20a), confirming that pigment is mainly made of iron hydroxides. In many samples different proportions of red ochre have been also detected.

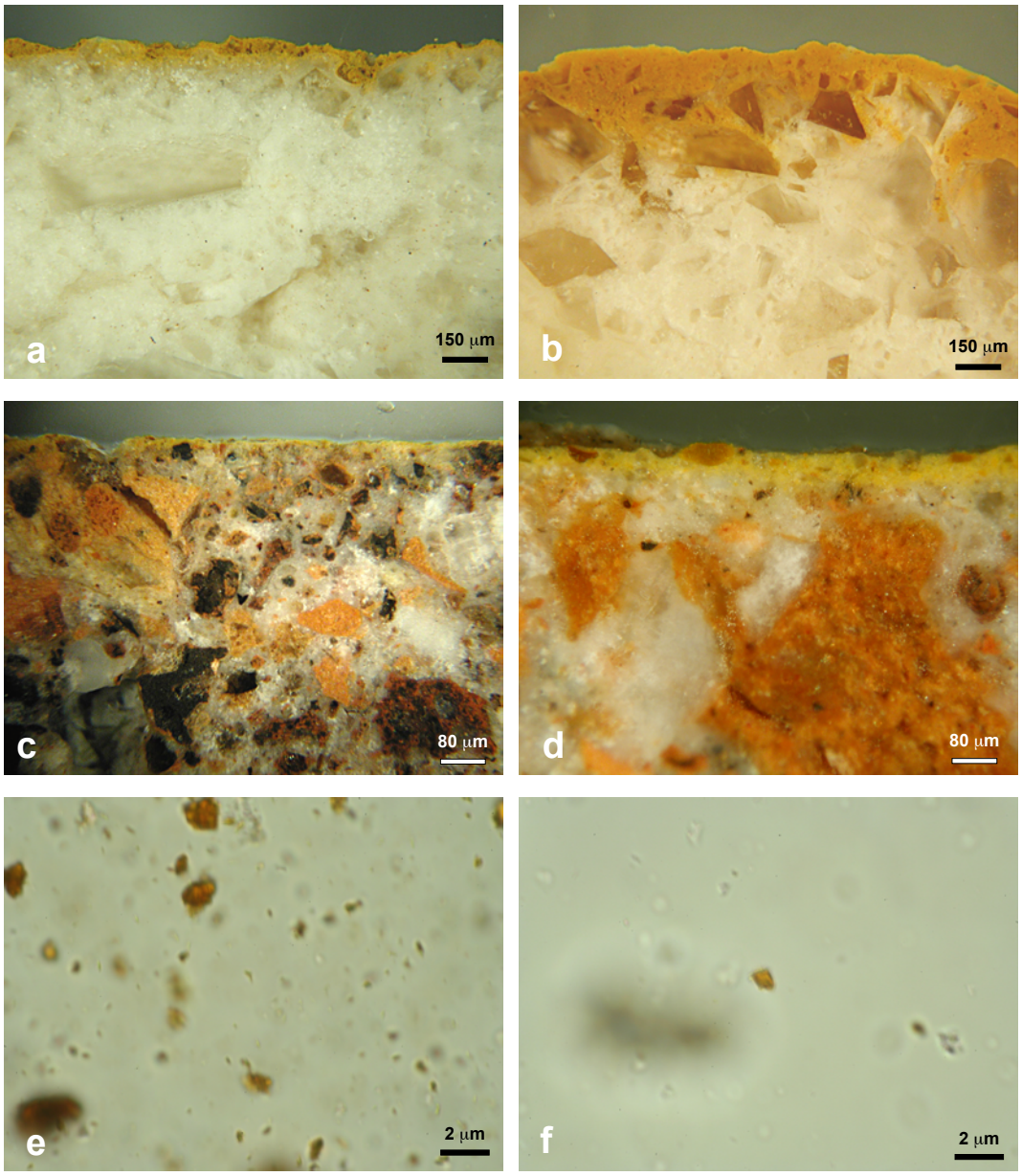

Figure 18. Yellow samples. Reflected light micrographs of: a) thin yellow layer on a *marmorino* preparation; b) thick yellow layer on a *marmorino* preparation; c) yellow layer on a *cocciopesto* preparation; d) yellow layer on a *cocciopesto* preparation with yellow glass particles. Polarising light micrographs of: e) yellow ochre; f) yellow glass. All images have been taken in PPL.

In few cases glassy yellow and brown fragments, displaying irregular shape and conchoidal fractures, have been recognised under TL-OM and RL-OM (Figure 18d and f). Under XPL these particles showed complete optical extinction. XRPD and FT-IR did not recognised any crystalline phase, a part from calcite of the binder, while EDS microanalysis showed that pigment particles have a silicate composition, containing Si, Al, Fe, Mg, Ca, Na, K and traces of other chemical elements (Figure 21a). EDS analyses were also performed on grains of yellow volcanic glass constituting the aggregate of the underlying *intonaco* and that of other mortars from the Temple of Venus, providing similar compositions (Figure 21a, b). EMPA microanalyses were performed on the pigment yellow grains and their compositions (Table 6) resulted to be compatible with those of the trachyandesitic-phonotephritic glasses

of the Somma-Vesuvius when plotted in the TAS diagram (Figure 22). This indicated that the yellow and brown glasses identified as pigments probably derive from a natural volcanic glass, which was deliberately ground by the artist to produce a yellow pigment.

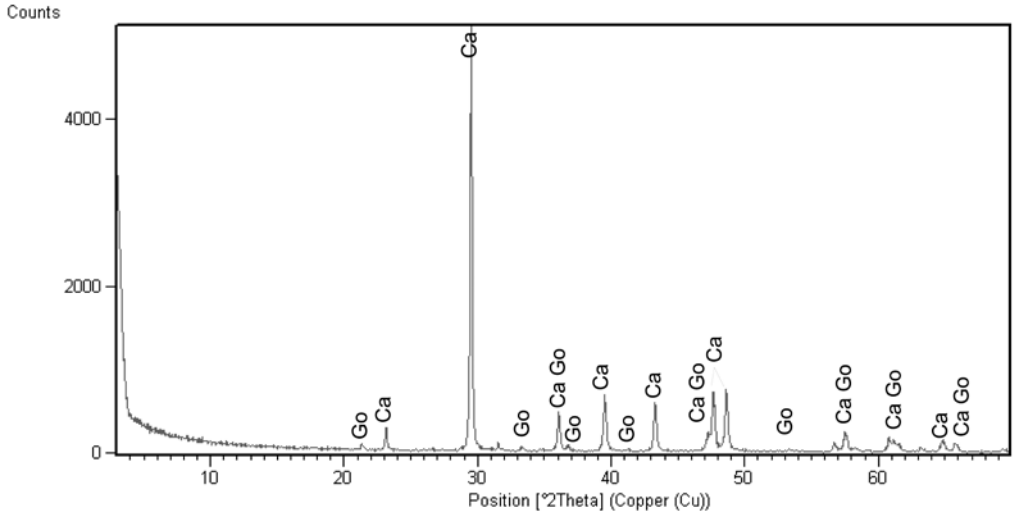

Figure 19. XRD pattern of a yellow sample with the following phases: calcite (Ca) and goethite (Go).

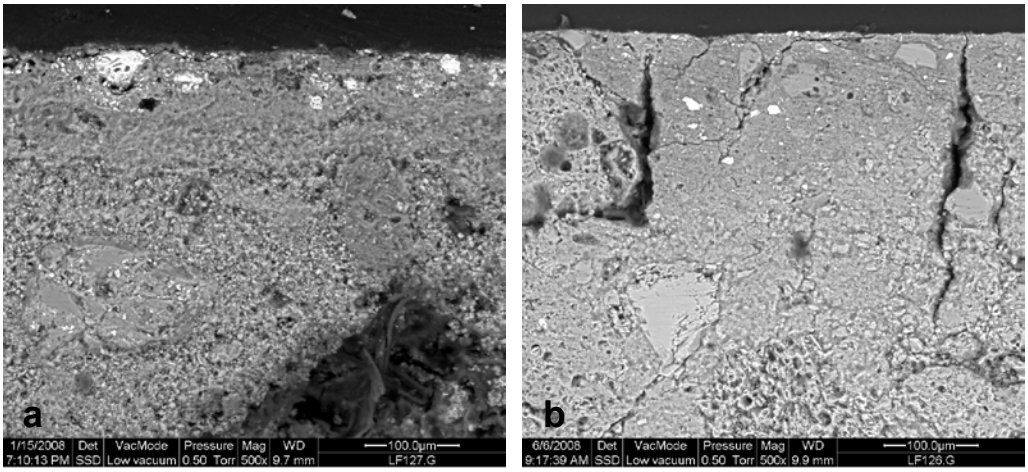

Figure 20. BSE images of wall painting samples analysed in this study: a) yellow ochre; b) yellow ochre in thick painting layer.

Considering the different components recognised in the yellow paints, four different recipes can be recognised, most of which based on the presence of a yellow ochre. The first recipe (yellow 1 in Table 3) refers to a pigment prevalently made of yellow ochre with traces of red ochre, which has been mainly used for paintings belonging to the second half of the 2nd century BC, but is also testified in an Imperial Age sample (LF028). The second recipe (yellow 2 in Table 3) also refers to a pigment rich in yellow ochre but with a higher content in red ochre (about 20-40% of the total pigment). These pigments also contain traces of a yellow glass and clay minerals. The majority of the yellow paints here considered were prepared according to this recipe, which resulted to have a wide chronological distribution, from the end of the 4th century BC to the Julio-Claudian Age, with the exception of the

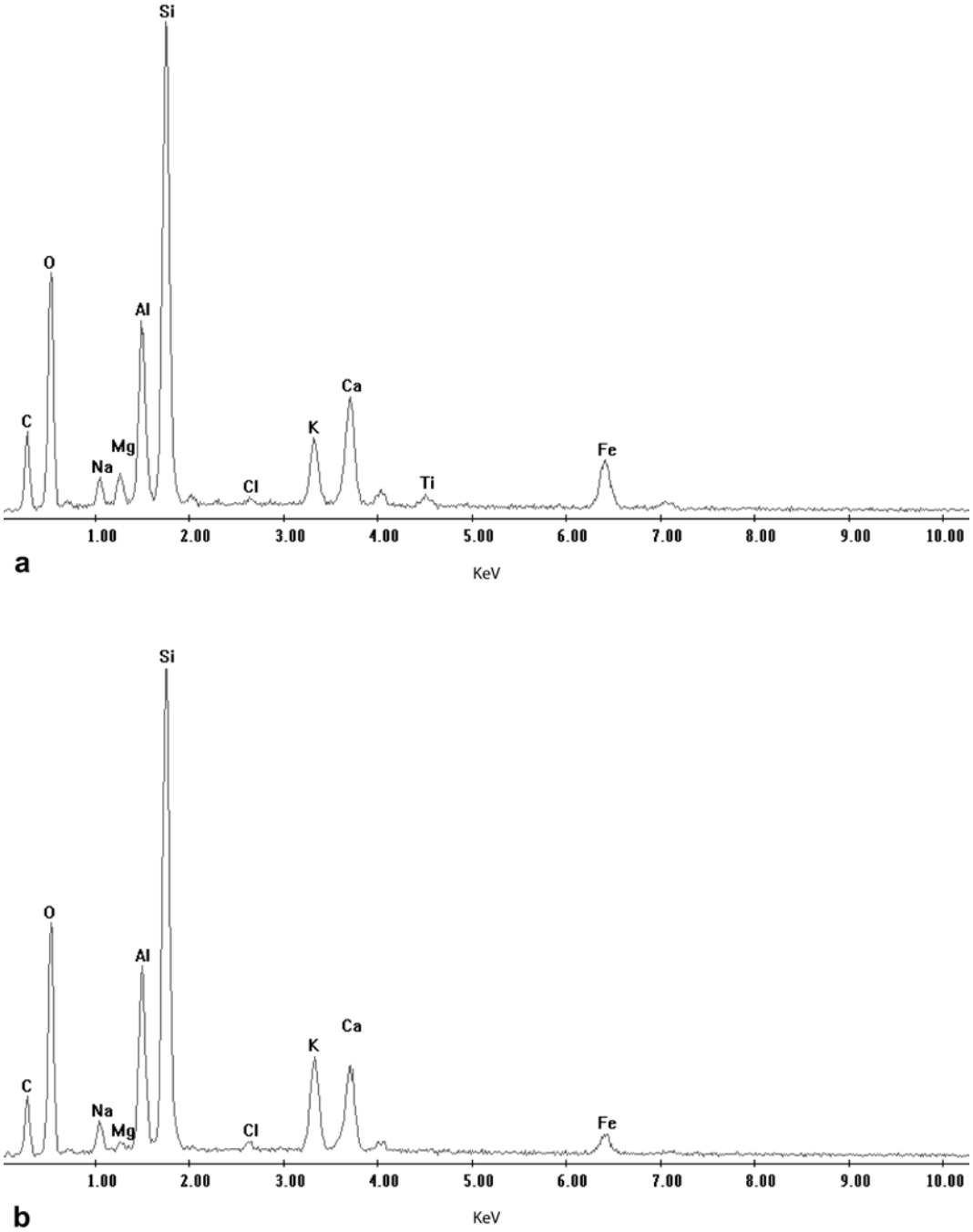

Figure 21. EDS spectra of yellow glassy particles: a) yellow glass in the painting layer; b) yellow glass in the plaster aggregate.

Augustan Age. The third recipe (yellow 3 in Table 3) represented by a single sample collected in a stratigraphic unit of the end of the 4th – 3rd century BC (LF057), is characterised by the prevalence of red ochre with a 20% of yellow glass. An additional recipe (yellow 4 in Table 3) describes a pigment prevalently composed by yellow and brown glasses with traces of yellow ochre, observed in a single sample Julio-Claudian in age (LF007). All these observations indicate that yellow ochre and yellow glass pigments were used in different paint recipes from Republican to Imperial times.

Table 6
Chemical composition of major elements (wt.%) for analysed grains of yellow glass pigment.

Analysis	SiO_2	TiO_2	Al_2O_3	FeO	MnO	MgO	CaO	Na_2O	K_2O	Cr_2O_3	Sum
LF007-1	50.48	1.11	16.55	7.99	0.25	2.65	8.37	3.30	5.38	0.03	96,11
LF007-2	51.84	1.18	16.25	8.11	0.15	2.07	11.09	3.04	5.25	0.12	99,10

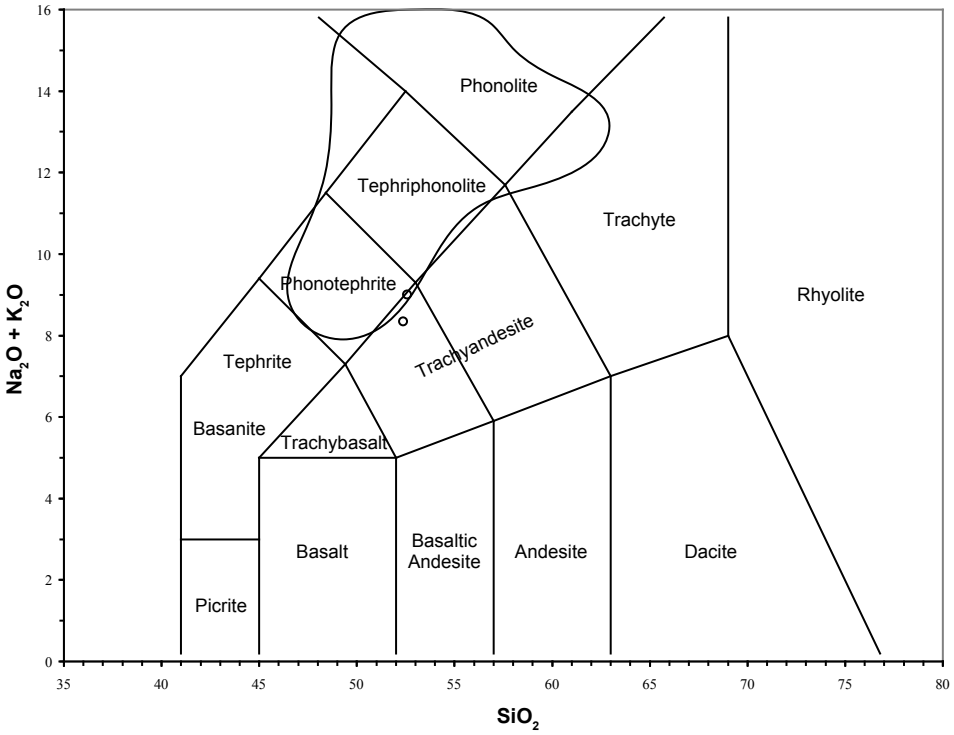

Figure 22. Total Alkali Silica diagrams of yellow glass particles (circles). Continue line delimits composition of glasses from Somma-Vesuvius volcanic deposits (unpublished data, Grifa, pers. comm.).

In all the samples, BSE images showed that the pictorial layer is well adherent to the preparation layer, without any net discontinuity, also in the samples in which the pictorial layer is particularly think (Figure 20b). This suggests that paint was applied on a wet surface and therefore that the adopted painting technique was the *fresco*. Nevertheless, the thickness of the samples LF107 and LF126.G and the dispersion of the particles within the entire painted layer suggest that sometimes pigment was mixed with limewash.

Two samples were also studied under Mössbauer spectroscopy (LF015, LF128.G), the former being a yellow 1 – i.e. made of yellow ochre – and the latter a yellow 2 – i.e. made of both yellow and red ochres. The spectra present the typical signal of oxide/oxyhydroxide species (Figure 23a and b). The parameters well fitted with those of goethite, as described by Murad and Johnston (1987). Also in this case, one of the analysed samples (LF015, Figure 23b) showed a doublet attributable to nanosized oxide/oxyhydroxide particles because of the absence or shortage of silicates. This data were also confirmed by XRPD, FT-IR, EDS and non-destructive XRF analyses, performed on the surface of the painting. The hyperfine parameters relative to the studied sample are reported in Table 5.

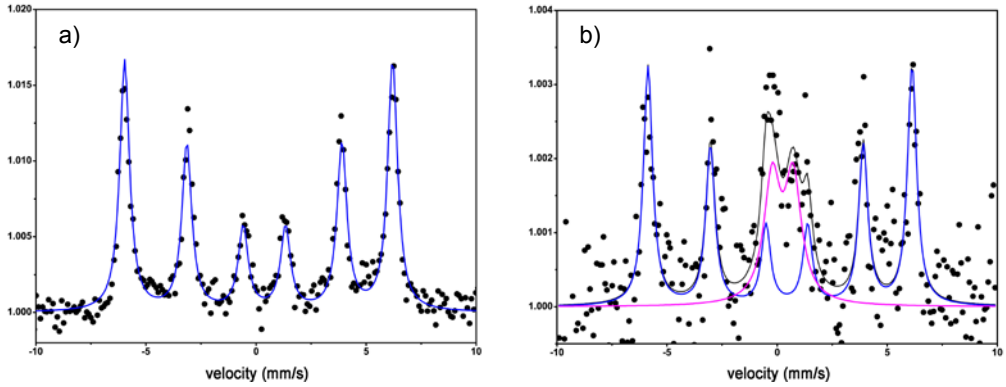

Figure 23. Backscattering Mössbauer spectra of: a) LF128-G; b) LF015-G. Blue line represents goethite; ciano lines nanosized oxide/oxyhydroxide particles.

Yellow ochres are composed primarily of goethite, which may derive from iron-rich soils or decomposition of ore deposits. In these cases it will be generally impure, the other phases associated being commonly quartz, feldspar, clay minerals and/or carbonate minerals in association with minor amounts of the red iron(III) oxide haematite (Eastaugh et al., 2004). As already described in the case of red ochre, also yellow ochres were widely used in Roman times (i.e. Bèarat, 1997; Meggiolaro et al., 1997; Bugini and Folli, 1997; Edwards et al., 2002; Villar and Edwards, 2005). According to Pliny the yellow ochre (*sil*) was an inexpensive pigment with a cost of approximately 2 *denarii* (32 *asses*) per *libra*. As regards the use of yellow and brown glasses as pigments, what discovered in this work represents the first evidence ever published of a pigment which was ignored even in the classical literature.

3.4 Light blue colour

This paint is characterised under RL-OM by the presence of fine- to medium-grained blue particles (up to 0.07 mm) homogeneously distributed in a thin light-blue layer with a thickness of 0.05 to 0.15 mm (Figure 24a, b). On the same samples TL-OM observations in PPL revealed the presence of glassy blue particles sometimes pleochroic from blue to pale blue with high relief, anhedral morphology and broken angular, sometimes displaying reddish hues (Figure 24c). In XPL the rare well-crystallised blue fragments show high birefringence partially covered by the pigment colour (Figure 24d). Moreover, when observed through a Chelsea filter, all blue particles transmit a dull red colour. Blue particles in BSE images appeared composed of different mineral phases also distinguishable on the basis of their atomic number contrast. Phases with high atomic number (Figure 25a, b), which appear bright in BSE images, resulted to be composed, in order of decreasing abundance, of C, O, Si, Cu and Ca, which is characteristic of the calcium copper tetrasilicate $CaCuSi_4O_{10}$ (cuprorivaite), the main component of the Egyptian blue (Figure 26a). Slightly darker inclusions in BSE images display a similar composition but with higher content in Si, suggesting the presence of a glassy phase not completely transformed into Egyptian blue crystals (Figure 25c, 26b).

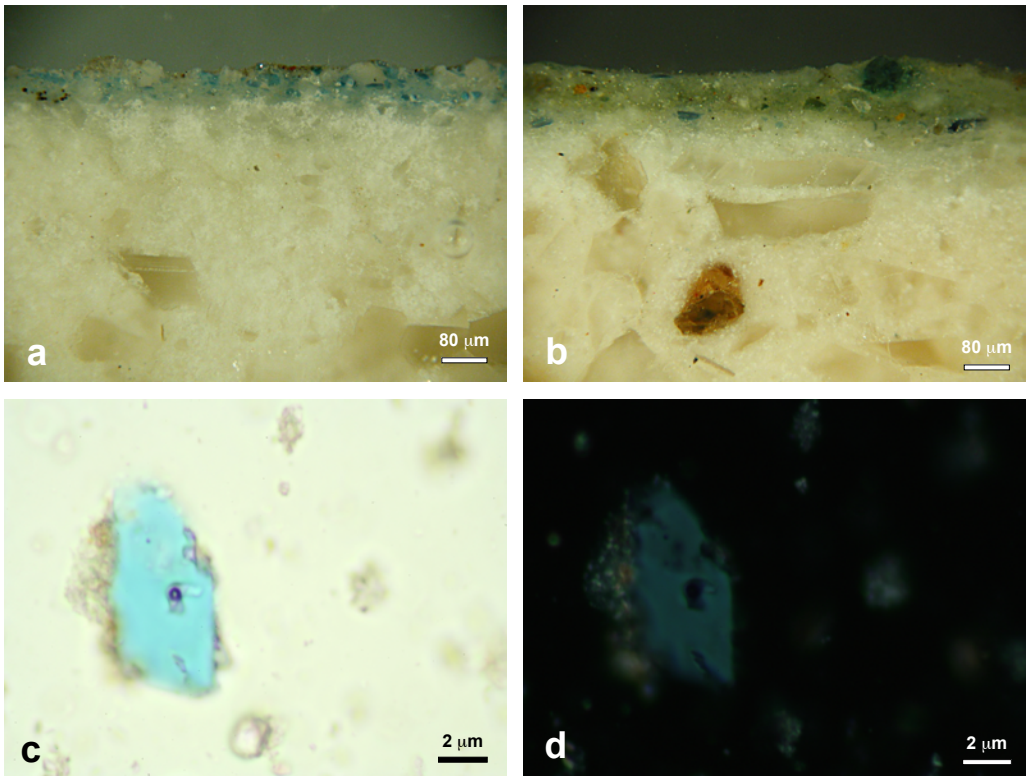

Figure 24. Light blue samples. Reflected light micrographs of: a) thin pale blue layer on a *marmorino* preparation; b) thin pale blue layer on a *marmorino* preparation under a green layer. Polarising light micrographs of: c) Egyptian blue in PPL; d) Egyptian blue in XPL.

More rarely, a mineral phase containing Sn have been identified in small inclusions within cuprorivaite crystals, which resulted to be malayaite ($CaSnSiO_5$) (Figure 25d, 26c). The identification of this component in the Egyptian blue suggests that the source of the copper was scale from bronze (Hatton et al., 2008). In the majority of the samples Egyptian blue particles display regular shape and sometime visible cleavage. Moreover, BSE images showed different characteristics in the two samples of blue. In the first one (LF024.V) paint is in continuity with the preparation layer, whereas in the second one (LF035.V) is clearly present a thin carbonation layer. This evidence suggests that the two pictorial layers were produced using two different techniques, i.e. *fresco* in the first case, and *mezzofresco* in the second case (see chapter 2 for the details on distinguishing criteria).

FT-IR spectra showed, besides the typical carbonate bands, two intense bands at 1000 and 1052 cm^{-1} and other two bands at 1162 and 1192 cm^{-1} with minor intensity, which are typical of the Egyptian blue (Figure 27). The blue particles are therefore constituted by Egyptian blue and dispersed in a calcite binder. Small grains of calcite, yellow ochre and particles of yellow glass already described in section 3.3, have been also recognised. These components were added to the blue pigment in different amounts obtaining lighter colours in the case of calcite, or greenish hues, in the case of yellow ochre and glass. Moreover, a minor fraction of Egyptian blue has been also identified in green and grey paintings (see section 3.5 and 3.6 respectively).

Egyptian blue is the earliest synthetic pigment synthesised and used extensively

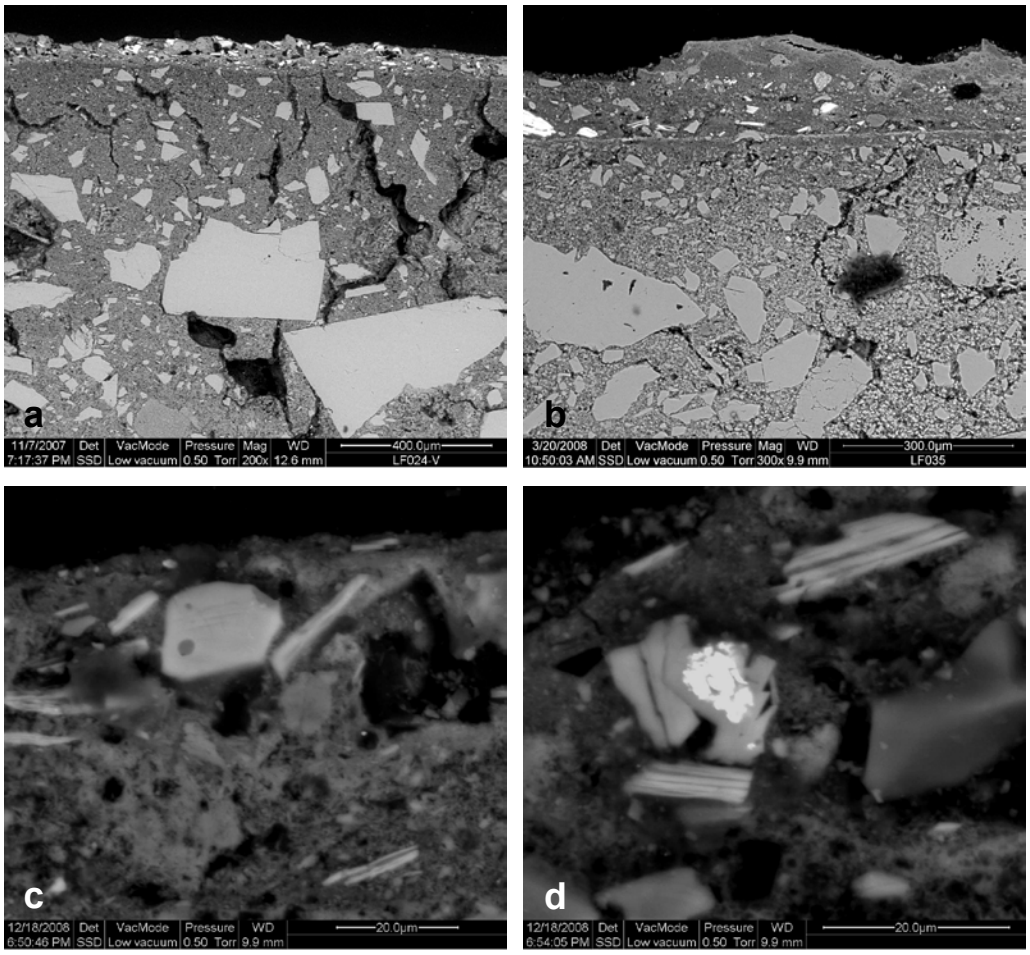

Figure 25. BSE images of wall painting samples analysed in this study: a) Egyptian blue particles in a *fresco* painting; b) Egyptian blue particles in a *mezzofresco* painting; c) Cuprorivaite crystal with glass phase (darker inclusion); d) Cuprorivaite crystals with Sn-rich phase (lighter inclusion).

starting from 4th Dynasty until the end of the Roman period in Europe. It is a multicomponent material that was produced by firing a mixture of quartz, lime, copper alloy and in an alkali flux to a temperature in the region 850-1000 °C (Tite et al., 1984). It is a quite precious and expensive pigment, worthing up to 40 *denarii* (640 *asses*) per *libra*, according to Augusti (1967). It was widely adopted by the Egyptians, the Mesopotamians, the Greeks and the Romans (Eastaugh et al. 2004 and references therein). In particular the Romans also set up local production centres. Both Pliny and Vituvius write that Eghyptian blue (*caeruleum*) was manufactured in Pozzuoli, near Naples, and called Puteolanum (Pozzuoli blue or Vestorian blue), but unfortunately a criteria for distinguishing relative productions areas is still missing. Egyptian blue was identified in many Roman contexts such as at Pompeii and in Switzerland (Béarat, 1997), in Rome (Bugini and Folli, 1997), at Paphos and Cyprus (Kakoulli, 1997), and in Northern Spain (Villar and Edwards, 2005). Canti and Heathcote (2002) also identified a local-produced Egyptian blue in west-central England. Blue samples were found in stratigraphic units dated to the Imperial Age.

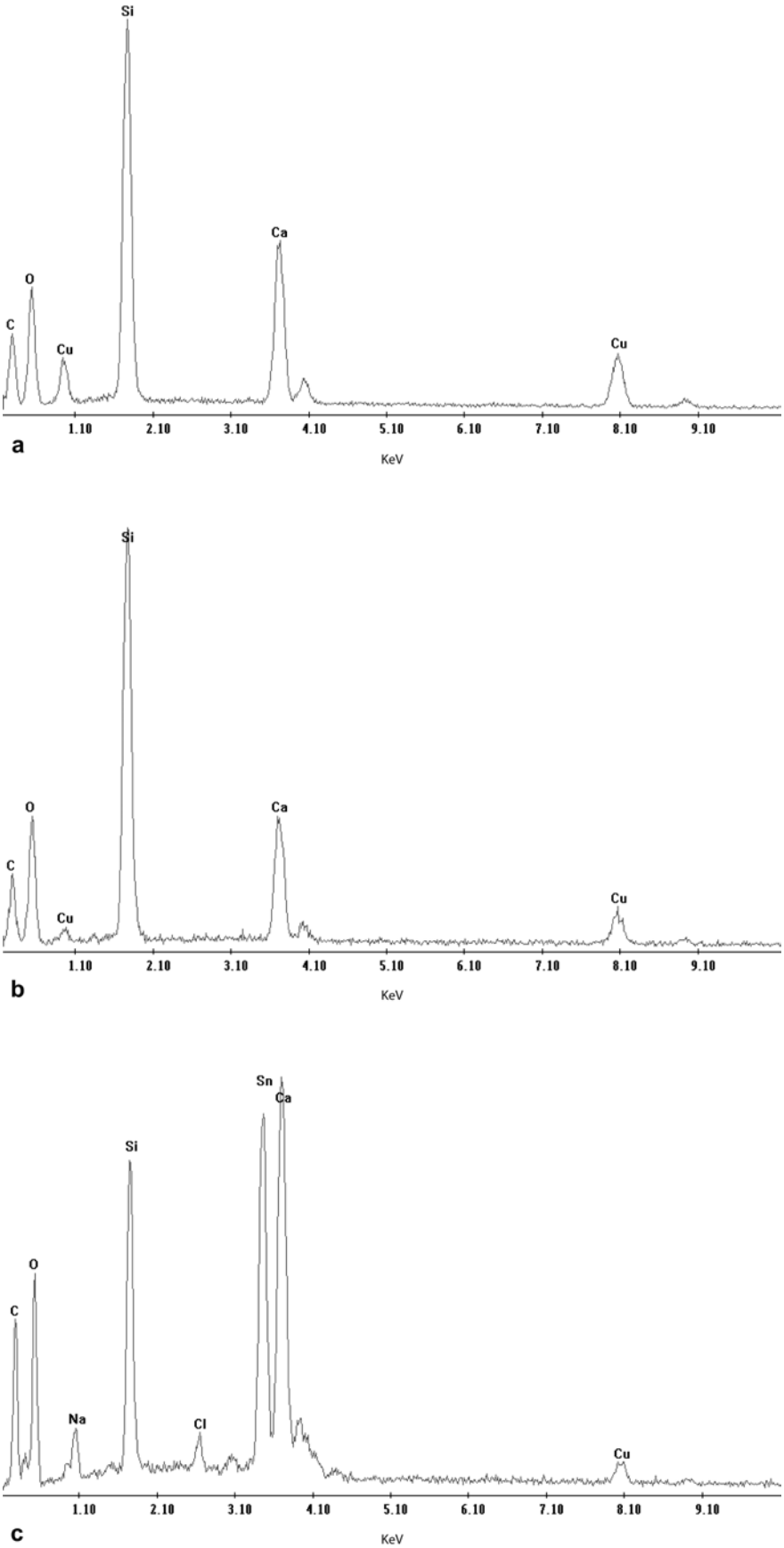

Figure 26. EDS spectra of Egyptian blue particles: a) cuprorivaite; b) glass phase; c) malayaite.

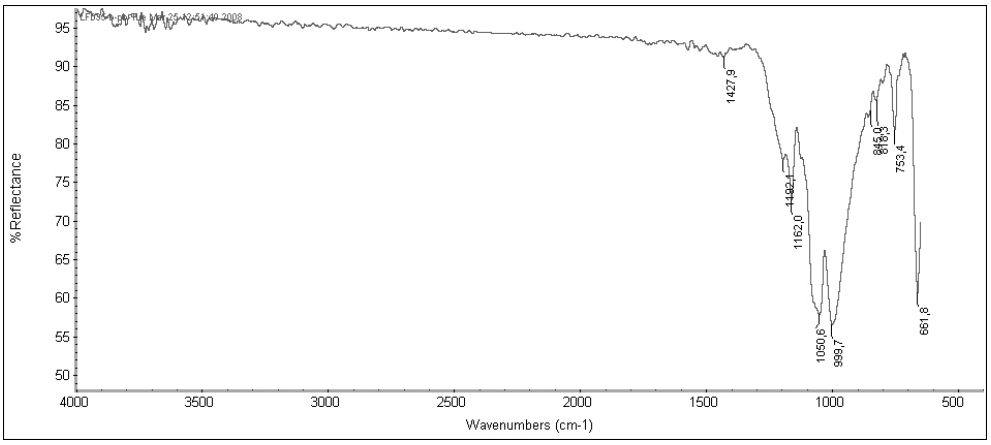

Figure 27. FT-IR spectrum of an Egyptian blue in light blue layer.

3.5 Green colour

The majority of the green samples (green 1 in Table 3) appears under RL-OM as a thin pale green pictorial layer with few green well-distinguishable particles and rare yellow and red fine particles (Figure 28a). The thickness of the painted layer is rather constant, and measures about 0.03 mm. In one sample where the green colour is applied on a previous red painting layer (Figure 11a), thickness reaches about 0.05 mm. TL-OM study revealed abundant rounded particles with a colour varying from bright emerald green to pale green. Green particles display a low relief and often result to be made of a polycrystalline aggregate (Figure 27c) as also shown by mottled extinction. In XPL they show moderate birefringence and second to third order interference colours, sometimes masked by the high body colours (Figure 27d). All these characteristics indicate that the green pigment is made of a green earth. Both in RL-OM and TL-OM few particles of red and yellow ochres, and traces of Egyptian blue were recognised, the latter showing the same optical and microtextural distinguishing features described for the blue paintings. However, further evidence of their mineralogical nature are missing because of the extremely fine grain size of the particles. XRPD analysis identified calcite, aragonite, quartz, and celadonite as primary components of the green earth (Figure 29). Celadonite is a green ferromagnesian silicate mineral belonging to the mica group with a general chemical formula $K(Mg,Fe^{2+})(Fe^{3+},Al)Si_4O_{10}(OH)_2$. The presence f this mineral phase was also confirmed by the analysis of an ESEM-EDS spectrum, where relative proportion of the different chemical components are compatible with celadonite associated to calcite (Figure 30). FT-IR spectra showed the presence of carbonates, due to the $CaCO_3$ of the binder (bands centred at 1400, 875 and 712 cm^{-1} assignable to $CO_3^{=}$) and silicates (bands centred at 1000 cm^{-1} assignable to the Si-O-Si stretching), possibly related to the pigment (Figure 31).

Other two recipes have been identified in two of the green samples (LF036, LF128. V). They differ from “green 1” for the different proportion of the same components described above (i.e. celadonite, red and yellow ochres, Egyptian blue). The first recipe (green 2 in

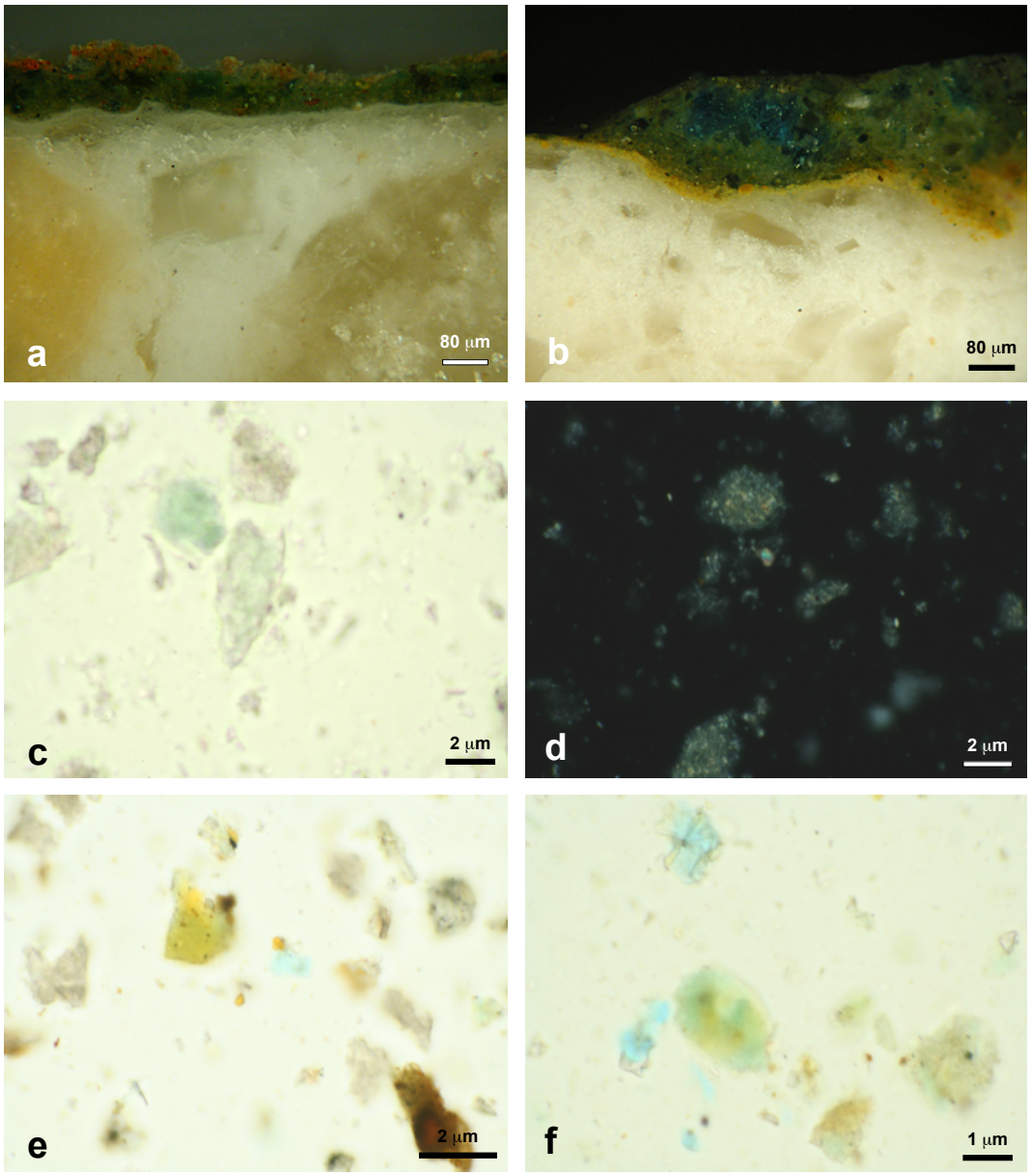

Figure 28. Green samples. Reflected light micrographs of: a) thin green layer on a *marmorino* preparation with traces of a red painting on the top; b) deep green layer on a yellow layer and a *marmorino* preparation. Polarising light micrographs of: c) green earth in PPL; d) green earth in XPL; e) Egyptian blue, green earth in PPL; f) Egyptian blue, green earth, ochres and lime in PPL.

Table 3, sample LF036) refers to a paint in which about 50% of the pigment particles are made of red and yellow ochres, 20% of Egyptian blue, 10% of celadonite and 20% of lime and calcite (Figure 28b, f). The second one (green 3 in Table 3, sample LF128.V) refers to sample displaying 70% of celadonite, 10% of Egyptian blue and 20% of ochres, lime and calcite (Figure 28e).

The main colouring agents in green earths are more commonly the green clay minerals glauconite and celadonite, which have very similar composition but precisely different environments of formation, in such a way that celadonite and glauconite are never associated (Eastaugh et al., 2004). Glauconite is present in many sandstones and marls deposited as marine sediments; it forms from the alteration of a variety of starting materials, especially

Mg,Fe-rich silicate minerals such as biotite, in many marine environments and therefore occurs worldwide (Deer, 1999). Celadonite, instead, occurs as the alteration product of basaltic igneous rocks and is therefore known from certain regions of onshore and offshore volcanic activity (Eastaugh et al., 2004). Like other earth pigments, this material has been widely used since antiquity as also described by both Vitruvius (as *creta viridis*) and Pliny (77 AD). According to the latter author, it was a rather inexpensive pigment, worth only one *sestertius* per *libra*.

The use of green earth, and especially celadonite, as a pigment is well documented in many examples of Roman art in Pompeii (Béarat, 1997; Varone and Béarat, 1997), Switzerland (Béarat, 1997), Rome (Bugini and Folli, 1997) and Paphos in Cyprus (Kakoulli, 1997). As concerns the age of the different samples, unfortunately all the green ones belong to units of unknown age, with the exception of the sample rich in Egyptian blue and produced following the "green 3" recipe (LF128.V), that belong to a unit of the 4th – 3rd BC centuries.

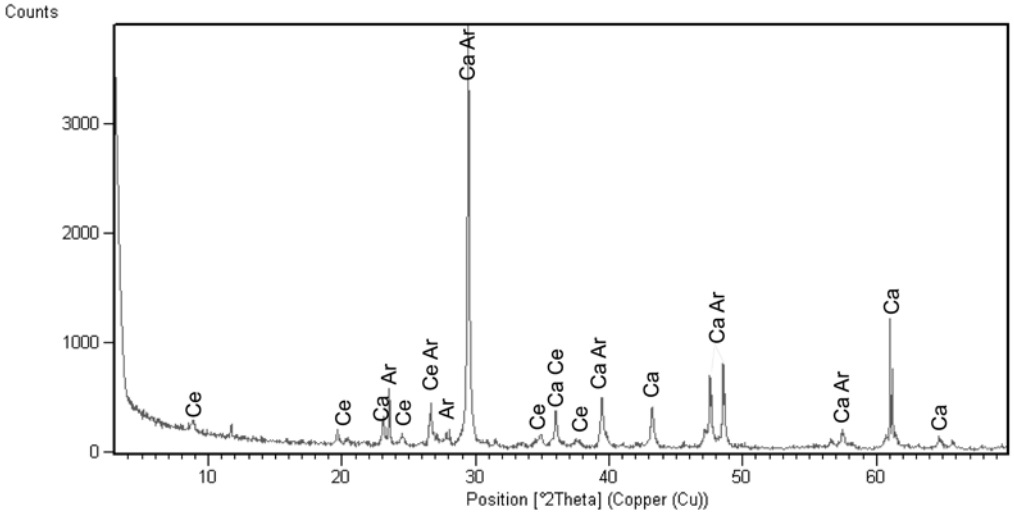

Figure 29. XRD of a green sample with the phases: calcite (Ca), celadonite (Ce) and anorthite (Ar).

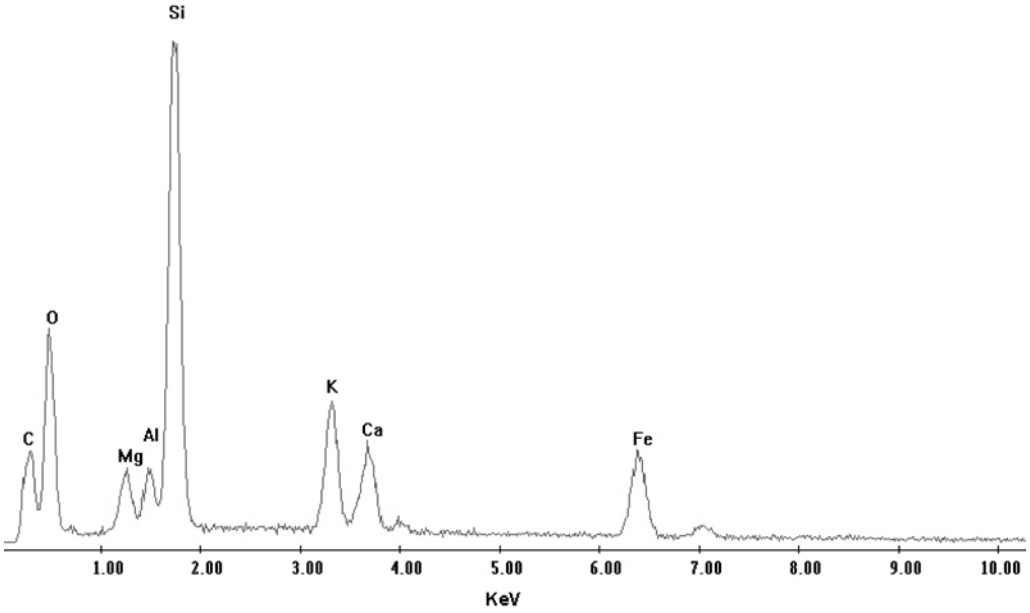

Figure 30. EDS spectrum of green particles in a green layer (celadonite).

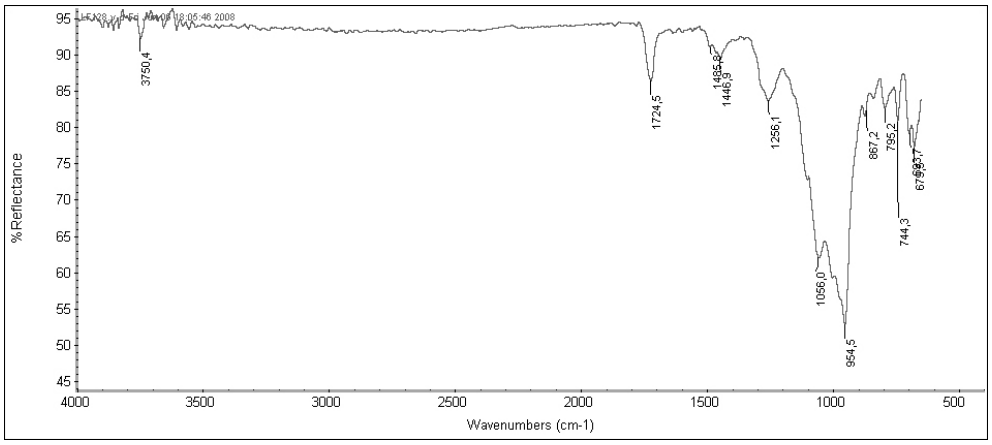

Figure 31. FT-IR spectrum of green earth in green layer.

3.6 Grey colour

Three different grey samples were also analysed (LF026.G, LF027.G, LF044.G). RL-OM study of the grey colours showed a thick grey layer of 0.1-0.2 mm with a bluish-greenish shade. The layer contains medium-grained red, yellow, brown and blue pigment particles up to 0.02 mm in diameter (Figure 32a). These particles appeared homogeneously distributed in the painted layer which is always applied on a previously painted layer, the colour of which resulted to be black, red and white, respectively, for the three considered grey samples. This complex microstructure was also confirmed by TL-OM (Figure 32b), FTIR and ESEM-EDS, which allowed identifying red, yellow and brown ochres, and Egyptian blue as major components (Figure 33a), and traces of glauconite, brown glass and cinnabar. For an exhaustive description of all this pigments see sections 3.2, 3.3, 3.4 and 3.5. As regards the Egyptian blue inclusions, the recognition of tiny K-Ca-Fe-bearing inclusions(Figure 33b) and the absence of malayaite, suggest that the source of Cu for the pigment preparation probably derived directly from copper ore or scale from copper metal (Hatton et al., 2008), indicating different manufactures for the production of Egyptian blue used in blue and grey paintings. Moreover, in low-magnification BSE images a thin carbonation layer has been recognised at the bottom of the grey painted layer, which is missing at the base of the underlying coloured layer (Figure 33a), indicating that the grey paint has been applied using the *mezzofresco* technique, while the underlying coloured layer has been applied with the *fresco* technique. Since grey paintings have been observed on limited areas such as stripes or geometric drawings, probably this colour was used for finishes and decorations applied on a painted surface.

Such a complex recipe for the production of a grey colour derived from the mixture of several pigments is unprecedented in other studies concerning Roman wall paintings. As concerns the age distribution, all these grey samples belong to the Imperial Age l.s., although a more precise chronological collocation was not possible to assess.

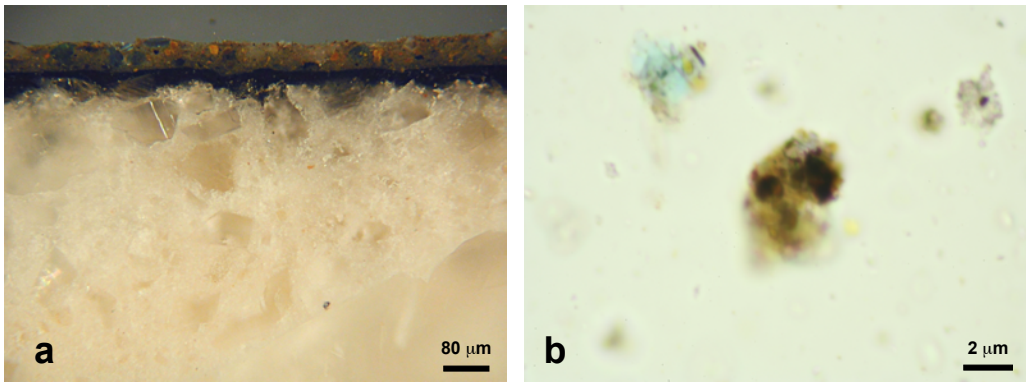

Figure 32. Grey samples: a) reflected light micrographs of grey painting layer; b) polarising light micrographs of ochre, Egyptian blue, green earth and lime particles. All images were taken in PPL.

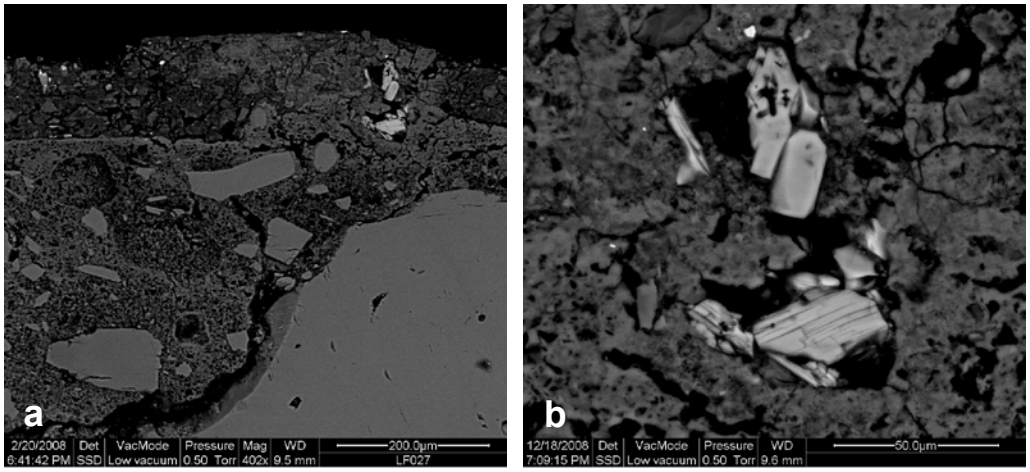

Figure 33. BSE images of wall painting samples analysed in this study: a) Egyptian blue particles in a grey *mezzofresco* painting; b) Egyptian blue particles in a grey painting with K-Ca-Fe-bearing inclusions (darker inclusion).

3.7 White colour

Twenty white fragments from the Temple of Venus have been analysed. TL-OM petrographic analyses allowed recognising in the majority of the samples abundant grains of calcite both as crystalline sparite and as cryptocrystalline micrite-like agglomerates which probably derived from the carbonation of lime. The former either display regular shape related to calcite cleavage, or from anhedral colourless crystals, the latter show agglomerates composed by indistinguishable very fine-grained crystals. When sufficiently large, crystals showed highly variable relief and high birefringence with interference colours of the third order or greater. XRPD, FT-IR and EDS analyses also indicated that calcite is almost the only mineral component, with the exception of samples LF037 and LF127.B, where few particles of red ochre and coal black, and of Egyptian blue, respectively, have been identified (Figure 34a). The presence of these particles may be due to a contamination during the implementation of the paint or to an intentional addition to obtain particular hues. Various percentages of fine-grained crystals of calcite or micrite-like agglomerates have been recognised also in other paintings (Figure 34c, d), where they were deliberately added to

extend other pigments and make their colour lighter. In petrographic thin section, most of the samples with a white surface appear as a very fine-grained mortar exclusively made of lime and calcite grains such as observed in *marmorino*, and therefore a true painted layer is apparently lacking (Figure 3a), while in others (LF037, LF097, LF101, LF108) a thick white smoothing layer result to be applied on an underlying *marmorino* preparation layer (Figure 34b). When associated with another coloured layer, the white paint always acts as a preparation layer (Figure 2e, f).

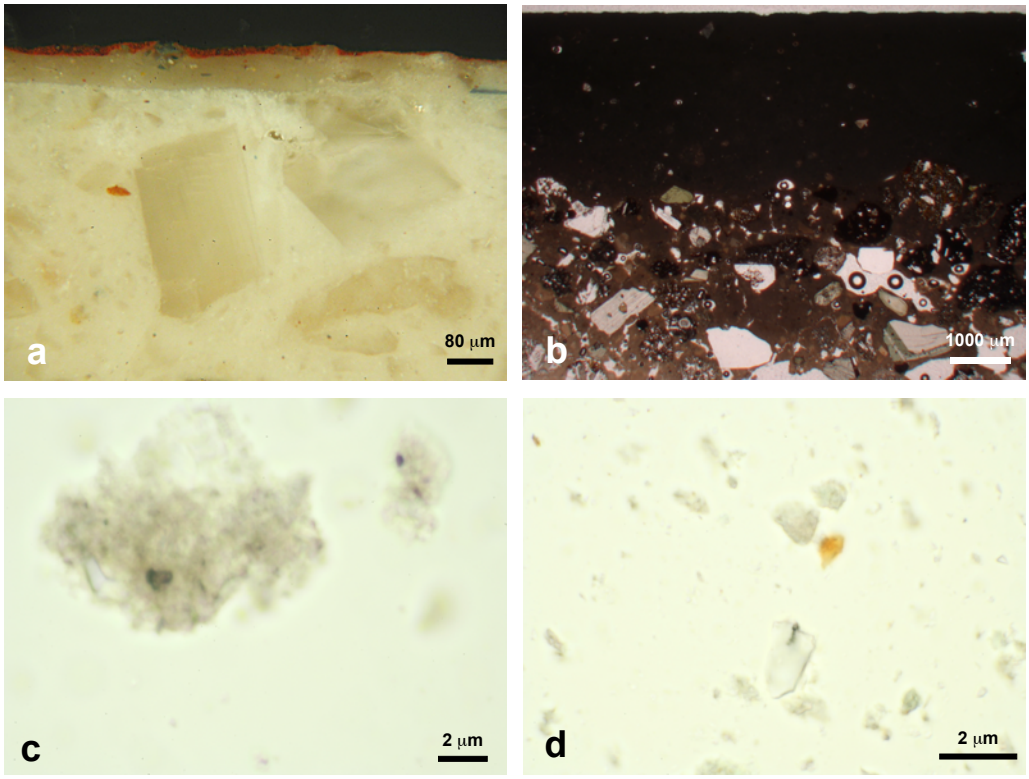

Figure 34. White samples. Reflected light micrographs of: a) white smoothing layer on a *marmorino* preparation with traces of a red painting. Polarising light micrographs of: b) smoothing layer on a *marmorino* preparation in XPL; c) lime in PPL; d) crystals of calcite in PPL.

A water-rich mixture of slaked lime was really used as paint in antiquity, known as lime white, limewash or whitewash (Gettens et al., 1993). As said in Eastaugh et al., 2004: "Lime derived calcium carbonates and calcium hydroxides are ubiquitous as pigments used in frescoes. Lime white, when used in this technique, required no binder and was a highly stable pigment". Pliny and Vitruvius report on a number of different white colours, including "earths" and organic dyes, but also indicate that whitewash was the most commonly used white pigment. Moreover, lime-based mortars were also widely used as final preparation coat on *intonaco* or *marmorino* for frescoes from the Greek period to present times, and ground marble was commonly used as an aggregate in this mortar layer (Eastaugh et al., 2004).

Whitewash as well as calcite and dolomite have been widely recognised as raw materials for pigments in Roman wall paintings in many archaeological context such as

Pompeii (Béarat, 1997; Varone and Béarat, 1997), various sites in Switzerland (Béarat, 1997), Rome (Bugini and Folli, 1997), Corinth (Meggiolaro et al., 1997) and Paphos in Cyprus (Kakoulli, 1997). Chronological dating of the samples confirmed persistence of the used of these simple white paints in time. Samples, indeed, belong to all the considered chronological units, from the end of the 4th-3rd century BC to the Augustan Age. On the contrary, paintings prepared in accordance to the "white 2" recipe are only testified in the second half of the 2nd century BC.

Conclusions

The colour palette of the Temple of Venus is relatively various, although the number of colours is not as high as found in other buildings in Pompeii. The types of pigments recognised are consistent with those observed elsewhere in Pompeii and more in general in the Roman Empire, and basically follows the palette described both by Pliny and Vitruvius, with the exception of a volcanic natural yellow glass. Ten different pigments have been found, either in a pure form or in admixtures in different proportions of two or more compounds. Inexpensive and widely distributed pigments such as yellow and red ochres, green earth and whitewash, were recognised as well as relatively precious pigments such as Egyptian blue and cinnabar, which all resulted to be relatively pure and of good quality. In particular, red ochre resulted to be haematite with high degree of crystallinity, and cinnabar and the two types of Egyptian blue resulted to be made of highly pure well-selected cinnabar crystals and cuprorivaite, respectively, with a negligible content of other mineral impurities. Mössbauer spectroscopy performed on both red and yellow ochres confirmed that these pigments are basically composed of a single phase (i.e. haematite and goethite, respectively) and that other K-Ca-Fe-bearing mineral phases are missing in these pigments. In two cases (LF013, LF015) the presence of nanosized oxide/oxyhydroxide particles were also recognised. It is also worth noting that Mössbauer spectra were acquired using a newly designed Mössbauer portable spectrometer which was tested on wall paintings for the first time. Statistics of the spectra was sufficiently good and acquisition time reasonably short to confirm the applicability of this new facility.

As regards Egyptian blue, the identification of malayaite ($CaSnSiO_5$) in a group of the samples and that of an unspecified K-Ca-Fe-bearing phase as tiny inclusions in pigment grains of another group of samples, clearly indicates two different manufacturing processes in the preparation of this specific pigment. In particular, the occurrence of malayaite indicates that Cu was derived from bronze, while the absence of this phase probably suggests a different origin for Cu, such as directly from copper ore deposits.

Paints were either constituted by pure pigments or prepared as admixtures of pigments following a series of seventeen recipes, to obtain different hues and shades. The majority of the recipes is rather simple and involves one or two main pigments, sometimes with the

addition of other minor impurities. In order to make colours darker or lighter, especially yellow and red, carbon (lampblack) and calcite (whitewash), respectively, have been used in admixture with the appropriate pigment. In other cases, paints contain the same pigments but were admixed in different relative proportions according to different recipes (i.e. recipes yellow 1 and red 1), obtaining a variety of hues. "Grey" and "green 2" resulted to be the most complex recipes, including four different pigments and several minor components. In particular, grey colour was made by deliberately admixing yellow, red and brown ochre, Egyptian blue, brown glass, cinnabar and glauconite in precise proportions to obtain the desired hue. There are no analogies in the literature of such a complex admixture of pigments, which may reflect the skill of a painter.

An additional important remark is that some of the colours, such as black, red, green and yellow, were prepared using different pigments. The adoption of different recipes for the same colour may suggest presence of several ateliers of painters working in the Temple of Venus who had preferences for different methods for the production of their colour tones. Chronological data show that the most common and inexpensive recipes are also widely diffused with time, such as pure haematite in "red 1", haematite and goethite in "yellow 2", *marmorino* in "white 1". "Black 1" seems to be the most used recipe for the black paints at least from the 1st century BC to the 1st AD (Julio-Claudian Age) while Egyptian blue in light blue paints seems to be exclusively used in the Imperial Age, although this pigment was certainly used since the end of the 4th century BC as demonstrated by its identification as a component in green admixtures. It is also relevant noting that the identification of different manufacturing of the Egyptian blue pigment in the Imperial Age, suggests that the pigment was purchased from different producers.

Furthermore, a new yellow and brown pigment never identified before has been also recognised and characterised. It is made of fragments of a yellow or brown natural volcanic glass which is chemically compatible with vulcanites of the Mount Somma-Vesuvius. This seems to suggest a local production for this pigment which is undocumented even by Pliny and Vitruvius. It is relatively common in many paints either as one of the main components (yellow 3, yellow 4) or as a minor component (red 2, yellow 2, light blue, green 2).

As regards the preparation layers, three different types of *intonaco* have been recognised, on the basis of the composition of their aggregate. *Intonachino* is characterised by an aggregate made of volcanic sand and represents 9% of the preparation layers, *cocciopesto* is made of grog and represents 19% of the preparation layers, while *marmorino* is prepared with limestone and calcite and represents 72% of the preparation layers of the analysed samples. Although all the *intonaco* layers are meticulously prepared, *marmorino* is realised as a multi-layered plaster, and reflects more closely Vitruvius's recommendations (Figure 3b).

All the data, and in particular the absence of a carbonation layer between the paint and the *intonaco* and of any trace of organic binders, confirmed that the most utilised painting technique was the *fresco*. All samples display very thin painting layers, with well dispersed

fine-grained pigment particles and sometimes medium to coarse grains well coated by a film of calcite (Figure 5a, c). In multi-layered coloured samples, when strips or figures were painted on a coloured background, thickness of the painted layers and the presence of a carbonation layer between the two differently coloured layers, suggests that the more superficial painted one was applied with a *mezzofresco* painting technique.

In conclusion, the importance and prestige of the Temple of Venus is also reflected in the quality and value of the pigments, and in the careful execution of the mortars.

REFERENCES

Augusti, S., 1967. *I colori pompeiani*. De Luca Editore. Rome.

Baxter, M. J., 1999. Detecting multivariate outliers in artefact compositional data, *Archaeometry* 41, 321–338.

Béarat, H., 1997. Quelle est la gamme exacte des pigments romains? Confrontation des resultats d'analyse et des textes de Vitruve et de Pline» (What is the exact scale of Roman pigments? Confrontation of the results of analysis with the texts of Vitruvius and Pliny). In: "Roman wall painting. Materials, techniques, analysis and conservation" Proceedings of the International Workshop on Roman Wall Painting, Fribourg, 7-9 March 1996. Institute of Mineralogy and Petrography Fribourg University: 11-34.

Bugini, R., and Folli, L., 1997. Materials and making techniques of Roman republican wall paintings (Capitolium, Brescia, Italy). In: "Roman wall painting. Materials, techniques, analysis and conservation" Proceedings of the International Workshop on Roman Wall Painting, Fribourg, 7-9 March 1996. Institute of Mineralogy and Petrography Fribourg University: 121-130.

Canti, M.G. and Heathcote, J.L., 2002. Microscopic Egyptian blue (Synthetic Cuprorivaite) fromsedimens at two archaeological sites in West Central England. Journal of Archaeological Science 29, 831-836.

Cioni, R., Gurioli, L., Lanza, R. and Zanella, E., 2004. Temperatures of the A.D. 79 pyroclastic density current deposits (Vesuvius, Italy). J. Geophys. Res. 109, B02207, doi:10.1029/2002JB002251.

Curti, E., 2007. La Venere Fisica trionfante: un nuovo ciclo di iscrizioni dal santuario di Venere a Pompei. In: Il filo e le perle. Studi per i 70 anni di Mario Torelli, Venosa: 57-71.

Curti, E., 2008. Il tempio di Venere Fisica e il porto di Pompei? In: Guzzo, P.G. and Guidobaldi, M.P. (Eds.) Nuove ricerche archeologiche nell'area vesuviana (scavi 2003-2006), Roma: 47-60.

Damiani, D., Gliozzo, E., Memmi Turbanti, I. and Spangenberg J.E., 2003. Pigments and plasters discovered in the House of Diana (Cosa, Grosseto, Italy): an integrated study between art history, archaeology and scientific analyses. Archaeometry 45, 2, 341-354.

Deer, W.A., Howie, R.A. and Zussman, J., 1999. An introduction to the rock-forming minerals. 2nd edition. Longman.

Eastaugh, N., Walsh, V., Chaplin, T. and Siddall, R., 2004. Pigment compendium. A dictionary of historical pigments. Butterworth-Heinemann.

Edwards, H.G.M., de Oliveira, L.F.C., Middleton, P. and Frost, R.L., 2002. Romano-British wall-painting fragments: a spectroscopic analysis. The analyst 127, 277-281.

Fairchild M.D., 2005. Color appearance models. 2nd edition. John Wiley & sons.

Fuchs, M. and Béarat, H.,1997. Analyses phisico-chimiques et peintures murales romaines à Avenches, Bosingen, Dietikon et Vallon. In: "Roman wall painting. Materials, techniques, analysis and conservation" Proceedings of the International Workshop on Roman Wall Painting, Fribourg, 7-9 March 1996. Institute of Mineralogy and Petrography Fribourg University: 181-191.

Gettens, R.J., FitzHugh, E.W. and Feller, R.L., 1993. "Calcium Carbonate Whites" In: Roy, A., (ed.) Artists' Pigments. A Handbook of their History and Characteristics. Vol. 2. National Gallery of Art, Washington and Oxford University Press, Oxford, 203-226.

Hatton, G.D., Shortland, A.J. and Tite, M.S., 2008. The production technology of Egyptian blue and green frits from second millennium BC Egypt and Mesopotamia. Journal of Archaeological Science 35, 1591-1604.

Kakoulli, I.,1997. Roman wall paintings in Cyprus: A scientific investigation of their technology. In: "Roman wall painting. Materials, techniques, analysis and conservation" Proceedings of the International Workshop on Roman Wall Painting, Fribourg, 7-9 March 1996. Institute of Mineralogy and Petrography Fribourg University: 105-117.

Mazzochin, G.A., Agnoli, F., Mazzochin, S. and Colpo, I., 2003. Analysis of pigments from Roman wall paintings found in Vicenza. Talanta, 61, 565-572.

Mazzochin, G.A., Agnoli, F. and Salvadori, M., 2004. Analysis of Roman Age wall paintings found in Pordenone,Trieste and Montegrotto. Talanta, 64, 732-741.

Meggiolaro, V., Molin, G., Pappalardo, U. and Vergerio, P.,1997. Contribution to studies on Roman wall painting materials and technique in Greece: Corinth, the southeast building. In: "Roman wall painting. Materials, techniques, analysis and conservation" Proceedings of the International Workshop on Roman Wall Painting, Fribourg, 7-9 March 1996. Institute of Mineralogy and Petrography Fribourg University: 105-117.

Murad, E. and Johnston, J. H., 1987. Iron oxides and hydroxides. In: Long, G. J. (Ed.), Mössbauer spectroscopy applied to inorganic chemistry, Vol. 2. Plenum Press, New York.

Pliny, 1999. Natural History H. Rackham trans., Loeb Classical Library, Harvard University Press, Cambridge, Massachusetts.

Prentice, J. E., 1990. Geology of construction materials, Chapman and Hall, London.

Rozenberg, S., 1997. Pigments and fresco fragments from Herod's palace at Jericho. In: "Roman wall painting. Materials, techniques, analysis and conservation" Proceedings of the International Workshop on Roman Wall Painting, Fribourg, 7-9 March 1996. Institute of Mineralogy and Petrography Fribourg University: 63-74.

Santacroce, R. (Ed.)., 1987. Somma-Vesuvius, Quaderni de "La Ricerca Scientifica". Progetto finanziato "Geodinamica". Monografie finali, 8. CNR Roma.

Tite, M.S., Bimson, M. and Cowell, M.R., 1984. Technological examination of Egyptian blue. In: Lambert, J.B. (Ed.), Archaeological Chemistry III. American Chemical Society Advances in Chemistry Series No. 205, pp. 215-242. Washington, DC.

Wallert, A., and Elston, M., 1997. Fragments of Roman wall painting in the J. Paul Getty Museum: a preliminarly technical investigation. In: "Roman wall painting. Materials, techniques, analysis and conservation" Proceedings of the International Workshop on Roman Wall Painting, Fribourg, 7-9 March 1996. Institute of Mineralogy and Petrography Fribourg University: 93-104.

Walsh, V., Siddall, R., Eastaugh, N. and Chaplin, T., 2003. Pigmenti di Pompeii: verso la definizione di uno standard di riferimento per la ricerca sui pigmenti romani. In: "Scienze e archeologia" Proceedings of giornate di studio: "Le scienze e l'ambiente" e "Le scienze chimico fisiche", Pompeii, 23 October and 19 November 2003. Università del Sannio-dipartimento di studi geologici e ambientali and Università di Modena e Reggio Emilia-dipartimento di chimica. 181-196.

Varone, A., and Béarat, H., 1997. Pittori romani al lavoro. Materiali, strumenti, tecniche: evidenze archeologiche e dati analitici di un recente scavo pompeiano lungo via dell'Abbondanza (Reg. IX ins. 12). In: "Roman wall painting. Materials, techniques, analysis and conservation" Proceedings of the International Workshop on Roman Wall Painting, Fribourg, 7-9 March 1996. Institute of Mineralogy and Petrography Fribourg University: 199-214.

Villar, S.E.J. and Edwards, H.G.M., 2005. An extensive colour palette in Roman villas in Burgos, Northern Spain: a Raman spectroscopic analysis. Analytical and Bioanalytical Chemistry 382: 283-289.

Vitali, V., and Franklin, U. M., 1986. New approaches to characterisation and classification of ceramics on the basis of their elemental composition. Journal of Archaeological Science 13, 161–170

Vitruvius, 1999. The ten books on architecture. I.D. Rowland trans., Cambridge university press.